

LU TP 17-20
June 2017

An Investigation of the Trinification Scalar Sector at One Loop

Laurie Walk

Department of Astronomy and Theoretical Physics, Lund University

Master thesis supervised by Roman Pasechnik



LUND
UNIVERSITY

In memory of my colleague and friend,

Erik Gustafsson

Abstract

Throughout this work we investigate a trinification-based grand unification theory (GUT) with a global family symmetry, as a radiative origin of the Standard Model (SM). We show that after spontaneous symmetry breaking of the trinification gauge group, we can in theory construct an effective left-right symmetric model (LRSM) which breaks to the SM gauge group through radiative breaking induced by the running of the model's parameters. We further argue that a low-energy limit of this effective LRSM can accommodate a realistic SM quark mass hierarchy and Cabibbo mixing. Upon close consideration, however, we show that we cannot impose a tree-level scalar mass hierarchy at the GUT scale significant enough to justify the effective LRSM as a physically viable low-energy limit of the trinification model. Thus, we compute the full one-loop scalar mass spectrum using the effective potential approach, and search for parameter space points for which such a hierarchy can be imposed at one loop. Upon implementation of a preliminary random scanning algorithm, no such parameter space points are found, and we conclude that more advanced scanning techniques are needed in future studies, and/or additional scalars should be kept in the effective theory.

Populärvetenskapligt sammanfattning

Standardmodellen inom partikelfysik beskriver de kända fundamentalkrafterna och klassificerar alla de experimentellt observerade elementarpartiklarna. Allmänt sett anses den vara en av de största bedrifterna inom modern vetenskap, tack vare sin förmåga att sammanlänka teoretiska förutsägelser med fenomenologi. Men trots att nästan hela vår förståelse av den subatomära världen ryms i denna modell så ger inte standardmodellen någon beskrivning av fenomen så som mörk materia, neutrinomassor och gravitation. Dessa luckor i teorin motiverar fysiker till att söka efter utvidgningar av standardmodellen som kan bidra till en mer övergripande teori.

Fysiker tror att luckorna i standardmodellen kan förklaras med hjälp av mekanismer och/eller partikelinteraktioner som inte kan observeras i ett universum med vår nuvarande energiskala. Därför konstruerar de så kallade 'storförenade teorier' inom vilka de elementära krafterna förenas på högre energiskalor. En framgångsrik sådan måste utvecklas till den observerade standardmodellen, och innehålla dennes parametrar och symmetrier, när energiskalorna sänks till de betingelser som råder idag. Därför skulle en sådan modell inte bara kunna ge svar på frågor inom modern vetenskap, utan också ge insikt i de högenergiförhållanden som rådde i det tidiga universum, ur vilka de nuvarande fysiklagarna uppstod.

I detta arbete föreslås ett exempel på en sådan storförenad modell. Vi undersöker hur dess symmetrigrupp, som beskriver teorins tillåtna partiklar och interaktioner, bryts ner till de inom standardmodellen när energiskalan sänks. Vi utforskar ett antal nyckelfenomen inom den så kallade trinifikationsmodellen, och använder denna för att förutsäga uppkomsten för standardmodellens fenomenologi. Slutligen söker vi efter värden av de av modellens parametrar, för vilka den utvecklas till en realistisk version av den observerbara standardmodellen.

Sökandet bortom standardmodellen banar väg för lösningar av de många mysterier inom modern fysik, vilka är nödvändiga för en djupare förståelse av vårt universum.

Contents

1	Introduction	3
2	The trinification model	6
2.1	Symmetry group	6
2.2	Field content	7
2.3	Lagrangian of the scalar sector	8
3	Spontaneous symmetry breaking in the trinification model	10
3.1	Tree-level minimization conditions	10
3.2	Tree-level particle spectrum	11
3.2.1	Scalars	12
3.2.2	Fermions	12
3.2.3	Gauge bosons	13
3.3	Breaking trinification symmetry	13
3.4	Quantum numbers	16
3.4.1	Example: Color-singlet scalar: $U(1)_{L+R}$	17
4	The left-right symmetric model	18
4.1	The tree-level mass spectrum	18
4.1.1	Scalar masses	18
4.1.2	Fermion masses	19
4.1.3	Gauge boson masses	19
4.1.4	Parameter constraints of the LRSM	20
4.2	The low-energy effective theory	22
4.2.1	Constructing an appropriate effective theory	22
4.2.2	Constraints of the effective LRSM	24
4.2.3	Discussion of the effective LRSM at tree-level	24
4.2.4	Field content and effective Lagrangian	25
4.3	Tree-level matching conditions	28
4.3.1	Example: Tree-level matching conditions for $(\tilde{H}\tilde{H}^*\tilde{H}\tilde{H}^*)$	28
4.3.2	Tree-level matching results	32
5	RG evolution of the LRSM	34
5.1	Obtaining β -functions with PyR@TE	34
5.1.1	Example: constructing contractions from PyR@TE invariants	35
5.2	Results	36
6	Radiative breaking to the SM	38
6.1	Symmetry breaking in the effective LRSM	39
6.2	Parameter constraints for radiative breaking	41
6.3	Scanning the parameter space with simulated annealing	42
6.3.1	Implementation in Python	43

7	The one-loop scalar mass spectrum	45
7.1	The effective potential method	46
7.1.1	Formalism of the effective potential	46
7.1.2	The Coleman-Weinberg effective potential	48
7.2	One-loop scalar masses in the LRSM	50
7.2.1	Renormalized one-loop contribution	50
7.2.2	Derivative formulas of the one-loop effective potential	51
7.2.3	Tri-linear couplings	53
7.2.4	Quartic couplings	54
7.2.5	The first derivative formula	55
7.2.6	One-loop tadpole condition	57
7.2.7	The second derivative formula	58
7.2.8	One-loop mass terms	58
7.3	Numerical results for the one-loop mass spectrum	60
7.3.1	Random point parameter scan	60
8	Conclusion	63
A	Full trinification breaking scheme	66
B	Gell-Mann matrices	68
C	Functional methods in quantum field theory	69
C.1	Path integral formulation	69
C.2	Correlation functions	69
C.3	Generating functionals	70
D	Full RG equations of the effective LRSM	72
D.1	Running of Yukawa couplings	72
D.2	Running of quartic couplings	73
D.3	Running of the Majorana mass term	76
E	One-Loop tadpole condition	77

1 Introduction

The Standard Model (SM) is widely considered one of the greatest achievements in modern science for its ability to correctly match the predictions of theoretical particle physics to experimentally obtained data. The long awaited discovery of the Higgs boson at CERN in 2012, almost 50 years after its theoretical prediction in the early 1960's, proved the true phenomenological power of the SM to physicists everywhere.

Today, most of our fundamental understanding of the subatomic universe is neatly embedded in this model. And yet, however adept, the SM still fails to provide a full description of all predicted and observed phenomena, such as dark matter, neutrino masses, and a fundamental theory of gravity. Furthermore, from a theoretical point of view, the SM can be considered rather *ad hoc* in its nature, compiling together theoretical concepts as a means of explaining experimental observations. As a theory, it remains unsatisfactory in its inability to justify its premises and explain the origins of its parameters.

This suggests that the SM cannot be a grand underlying theory incorporating the full physical laws of nature, but rather exists as an effective theory, applicable at the low-energy scale of our current observations. The idea of the SM as an effective theory invites us to explore so-called Beyond Standard Model (BSM) theories as extensions to its boundaries. Furthermore, it entices physicists to search for a grand unified theory (GUT) in which the gauge interactions of the SM are unified into a single coupling at a corresponding high-energy scale.

Radiative breaking refers to spontaneous symmetry breaking of a model's gauge group, induced by the renormalization group (RG) evolution of its parameters. As such, radiative breaking of certain GUT models can provide a natural origin of the SM. However, as a GUT embodies larger symmetries at high energies, they consist of additional particles and interaction, which lead to compelling arguments for observable phenomena at lower energies.

One such GUT group candidate is the trinification gauge group, $[SU(3)]^3$. It is one of the four maximal subgroups of the exceptional Lie group E_6 , and on its own, forms the minimal trinification model, first proposed as a viable GUT candidate by Sheldon Lee Glashow, Howard Georgi and Alvaro de Rujula, in 1984 [1].

Since then, trinification-based GUT models have become increasingly popular as their low-energy phenomenology remarkably resembles the SM. For instance, in [2] it is argued that spontaneous symmetry breaking of the trinification group can provide an account parity violation in the SM. Furthermore, as is shown in [3] and [4], E_6 -inspired models can naturally account of the lightness of right-handed neutrinos, by predicting that their masses originate from loop interactions with scalars and heavy fermions at the unification scale. Finally, in [5] it is shown that trinification models are flexible enough to accommodate any quark and lepton masses and mixing angles, and that their naturally arising baryon conservation provides a inherent opposition to proton decay.

Although the minimal trinification model makes an attractive GUT candidate, it brings about several concerns. For instance, it fails to justify the considerable hierarchy between the trinification and electroweak breaking scales, and it contains a large number of free parameters,

even at high energies. In [6], it is suggested that the latter can be significantly reduced when Yukawa couplings, in addition to gauge couplings, are unified at GUT scale. After spontaneous symmetry breaking of the trinification gauge group, however, many Yukawa couplings will be allowed under the new symmetry group, and the (RG) evolution of these couplings can provide an origin of fermion mass hierarchies at lower energies.

With the outlined concepts as motivation, throughout this work we explore whether radiative breaking of a trinification-based GUT model with an added global family symmetry acts as a possible origin of the SM. This scenario is inspired by a natural reduction from an E_8 symmetry, and, as we will see, the addition of the global family symmetry will ensure a single unified Yukawa coupling at GUT scale. Consequently, this model will maintain the desirable properties of the minimal trinification model, while significantly decreasing the number of free parameters at high energies.

We begin by investigating spontaneous symmetry breaking of the model's trinification gauge group into the so-called Left-Right Symmetric Model (LRSM). At high energies, the LRSM will contain a large number of particles, making its full RG evolution difficult to study. Thus, we will attempt to construct a low-energy limit of the LRSM by tuning the model parameters in such a way that heavy states can be integrated out at the breaking scale. Then, the aim of this work is to investigate whether radiative breaking of such a low-scale effective theory leads to a SM-like model.

In [7], it is shown that at tree-level, radiative breaking from this trinification model to the SM gauge group is possible upon inclusion of two light scalar multiplets in the effective theory. Although the resulting theory contains massive particles which can be identified with certain heavy SM quarks, the remaining unbroken global group prohibits non-zero tree-level masses for lighter quarks and color neutral fermions. It is further argued that the structure of the SM Cabibbo-Kobayashi-Maskawa (CKM) mixing matrix emerges naturally as a consequence of the global family symmetry, when keeping additional scalars in the effective LRSM.

Thus, this work aims to upgrade the effective theory proposed in [7] by keeping additional scalars light. More specifically, we include a color-singlet, tri-doublet scalar field, which after induced breaking is hypothesized to split into viable SM Higgs-doublet candidates. In [7] is argued that correctly engineering the model such that certain masses can again be integrated out at this breaking scale, will result in an effective theory exhibiting the observable quark mass hierarchy and CKM mixing of the SM.

After constructing the upgraded low-energy limit of the LRSM, it is matched to the trinification model at the breaking scale, and the full set of RG equations describing the running of the model is calculated. Finally, radiative breaking of the effective theory is studied, and the properties of the resulting SM-like theory are investigated. As will become apparent, construction of our upgraded effective LRSM will require the addition of one-loop mass corrections to the scalar sector. Thus, the final aim of this work is to obtain the full one-loop scalar mass spectrum of the LRSM, and search for physically viable parameter space points which constitute radiative breaking to a SM-like theory with the proposed features.

To obtain the one-loop scalar mass spectrum we formulate the effective potential method, which allows us to use the effective potential of the trinification model to determine loop corrections to any n -point functions of the theory. Due to the large number of particles at GUT scale, derivatives of the one-loop effective potential describing such corrections are difficult to compute. For this objective, we use a set of general analytical expressions for these derivatives derived from the Coleman-Weinberg effective potential in [8].

Finally, upon determining the one-loop scalar mass spectrum, we can investigate the mass hierarchy of scalars at the trinification breaking scale. The observation of a natural spitting between scalars is a clear indication that our constructed effective LRSM is truly a low-energy limit of the model. This would justify our choice to greatly simplify the investigation of the RG evolution of the model by considering only the fields in the effective theory.

The content of this work is organized as follows. In Section 2, we outline the main features of the proposed trinification model. In Section 3, spontaneous breaking of its symmetry group is investigated, and the resulting (un)broken group generators are found. In Section 4, we obtain the tree-level particle content of the LRSM, construct the effective theory, and calculate the matching conditions. In Section 5, the full set of RG equations are found. Throughout Section 6, these are used to study the evolution of the model, and look for parameter space points which indicate radiative breaking. Finally, in Section 7 we calculate the full one-loop scalar mass spectrum, and consider the one-loop scalar mass hierarchy at the trinification scale. The appendices contain further theoretical background information, details of several calculations throughout this work, and raw results of certain computations.

2 The trinification model

The first essential part of this work is a thorough formulation of the high-scale GUT model. Throughout this section, we state the symmetry group, field content, and the Lagrangian of the trinification model, as well as outline some essential notation used throughout the rest of this work.

2.1 Symmetry group

The proposed model is non-supersymmetric, and has the trinification gauge group

$$[\mathrm{SU}(3)_C \times \mathrm{SU}(3)_L \times \mathrm{SU}(3)_R],$$

where the labels C, L, R will refer to color, left, and right symmetry respectively throughout the rest of this work. Here after, gauge groups are denoted with [...], and global symmetries with {...}.

The trinification group is one of the four maximal subgroups of the exceptional Lie group E_6

$$[\mathrm{SU}(3)]^3 \subset E_6,$$

which has a fundamental **27** representation. Under this symmetry group, fermions and scalars decompose into three matter fields, and each family can be arranged in a fundamental **27**-plet

$$\mathbf{27} = (\mathbf{3}, \bar{\mathbf{3}}, \mathbf{1}) \oplus (\mathbf{1}, \mathbf{3}, \bar{\mathbf{3}}) \oplus (\bar{\mathbf{3}}, \mathbf{1}, \mathbf{3}). \quad (2.1)$$

Fundamental and anti-fundamental representations ensure that the trinification model is free of gauge anomalies¹.

The \mathbb{Z}_3 group, which is the group of all cyclic permutations of C, L, and R, is included. It permutes scalar, fermion, and gauge fields in the trinification model accordingly, and invariance under these transformations indicates that the three gauge couplings are unified at GUT scale, such that $g_C = g_L = g_R = g$.

When breaking to the SM, the $[\mathrm{SU}(3)_C]$ of the trinification model must remain intact, while the left and right $\mathrm{SU}(3)$ product group should break to the electroweak sector of the SM. That is, the trinification gauge group should be broken as

$$\begin{array}{c} [\mathrm{SU}(3)_C \times \mathrm{SU}(3)_L \times \mathrm{SU}(3)_R] \\ \downarrow \\ [\mathrm{SU}(3)_C \times \mathrm{SU}(2)_L \times \mathrm{U}(1)_Y]. \end{array}$$

The spontaneous symmetry breaking of the trinification model is investigated in the following section.

¹An anomaly free theory is ensured when field representations under each $[\mathrm{SU}(3)]$ group add to one. For additional details on anomalies in gauge theories, see for example [9]

We further extend the model with a global $\{\text{SU}(3)_F\}$ family symmetry, such that

$$[\text{SU}(3)_C \times \text{SU}(3)_L \times \text{SU}(3)_R] \times \mathbb{Z}_3 \times \{\text{SU}(3)_F\}. \quad (2.2)$$

Inspired by supersymmetry, the family group is imposed in such a way that it acts on fermions and scalars equally. An extended supersymmetric version of the trinification model is proposed in [10].

When considering the full symmetry group, the proposed model originates as the natural reduction from a E_8 symmetry

$$E_8 \rightarrow E_6 \times \text{SU}(3).$$

An E_8 symmetry can be considered a low-energy remnant of the $E_8 \times E_8$ gauge group of the heterotic superstring theory proposed in [11], further motivating the inclusion of the global $\{\text{SU}(3)_F\}$ family symmetry in this model.

2.2 Field content

Under the symmetry group given in (2.2), scalars and fermions decompose into three matter fields, denoted by \tilde{L} , \tilde{Q}_L , \tilde{Q}_R and L , Q_L , Q_R respectively. There are eight gauge bosons for each $[\text{SU}(3)]$ group, expressed as G_C , G_L , and G_R . Both fermions and scalars in the model form bi-triplet representations under the trinification gauge group, and tri-triplets under the full symmetry group.

Throughout this work, we adopt a specific notation for fields. All fundamental representations are denoted with superscripts and anti-fundamental representations with subscripts. The indices i , l , r , c are used for family, left, right, and color charges respectively. Capitalized indices refer to representations in $\text{SU}(2)$ -space while lowercase indices refer to representations in $\text{SU}(3)$ -space [7]. The fields content and corresponding representations of the trinification model, are summarized in Table 1.

Because each scalar and fermion matter field is in a tri-triplet/singlet representation under the full symmetry group, we can illustrate each with a $3 \times 3 \times 3$ object. For simplicity we use 3×3 matrices, where the $[\text{SU}(3)_L]$ index, l , denotes the column, and the $[\text{SU}(3)_R]$ index, r , denotes the row. The family index is assigned to the matrix as a whole, and the color index is labeled on each matrix element separately. Using this notation, the scalar sector of the trinification model is denoted

$$(\tilde{L}^i)_r^l = \begin{pmatrix} \tilde{L}_1^1 & \tilde{L}_1^2 & \tilde{L}_1^3 \\ \tilde{L}_2^1 & \tilde{L}_2^2 & \tilde{L}_2^3 \\ \tilde{L}_3^1 & \tilde{L}_3^2 & \tilde{L}_3^3 \end{pmatrix}^i, \quad (\tilde{Q}_R^i)_c^r = \begin{pmatrix} (\tilde{Q}_R^i)_c^1 \\ (\tilde{Q}_R^i)_c^2 \\ (\tilde{Q}_R^i)_c^3 \end{pmatrix}^i, \quad (\tilde{Q}_L^i)_l^c = \left((\tilde{Q}_L^i)_1^c \quad (\tilde{Q}_L^i)_2^c \quad (\tilde{Q}_L^i)_3^c \right)^i, \quad (2.3)$$

where $i, c = \{1, 2, 3\}$.

Table 1: Field content and corresponding representations of the trinification model at GUT scale. Each index a takes on values from 1 to 8, while the indices i , l , r , and c take on values from 1 to 3. The model has 162 scalar field components, 81 (Weyl) fermions, and 24 gauge bosons.

		$SU(3)_C$	$SU(3)_L$	$SU(3)_R$	$\{SU(3)_F\}$	Notation
Scalars	\tilde{L}	1	3	$\bar{\mathbf{3}}$	3	$(\tilde{L}^i)_r^l$
	\tilde{Q}_L	3	$\bar{\mathbf{3}}$	1	3	$(\tilde{Q}_L^i)_l^c$
	\tilde{Q}_R	$\bar{\mathbf{3}}$	1	3	3	$(\tilde{Q}_R^i)_c^r$
Fermions	L	1	3	$\bar{\mathbf{3}}$	3	$(L^i)_r^l$
	Q_L	3	$\bar{\mathbf{3}}$	1	3	$(Q_L^i)_l^c$
	Q_R	$\bar{\mathbf{3}}$	1	3	3	$(Q_R^i)_c^r$
Gauge Bosons	G_C	8	1	1	1	G_C^a
	G_L	1	8	1	1	G_L^a
	G_R	1	1	8	1	G_R^a

Throughout this work, we will focus mainly on the scalar sector. At the trinification scale, however, fermions are organized in the same notation as (2.3). Fermions in the trinification model are left-handed Weyl fermions [7].

2.3 Lagrangian of the scalar sector

For the sake of this work, it is sufficient to consider the Lagrangian of the scalar sector. When we refer to the Lagrangian of the scalar sector, we refer to terms in the full Lagrangian which involve interactions with at least one scalar field. The Lagrangian of scalar sector of the trinification model consists of three essential parts: a gauge term, $\mathcal{L}_{\text{gauge}}$, which contains interactions between the three non-Abelian gauge fields and the scalars in the model, a Yukawa term, \mathcal{L}_Y , which contains interactions between fermion fields and scalars, and the classical scalar potential, $V^{(0)}$, which contains scalar self-interaction terms.

Interactions between gauge bosons and scalars are given by kinetic terms in the Lagrangian, such that

$$\mathcal{L}_{\text{gauge}} = [\mathcal{D}_\mu(\tilde{L}^i)_r^l][\mathcal{D}^\mu(\tilde{L}^i)_r^l]^\dagger + (\mathbb{Z}_3 \text{ permutations}), \quad (2.4)$$

with the covariant derivative given by

$$\mathcal{D}_\mu = \partial_\mu + igT_L^a G_{L\mu}^a - igT_R^a G_{R\mu}^a. \quad (2.5)$$

Here, g denotes the GUT scale gauge coupling, and the generators, T^a of each $[SU(3)]$ are defined $T^a = \frac{\lambda_a}{2}$, where λ_a are the eight Gell-Mann matrices [12].

Requiring the Lagrangian to be Lorentz invariant yields Yukawa interactions in the trification model of the form

$$\mathcal{L}_Y = -y\epsilon_{ijk}(\tilde{L}^i)_r^l(Q_L^j)_l^c(Q_R^k)_c^r + \text{c.c.} + (\mathbb{Z}_3 \text{ permutations}) \quad (2.6)$$

Here, the Levi-Cevita tensor is necessary for invariance under $\{\text{SU}(3)_F\}$.

Because the global family group acts on scalars and fermions equally, this is the only type of contraction which can form Yukawa terms in the trification model. Furthermore, invariance under cyclic \mathbb{Z}_3 permutations ensures that each permuted term of \mathcal{L}_Y will have the same coupling, y . This unification of the Yukawa coupling at GUT scale is a key feature of this model, and significantly reduces the number of free parameters in the theory [7]. As will become apparent in further sections, after spontaneous symmetry breaking of the trification model, the Lagrangian will contain many more Yukawa terms. Thus, the unified coupling, y , “splits” at the breaking scale, and we will study the RG evolution of these newly emerging couplings.

Finally, by enforcing the Lagrangian to be real, invariant, and renormalizable, the most general, classical scalar potential can be built out of three parts as follows [7]

$$V^{(0)} = V_1 + V_2 + V_3, \quad (2.7)$$

where

$$\begin{aligned} V_1 = & -\mu^2(\tilde{L}^i)_r^l(\tilde{L}_i^*)_l^r \\ & + \lambda_1 \left[(\tilde{L}^i)_r^l(\tilde{L}_i^*)_l^r \right]^2 \\ & + \lambda_2(\tilde{L}^i)_r^l(\tilde{L}^j)_{r'}^{l'}(\tilde{L}_j^*)_l^r(\tilde{L}_i^*)_{l'}^{r'} \\ & + \lambda_3(\tilde{L}^i)_r^l(\tilde{L}^j)_{r'}^{l'}(\tilde{L}_i^*)_{l'}^{r'}(\tilde{L}_j^*)_l^r \\ & + \lambda_4(\tilde{L}^i)_r^l(\tilde{L}^j)_{r'}^{l'}(\tilde{L}_j^*)_l^r(\tilde{L}_i^*)_{l'}^{r'} \\ & + (\mathbb{Z}_3 \text{ permutations}) \end{aligned} \quad (2.8)$$

$$\begin{aligned} V_2 = & +\alpha_1(\tilde{L}^i)_r^l(\tilde{L}_i^*)_l^r(\tilde{Q}_L^j)_l^c(\tilde{Q}_{Lj}^*)_c^{l'} \\ & +\alpha_2(\tilde{L}^i)_r^l(\tilde{L}_j^*)_l^r(\tilde{Q}_L^j)_l^c(\tilde{Q}_{Li}^*)_c^{l'} \\ & +\alpha_3(\tilde{L}^i)_r^l(\tilde{L}_i^*)_{l'}^r(\tilde{Q}_L^j)_l^c(\tilde{Q}_{Lj}^*)_c^{l'} \\ & +\alpha_4(\tilde{L}^i)_r^l(\tilde{L}_j^*)_{l'}^r(\tilde{Q}_L^j)_l^c(\tilde{Q}_{Li}^*)_c^{l'} \\ & + (\mathbb{Z}_3 \text{ permutations}) \end{aligned} \quad (2.9)$$

$$\begin{aligned} V_3 = & \gamma \epsilon_{ijk}(\tilde{L}^i)_r^l(\tilde{Q}_L^j)_l^c(\tilde{Q}_R^k)_c^r \\ & + \text{c.c.} \end{aligned} \quad (2.10)$$

Finally, in addition to the symmetries of (2.2), we can identify two accidental global $\text{U}(1)$ symmetries² of the Lagrangian, and denoted them by $\text{U}(1)_A$ and $\text{U}(1)_B$. This choice of labels

²Accidental symmetries arise from imposing gauge invariance and renormalizability of a theory. They are essential tools in BSM physics, because proposed extensions should either also contain the accidental symmetries of the SM Lagrangian, or, they have to be promoted to fundamental symmetries in the model's higher symmetry group [13].

is motivated by the identification of $\{U(1)_B\}$ symmetry as baryon conservation. The natural emergence of baryon conservation provides additional motivation for this trinification based GUT model. We will see that this symmetry remains intact as the trinification model is reduced to the SM throughout this work [7].

Including the accidental symmetries, the full symmetry group of the trinification model is given by

$$[SU(3)_C \times SU(3)_L \times SU(3)_R] \times \mathbb{Z}_3 \times \{SU(3)_F \times U(1)_A \times U(1)_B\}. \quad (2.11)$$

3 Spontaneous symmetry breaking in the trinification model

The next aim of this work is to investigate spontaneous symmetry breaking in the trinification model and obtain the resulting tree-level mass spectrum.

Spontaneous symmetry breaking occurs when a symmetry is valid for the Lagrangian of a system, but not for its (degenerate) ground state. In quantized theories, the ground state corresponds to the vacuum of the theory, and the expectation value of a field operator at the vacuum (VEV) can take on non-zero values [14]. Furthermore, the effects of quantum fluctuations on the vacuum state are studied using perturbation theory, such that the VEV of a field operator corresponds to its value at the minimum of the potential, plus higher order corrections [12]. The effects of such radiative corrections on the vacuum state of the theory will be revisited in later sections, through the formulation of the effective potential.

In this section, we investigate spontaneous symmetry breaking of the trinification model due to the classical (leading order) non-zero VEV of one of its scalar components.

3.1 Tree-level minimization conditions

In [7], it is argued that the simplest way to break the trinification model into a SM-like theory is when only one of its real scalar components obtains a non-zero VEV. More specifically, the color-singlet scalar, $(\tilde{L}^i)_r^l = (\tilde{L}^3)_3^3$, obtains the VEV, which we will see ensures the $[SU(3)_L]$, $[SU(3)_R]$, and $[SU(3)_F]$ symmetries of the trinification model are broken, while the $SU(3)_C$ gauge group remains intact.

Thus, in this scenario, a single VEV, v , is placed in real component of the $(\tilde{L}^3)_3^3$ scalar, such that

$$(\tilde{L}^3)_3^3 = \frac{1}{\sqrt{2}} \begin{pmatrix} 0 & 0 & 0 \\ 0 & 0 & 0 \\ 0 & 0 & v \end{pmatrix}^3. \quad (3.1)$$

Here, we have used the notation presented in (2.3).

More specifically, we define the VEV as

$$\langle (\tilde{L}^i)_r \rangle \equiv \delta_3^i \delta_3^l \delta_3^r \frac{v}{\sqrt{2}}. \quad (3.2)$$

The minimization condition of the model gives the conditions on a particular parameter of the theory for which the classical scalar potential, $V^{(0)}$, is ensured to have a local minimum at the VEV. We define

$$\frac{\partial V^{(0)}}{\partial \phi_i} = \Lambda_{(s)}^i, \quad (3.3)$$

and minimize this derivative in the vacuum state as

$$\Lambda_{(s)}^i \Big|_{\phi_i = \langle \phi_i \rangle} = \Lambda_{(s)}^i, \quad (3.4)$$

where

$$\langle \phi_i \rangle = \begin{cases} \frac{v^2}{\sqrt{2}} & \text{for } \phi_i = (\tilde{L}^3)_3^3 \\ 0 & \text{for } \phi_i = \text{other} \end{cases} \quad (3.5)$$

The requirement that $\Lambda_{(s)}^i = 0$ leads to the minimization condition

$$\mu^2 = (\lambda_1 + \lambda_2 + \lambda_3 + \lambda_4)v^2. \quad (3.6)$$

Finally, we must verify that the placement of a single VEV in the $(\tilde{L}^i)_r^l = (\tilde{L}^3)_3^3$ scalar indeed corresponds to a global minimum of the classical scalar potential. In [7], the homotopy continuation method³ is implemented to search for parameter space points for which the minimum of the scalar potential does not correspond to the VEV setting in (3.2). Of the performed random scan, all points had this scenario as a global minimum of $V^{(0)}$.

Throughout this work, we will continue to define the Λ -basis, as used above, as the gauge eigenbasis. It is constructed by taking direct n^{th} -order derivatives of the Lagrangian. Hereafter, a lower case label $t = \{s, f, g\}$, indicating scalars, fermions, or gauge bosons respectively, indicates a field dependent derivative. Capital labels $T = \{S, F, G\}$, refer to derivatives evaluated at the VEV.

3.2 Tree-level particle spectrum

Upon symmetry breaking, the particles in the model will acquire mass. Mass terms in the Lagrangian correspond to two-point self-interactions. Such terms are isolated by taking the second derivative of the Lagrangian with respect to desired field, and removing any other non-contributing n -point terms by setting all other fields to zero [12]. Throughout this section, we will outline the method used to find the physical masses of particles after spontaneous symmetry breaking, as well as define important notation used throughout the rest of this work.

³Homotopy continuation methods provide a useful approach to finding the zeros of a function in a globally convergent manner. A detailed discussion of this method can be found in [15].

3.2.1 Scalars

To obtain the classical scalar mass-squared matrix in Λ -basis, we take the second derivative to the scalar fields, such that

$$\frac{\partial^2 V^{(0)}}{\partial \phi_i \partial \phi_j} = \Lambda_{(s)}^{ij} \quad (3.7)$$

To isolate mass terms, all scalars with exception of the $(\tilde{L}^3)_3$ field are set to zero, such that

$$\Lambda_{(s)}^{ij} \Big|_{\phi_i = \langle \phi_i \rangle} = \Lambda_{(S)}^{ij}, \quad (3.8)$$

where, again, (3.5) holds.

Throughout this work, we define the λ -basis as the mass eigenbasis which diagonalizes the tree-level mass-squared matrices. To go from the gauge eigenbasis to the mass eigenbasis, scalar fields must be rotated by an orthogonal rotation matrix. The mass-squared matrix in the λ -basis is then found by taking the second derivative of the potential in terms of the rotated fields. Alternatively,

$$O_{(s)} \Lambda_{(s)}^{ij} O_{(s)}^\dagger = \lambda_{(s)}^{ij}, \quad (3.9)$$

where $\lambda_{(s)}^{ij}$ is the diagonal mass-squared matrix. Elements on the diagonal correspond to mass-squared eigenvalues of the scalar fields such that at tree-level

$$diag\{\lambda_{(s)}^{ij}\} = m_{(s)a}^2. \quad (3.10)$$

To eliminate μ^2 , we can insert the minimization condition of (3.6) into the mass matrix.

3.2.2 Fermions

Similarly, fermion masses are found by taking the second derivative of the Yukawa term of (2.6). However, due to the complex conjugate component, to ensure positive squared-masses the resulting matrix must be multiplied by its hermitian conjugate [8]. For convenience, upper case matrix indices $\{I, J\}$ to refer to fermions, while lower case indices remain for scalars. Thus,

$$\frac{\partial^2 \mathcal{L}_Y}{\partial \psi_I \partial \psi_J} = M^{IJ}, \quad (3.11)$$

and the classical fermion mass-squared matrix in the Λ -basis is given by

$$M^{*IK} M_K^J = \Lambda_{(f)}^{IJ}. \quad (3.12)$$

Again isolating mass terms by setting non-VEV acquiring fields to zero defines

$$\Lambda_{(f)}^{IJ} \Big|_{\phi_i = \langle \phi_i \rangle} = \Lambda_{(F)}^{IJ}, \quad (3.13)$$

Rotating by a diagonalizing unitary matrix gives

$$U_{(\text{F})} \Lambda_{(\text{F})}^{IJ} U_{(\text{F})}^\dagger = \lambda_{(\text{F})}^{IJ}, \quad (3.14)$$

and finally, just as before, physical masses are found as diagonal elements

$$\text{diag}\{\lambda_{(\text{F})}^{IJ}\} = m_{(\text{F})a}^2. \quad (3.15)$$

3.2.3 Gauge bosons

In theories with spontaneously broken continuous symmetries, a single massless scalar particle arises for each broken group generator. These so-called Goldstone bosons can be interpreted as the additional longitudinal degrees of freedom required to turn a massless gauge field into a massive spin-1 vector boson [14]. In this way, massive gauge bosons arise as a consequence of the acquisition of a non-zero VEV by one or more scalars in a theory.

The gauge boson masses are found, similarly to the scalars and fermions, by taking the second derivative of the scalar/boson interaction given in (2.4), with respect to each of the gauge fields, such that

$$\frac{\partial^2 \mathcal{L}_{\text{gauge}}}{\partial G_\mu^a \partial G_\nu^b} = \Lambda_{(\text{g})}^{ab}, \quad (3.16)$$

and again in the direction of the VEV,

$$\Lambda_{(\text{g})}^{ab} \Big|_{\phi_i = \langle \phi_i \rangle} = \Lambda_{(\text{G})}^{ab}. \quad (3.17)$$

The $\Lambda_{(\text{G})}^{ab}$ matrix is diagonalized and the mass eigenvalues are found as

$$O_{(\text{G})} \Lambda_{(\text{G})}^{ab} O_{(\text{G})}^\dagger = \lambda_{(\text{G})}^{ab}, \quad (3.18)$$

with again,

$$\text{diag}\{\lambda_{(\text{G})}^{ab}\} = m_{(\text{G})a}^2. \quad (3.19)$$

3.3 Breaking trinification symmetry

The breaking scheme of the trinification model describes how its symmetry group is broken by the VEV into the resulting new symmetry group. It is found by considering which group generators are (un)broken throughout spontaneous symmetry breaking.

Finding all the (un)broken generators and obtaining the full breaking scheme is an extensive calculation. In this section, we outline the general idea of the method used in this work, by considering only the gauge part of (2.11). The full set of calculations is included in Appendix A.

We examine the (un)broken gauge group generators in the trinification model. We will see that this leads to the following breaking scheme

$$\begin{aligned} & [\text{SU}(3)_C \times \text{SU}(3)_L \times \text{SU}(3)_R] \\ & \quad \downarrow \\ & [\text{SU}(3)_C \times \text{SU}(2)_L \times \text{SU}(2)_R \times \text{U}(1)_{L+R}] \end{aligned}$$

Unbroken generators correspond to those which leave the vacuum state invariant upon transformations, even after symmetry breaking [16]. We apply a infinitesimal gauge transformation on $(\tilde{L})_r^l$ such that⁴

$$\delta(\tilde{L})_r^l = \underbrace{i\omega_L^a (T_L^a)_{r'}^l (\tilde{L})_r^{l'}}_{\text{SU}(3)_L} - \underbrace{i\omega_R^a (T_R^a)_{r'}^r (\tilde{L})_r^l}_{\text{SU}(3)_R}, \quad (3.20)$$

where the minus sign comes from the fact that $(\tilde{L})_r^l$ is anti-fundamental in $[\text{SU}(3)_R]$. For reference, the Gell-Man matrices, given in Appendix B.

Then, the requirement for an unbroken generator becomes $\delta\langle(\tilde{L}^i)_r^l\rangle = 0$. Implementing (3.2) in to (3.20) yields

$$\delta\langle(\tilde{L}^i)_r^l\rangle = i\frac{v}{\sqrt{2}}\omega_L^a (T_L^a)_3^l \delta_r^3 - i\frac{v}{\sqrt{2}}\omega_R^a (T_R^a)_r^3 \delta_3^l, \quad (3.21)$$

where

$$\delta_j^i = \begin{cases} 1, & i = j \\ 0, & i \neq j \end{cases} \quad (3.22)$$

and equating this to zero gives the condition for unbroken gauge group generator as

$$0 = i\omega_L^a (T_L^a)_3^l \delta_r^3 - i\omega_R^a (T_R^a)_r^3 \delta_3^l. \quad (3.23)$$

Thus, for a gauge group generator to remain **unbroken**, it must satisfy the above relation.

We investigate for which generators this relation is satisfied. There are non-trivial results in three cases.

Case 1 : $r = 3, l \neq 3$ such that: $0 = i\omega_L^a (T_L^a)_3^l$

→ Choose $l = 1$ such that $(T_L^a)_3^1$.

In this case, there are non-trivial results for $a = 4, 5$ giving

$$\begin{aligned} (T^4)_3^1 &= \frac{(\lambda^4)_3^1}{2} = \frac{1}{2} \\ (T^5)_3^1 &= \frac{(\lambda^5)_3^1}{2} = \frac{i}{2} \end{aligned}$$

⁴This transformation does not act on the family (i) index. Thus, for convenience we leave this index off the field notations throughout this calculation.

Applying this, we obtain: $0 = -i(\omega_L^4 + i\omega_L^5)$. Thus,

$$i\omega_L^4 = \omega_L^5 \quad (3.24)$$

→ Choose $l = 2$ such that $(T_L^a)_3^2$.

In this case, there are non-trivial results for $a = 6, 7$ giving

$$\begin{aligned} (T^6)_3^2 &= \frac{(\lambda^6)_3^2}{2} = \frac{1}{2} \\ (T^7)_3^2 &= \frac{(\lambda^7)_3^2}{2} = \frac{i}{2} \end{aligned}$$

Applying this, we obtain: $0 = -i(\omega_L^6 + i\omega_L^7)$. Thus,

$$i\omega_L^6 = \omega_L^7 \quad (3.25)$$

Case 2 : $r \neq 3, l = 3$ such that: $0 = -i\omega_R^a (T_R^a)_r^3$.

Due to symmetry of the Gell-Mann matrices, this case yields the same results as in Case 1, such that

$$i\omega_R^4 = \omega_R^5, \quad i\omega_R^6 = \omega_R^7. \quad (3.26)$$

Case 3 : $r = 3, l = 3$ such that: $0 = i\omega_L^a (T_L^a)_3^3 - i\omega_R^a (T_R^a)_3^3$.

In this case there are non-trivial results for $a = 8$, such that

$$0 = i\omega_L^8 (T_L^8) - i\omega_R^8 (T_R^8). \quad (3.27)$$

Here, we see that under the condition

$$\omega_L^8 = \omega_R^8 \equiv \omega^8,$$

the generator

$$(T_L^8 - T_R^8)$$

can be an unbroken generator. For generality, we write this generator as $(T_L^8 + T_R^8)$, as it would appear for transformations of fundamental representations.

The $(T_L^8 + T_R^8)$ generator transforms fields as

$$(\tilde{L}^i)_r^l \longrightarrow e^{i\omega^8 (T_L^8 + T_R^8)} (\tilde{L}^i)_r^l \quad (3.28)$$

implying that it corresponds to a remaining $U(1)_{L+R}$ gauge symmetry.

In addition to breaking the trinification gauge group, the global symmetry group of the model will also undergo spontaneous symmetry breaking due to the non-zero VEV. Finding the unbroken generators and the new symmetry group is done in the same way as for the trinification gauge group. The full set of calculations for the breaking scheme can be found in Appendix A.

Combining all obtained algebraic results, the full breaking scheme of the trinification model as a result of the VEV in (3.1) can be written as

$$[SU(3)_C \times SU(3)_L \times SU(3)_R] \times \mathbb{Z}_3 \times \{SU(3)_F \times U(1)_A \times U(1)_B\}$$

↓

$$[SU(3)_C \times SU(2)_L \times SU(2)_R \times U(1)_{L+R}] \times \mathbb{Z}_2 \times \{SU(2)_F \times U(1)_X \times U(1)_Z \times U(1)_B\}$$

with the unbroken group generators

$$\begin{aligned} T_C^{1\dots 8} \quad , \quad T_L^{1\dots 3} \quad , \quad T_R^{1\dots 3} \quad , \quad T_F^{1\dots 3} \\ T_{L+R} \equiv \frac{2}{\sqrt{3}}(T_L^8 + T_R^8) \\ T_X \equiv \frac{2}{\sqrt{3}}(T_L^8 - T_R^8 - 2T_F^8) \\ T_Z \equiv \frac{2}{3}(T_A + \sqrt{3}T_F^8) \end{aligned}$$

Motivated by the apparent symmetry in left and right-space, we will refer to the trinification model after spontaneous symmetry break as the **Left-Right Symmetric Model** (LRSM), throughout the rest of this work.

3.4 Quantum numbers

Finally, we can determine the charges of fields under each symmetry group after spontaneous symmetry breaking. Due to the principles of charge conservation, knowing the quantum numbers of the obtained particles under each group is essential in determining the allowed interactions of the theory. These charges are found by applying the unbroken generators to the field components.

As obtaining the full set of quantum numbers of all the fields is mathematically extensive, the general method used is best illustrated through an example. As we will see in more detail in the following section, scalar fields will have a different representation once trinification has been broken. Recall from Section 2.2 that the field indices $\{i, l, r, c\}$ refer to representations in $SU(3)$ -space while $\{I, L, R, C\}$ refer to representations in $SU(2)$ -space.

3.4.1 Example: Color-singlet scalar: $U(1)_{L+R}$

Throughout this example, we find the charge of the leptonic scalar fields under the $U(1)_{L+R}$ gauge group of the LRSM.

The corresponding generator, as found in Section 3.3 is given by

$$T_{L+R} \equiv \frac{2}{\sqrt{3}}(T_L^8 + T_R^8).$$

Applying this to $(\tilde{L}^I)_R^L$ gives

$$T_{L+R}(\tilde{L}^I)_R^L = \left(\frac{2}{\sqrt{3}}\right)\left(\frac{1}{2}\right)\left[\lambda_L^8|_{L'}^R \delta_{r'}^R - \lambda_R^8|_{r'}^R \delta_{l'}^L\right](\tilde{L}^I)_R^L, \quad (3.29)$$

where, again, the minus sign comes from the fact that $(\tilde{L}^I)_R^L$ is anti-fundamental in $SU(2)_R$. Using λ^8 , given in Appendix B, it is clear that for any combinations of L, R where $L = R$, this expression reduces to

$$\begin{aligned} T_{L+R}(\tilde{L}^I)_R^L &= \left(\frac{2}{\sqrt{3}}\right)\left(\frac{1}{2}\right)\left[\left(\frac{1}{\sqrt{3}}\right) - \left(\frac{1}{\sqrt{3}}\right)\right](\tilde{L}^I)_R^L \\ &= 0 \end{aligned} \quad (3.30)$$

Due to the fact that $\lambda^8|_1^1 = \lambda^8|_2^2$, combinations where $L \neq R$ will also be 0, indicating that all field components of $(\tilde{L}^I)_R^L$ are uncharged under $U(1)_{L+R}$.

However, the corresponding $SU(2)_{L,R}$ -singlet states will be charged under this group. The charges for these states are found as

$$\begin{aligned} T_{L+R}(\tilde{L}^I)_R^3 &= \left(\frac{2}{\sqrt{3}}\right)\left(\frac{1}{2}\right)\left[\lambda_L^8|_3^3 \delta_{r'}^R - \lambda_R^8|_{r'}^R\right](\tilde{L}^I)_R^3 \\ &= \left(\frac{2}{\sqrt{3}}\right)\left(\frac{1}{2}\right)\left[\left(\frac{-2}{\sqrt{3}}\right) - \left(\frac{1}{\sqrt{3}}\right)\right](\tilde{L}^I)_R^3 \\ &= -(\tilde{L}^I)_R^3 \end{aligned} \quad (3.31)$$

$$\begin{aligned} T_{L+R}(\tilde{L}^I)_3^L &= \left(\frac{2}{\sqrt{3}}\right)\left(\frac{1}{2}\right)\left[\lambda_L^8|_{L'}^L - \lambda_R^8|_3^3 \delta_{l'}^L\right](\tilde{L}^I)_3^L \\ &= \left(\frac{2}{\sqrt{3}}\right)\left(\frac{1}{2}\right)\left[\left(\frac{1}{\sqrt{3}}\right) - \left(\frac{-2}{\sqrt{3}}\right)\right](\tilde{L}^I)_3^L \\ &= (\tilde{L}^I)_3^L \end{aligned} \quad (3.32)$$

In conclusion, the charge of color-singlet scalar under $U(1)_{L+R}$ is summarized as

Field Component	$\mathbf{U(1)}_{\mathbf{L+R}}$
$(\tilde{L}^I)_R^L$	0
$(\tilde{L}^I)_3^3$	0
$(\tilde{L}^I)_R^3$	-1
$(\tilde{L}^I)_3^L$	+1

Similarly, the charges of all field components under any of the symmetry groups of the model are found.

4 The left-right symmetric model

Throughout the previous chapter, spontaneous breaking of trinification due to the non-zero VEV of the $(\tilde{L}^3)_3^3$ scalar component was investigated. The resulting symmetry group of the LRSM was found to be

$$[\mathrm{SU}(3)_C \times \mathrm{SU}(2)_L \times \mathrm{SU}(2)_R \times \mathrm{U}(1)_{\mathbf{L+R}}] \times \{\mathrm{SU}(2)_F \times \mathrm{U}(1)_X \times \mathrm{U}(1)_Z \times \mathrm{U}(1)_B\}.$$

We are interested in determining whether the RG evolution of the LRSM can induce a second case of spontaneous symmetry breaking, such that this group is further broken down into the SM gauge group. Due to the large number of particles in the LRSM, calculating the full RG running is greatly simplified by constructing an appropriate effective field theory (EFT). In doing so, particles which are heavy compared to others can be integrated out, and we can focus on a low-energy limit of the LRSM alone.

Throughout this chapter, we first determine the tree-level particle mass spectrum using the method described in Section 3.2. Secondly, knowledge of the SM is used to construct a low-energy limit of the LRSM. This EFT becomes the model of interest when investigating radiative breaking to the SM.

4.1 The tree-level mass spectrum

The tree-level particle masses are obtained using `Mathematica`. The essential components of the trinification model are implemented, and the method described in Section 3.2 is applied to obtain the mass-squared eigenvalues in each sector.

4.1.1 Scalar masses

Upon breaking trinification, the scalar fields split from their tri-triplet representations into doublet and singlet states in $\mathrm{SU}(2)_{\mathbf{L,R,F}}$. This decomposition is given by [7]

$$\begin{aligned}
(\tilde{L}^i)_r^l = & \delta_I^i \left[\delta_L^l \delta_r^R (\tilde{L}^I)_R^L + \delta_L^l \delta_r^3 (\tilde{L}^I)_3^L + \delta_3^l \delta_r^R (\tilde{L}^I)_R^3 + \delta_3^l \delta_r^3 (\tilde{L}^I)_3^3 \right] \\
& + \delta_3^i \left[\delta_L^l \delta_r^R (\tilde{L}^3)_R^L + \delta_L^l \delta_r^3 (\tilde{L}^3)_3^L + \delta_3^l \delta_r^R (\tilde{L}^3)_R^3 + \delta_3^l \delta_r^3 (\tilde{L}^3)_3^3 \right],
\end{aligned} \tag{4.1}$$

$$(\tilde{Q}_L^i)_l^c = \delta_I^i \left[\delta_L^l (\tilde{Q}_L^I)_L^c + \delta_3^l (\tilde{Q}_L^I)_3^c \right] + \delta_3^i \left[\delta_L^l (\tilde{Q}_L^3)_3^c + \delta_3^l (\tilde{Q}_L^3)_L^c \right], \tag{4.2}$$

$$(\tilde{Q}_R^i)_c^r = \delta_I^i \left[\delta_R^r (\tilde{Q}_R^I)_c^R + \delta_3^r (\tilde{Q}_R^I)_c^3 \right] + \delta_3^i \left[\delta_R^r (\tilde{Q}_R^3)_c^R + \delta_3^r (\tilde{Q}_R^3)_c^3 \right]. \tag{4.3}$$

As mentioned in Section 3.2.3, each broken generator will lead to the emergence of one Goldstone boson which provides the additional longitudinal degree of freedom needed for one massive spin-1 vector boson. The breaking scheme found in Section 3.3 shows a reduction from 24 generators of the trinification gauge group, to 15 for the left-right symmetric gauge group. Thus, the LRSM will have nine massless scalar degrees of freedom, and consequently, nine massive vector bosons.

Similarly, the reduction from the ten generators of the global $\{\text{SU}(3)_F \times \text{U}(1)_A \times \text{U}(1)_B\}$ group, to the six generators of the $\{\text{SU}(2)_F \times \text{U}(1)_X \times \text{U}(1)_Z \times \text{U}(1)_B\}$ group, leads to four so-called global Goldstone bosons. These additional degrees of freedom are not absorbed by gauge bosons, but rather, remain as scalars in the model. In [7], it is shown that global Goldstones will decouple at energies much lower than the VEV. The consequence of this will become apparent in the following sections, when the effective theory is matched to the high-scale trinification model.

The obtained scalar tree-level mass-squared eigenvalues, as defined by (3.10), are summarized in Table 2. A name is assigned to each field for future reference throughout this work.

4.1.2 Fermion masses

Using the method in Section 3.2, it is clear that only fermions which couple to the $(\tilde{L}^3)_3^3$ scalar via the Yukawa term in (2.6) will obtain a mass after spontaneous symmetry breaking in the trinification model. This is because when taking the second derivative in the direction of the VEV only terms proportional to the VEV will be non-zero.

The only fields which satisfy this condition are the $(Q_L^I)_3^c$ and $(Q_R^I)_c^3$ fermion fields. Thus, these twelve fermions will obtain a mass at tree-level, and each of these are found to have the same mass-squared eigenvalue given by

$$m_{(F)}^2 = \frac{1}{2} y^2 v^2. \tag{4.4}$$

4.1.3 Gauge boson masses

As mentioned in Section 4.1.1, nine gauge fields will become massive vector bosons. Additionally, the LRSM will have 15 massless gauge fields corresponding to the

Table 2: The scalar particle content and corresponding mass-squared eigenvalues of the LRSM. Here, $(\tilde{Q}_{LR\pm}^I)^c \equiv \frac{1}{\sqrt{2}} [(\tilde{Q}_L^I)^c \pm \epsilon^{IJ} (\tilde{Q}_{RJ}^*)^c]$. The abbreviation ‘‘GS’’ refers the *Goldstone Boson*

	Name	Field	Mass ²
Color-Singlet Sector	\tilde{H}	$(\tilde{L}^I)_R^L$	$-(\lambda_2 + \lambda_3 + \lambda_4) v^2$
	\tilde{h}	$(\tilde{L}^3)_R^L$	$-(\lambda_3 + \lambda_4) v^2$
	\tilde{l}_R	$(\tilde{L}^I)_R^3$	$-(\lambda_2 + \lambda_3) v^2$
	\tilde{l}_L	$(\tilde{L}^I)_3^L$	$-(\lambda_2 + \lambda_4) v^2$
	$\tilde{\Phi}^s$	$\text{Re} \left[(\tilde{L}^3)_3^3 \right]$	$2(\lambda_1 + \lambda_2 + \lambda_3 + \lambda_4) v^2$
	$\tilde{\Phi}_{\text{Im}}^s$	$\text{Im} \left[(\tilde{L}^3)_3^3 \right]$	0
	\tilde{l}_R^s	$(\tilde{L}^3)_R^3$	0
	\tilde{l}_L^s	$(\tilde{L}^3)_3^L$	0
	$\tilde{\Phi}$	$(\tilde{L}^I)_3^3$	0 Global GS
Colored Sector	\tilde{Q}_L	$(\tilde{Q}_L^I)_L^c$	$\frac{1}{2}[\alpha_1 - 2(\lambda_1 + \lambda_2 + \lambda_3 + \lambda_4)] v^2$
	\tilde{Q}_R	$(\tilde{Q}_R^I)_c^R$	$\frac{1}{2}[\alpha_1 - 2(\lambda_1 + \lambda_2 + \lambda_3 + \lambda_4)] v^2$
	\tilde{Q}_{LR}	$(\tilde{Q}_{LR\pm}^I)^c$	$\frac{1}{2}[(\alpha_1 + \alpha_3 \pm \frac{\gamma}{\sqrt{2}v}) - 2(\lambda_2 + \lambda_3 + \lambda_4)] v^2$
	\tilde{Q}_L^s	$(\tilde{Q}_L^3)_L^c$	$\frac{1}{2}[(\alpha_1 + \alpha_2) - 2(\lambda_1 + \lambda_2 + \lambda_3 + \lambda_4)] v^2$
	\tilde{Q}_R^s	$(\tilde{Q}_R^3)_c^R$	$\frac{1}{2}[(\alpha_1 + \alpha_2) - 2(\lambda_1 + \lambda_2 + \lambda_3 + \lambda_4)] v^2$
	$(\tilde{Q}_L^s)_s$	$(\tilde{Q}_L^3)_3^c$	$\frac{1}{2}[(\alpha_1 + \alpha_2 + \alpha_3 + \alpha_4) - 2(\lambda_1 + \lambda_2 + \lambda_3 + \lambda_4)] v^2$
	$(\tilde{Q}_R^s)_s$	$(\tilde{Q}_R^3)_c^3$	$\frac{1}{2}[(\alpha_1 + \alpha_2 + \alpha_3 + \alpha_4) - 2(\lambda_1 + \lambda_2 + \lambda_3 + \lambda_4)] v^2$

$$[\text{SU}(3)_C \times \text{SU}(2)_L \times \text{SU}(2)_R \times \text{U}(1)_{L+R}]$$

gauge group, which remains intact after spontaneous symmetry breaking.

The resulting tree-level mass-squared eigenvalues of the gauge bosons in the LRSM are found to be

$$m^2_{(G_R^{4\dots 7}, G_L^{4\dots 7})} = \frac{1}{4}g^2v^2 \quad , \quad m^2_{(\frac{1}{\sqrt{2}}[G_L^8 - G_R^8])} = \frac{2}{3}g^2v^2. \quad (4.5)$$

4.1.4 Parameter constraints of the LRSM

We can use the obtained expressions of the tree-level particle masses to conclude that the LRSM is fully described by the parameter space

$$\mathcal{P}_{\text{LRSM}}^{(\text{HS})} = \{\lambda_{1\dots 4}, \alpha_{1\dots 4}, \gamma, y, g, v\}. \quad (4.6)$$

Here, the (HS) label refers to ‘‘high-scale’’, and is included to distinguish this parameter space from that of the low-scale effective LRSM, which is constructed in the following section.

Furthermore, we can formulate an essential set of constraints on these parameters by requiring that the mass-squared matrix of each sector be positive definite. This ensures the positiveness of the mass-squared eigenvalue of each particle. This requirement places significant constraints on the parameter space.

In the scalar sector, the requirement that $m_{(S)}^2 > 0$ leads to the following set of constraints:

$$\begin{aligned}
(\lambda_2 + \lambda_3 + \lambda_4) &\leq 0 & \alpha_1 &\geq 2(\lambda_1 + \lambda_2 + \lambda_3 + \lambda_4) & (4.7) \\
(\lambda_2 + \lambda_3) &\leq 0 & (\alpha_1 + \alpha_2) &\geq 2(\lambda_1 + \lambda_2 + \lambda_3 + \lambda_4) \\
(\lambda_2 + \lambda_4) &\leq 0 & (\alpha_1 + \alpha_3) - \frac{|\gamma|}{\sqrt{2}v} &\geq 2(\lambda_1 + \lambda_2 + \lambda_3 + \lambda_4) \\
(\lambda_3 + \lambda_4) &\leq 0 & (\alpha_1 + \alpha_2 + \alpha_3 + \alpha_4) &\geq 2(\lambda_1 + \lambda_2 + \lambda_3 + \lambda_4)
\end{aligned}$$

Additionally, the requirement that $\mu^2 > 0$, needed to break trinification, automatically implies that

$$(\lambda_1 + \lambda_2 + \lambda_3 + \lambda_4) > 0, \quad (4.8)$$

through the minimization condition given in (3.6).

The requirements that $m_{(F)}^2 > 0$ and $m_{(G)}^2 > 0$ do not place any additional constraints on the parameter space, as y and g enter the fermion and gauge boson masses quadratically.

Only parameter space points of $\mathcal{P}_{\text{LRSM}}^{(\text{HS})}$ satisfying the conditions in (4.7) will constitute physical particle masses for the LRSM.

4.2 The low-energy effective theory

Throughout the rest of this work, we wish to investigate the radiative breaking of the LRSM to a SM-like theory. As can be seen from Table 2, the model contains many massive scalars which can be grouped into twelve matter fields, greatly increasing the number of parameters in the full Lagrangian of the LRSM from that of the unbroken trinification model in (2.7). All of these parameters will run as a function of the energy scale in the RG evolution of the model.

To simplify the investigation, we create an appropriate EFT as a low-energy limit of the LRSM, by integrating out heavy scalars at the spontaneous symmetry breaking scale⁵. Essentially, this implies that we remove any particles from the theory which are too heavy to be produced at lower energies. More specifically, we can discard particles from our theory if their mass is of the order of the renormalization scale [17]. Once heavy particles are integrated out, the resulting Lagrangian of the low-scale theory is matched to the original high-scale Lagrangian. In this way, the low-scale parameters are expressed in terms of high-scale counterparts, and the RG evolution can be studied with significantly fewer fields.

4.2.1 Constructing an appropriate effective theory

As such, the next aim of this work is to create an appropriate low-energy effective LRSM. We begin by applying knowledge of the SM gauge group and phenomenology to engineer a EFT. We choose its features such that it will provide a radiative origin for a model which best fits the SM. We then examine the scalar hierarchy at the trinification breaking scale to determine if our choice of EFT is physically viable.

In [7] it is shown that an EFT consisting of the \tilde{h} and \tilde{l}_R scalars, as defined in Table 2, can undergo radiative breaking to a SM-like theory. This choice of EFT is justified by showing that physically viable parameter space points can be found such that these fields are light

⁵In fact, the construction of an appropriate EFT is needed in order to deal with ultraviolet divergences, and as such, provides a number of additional key advantages for the investigation. For instance, going to the EFT changes the running of coupling constants from a logarithmic dependence on the masses of heavy particles, to a logarithmic energy scale dependence. Such details of renormalization theory and EFT's are beyond the scope of this work, but can be found in, for example, [17].

compared to all other scalars.

It is further shown that in addition to successfully yielding the gauge group of the SM, spontaneous symmetry breaking induced by the running of this EFT, leads to massive particles which can be identified with certain heavy SM quarks. However, it fails to break family symmetry in such a way that non-zero tree-level masses for lighter quarks and color neutral fermions arise naturally [7].

Thus, throughout this work, we propose an upgraded EFT. The proposed EFT will aim to keep the \tilde{l}_R field light, and in addition, include the color-singlet Higgs tri-doublet \tilde{H} field, instead of \tilde{h} . The choice of this particular combination can be motivated by several arguments.

First and foremost, keeping the \tilde{l}_R field is motivated by the need to ensure that the SM gauge group will arise from spontaneous symmetry breaking. This means preserving $[\text{SU}(3)_C]$, and breaking $[\text{SU}(2)_L \times \text{SU}(2)_R \times \text{U}(1)_{L+R}]$ into the electroweak sector. Furthermore, we need to break the global $\{\text{SU}(2)_F\}$ group, which is also not present in the SM. The \tilde{l}_R field is a singlet in C and L-space, and thus, if one of its field components acquires a non-zero VEV, it can lead to this desired breaking scheme.

Secondly, our choice to keep the \tilde{H} field can be motivated as follows. When spontaneous symmetry breaking is induced, this field will decompose in a similar way as in (4.1). We predict that the splitting of this field will yield particles which form viable SM Higgs doublet candidates. In [7], it is argued that if we can again integrate out heavy particles at this stage, the resulting effective theory can acquire VEVs which can be identified as the SM-breaking Higgs VEVs. Upon breaking, this gives promising predictions for the masses of W^\pm and Z^0 gauge bosons, the quark hierarchy, and the CKM mixing of the SM.

Finally, it should be noted that the global Goldstone field, $\tilde{\Phi}$, must also remain in the particle content of our proposed EFT. It is massless, but unlike the Goldstone bosons arising from broken gauge group generators, it is not absorbed by a massive gauge boson.

All other scalars are integrated out, that is, their masses are required to be of the order of the VEV, v . Finally, the scalar particle content of our proposed EFT is summarized as

$$\begin{aligned}\tilde{H} &= (\tilde{L}^I)_R^L \\ \tilde{l}_R &= (\tilde{L}^I)_R^3 \\ \tilde{\Phi} &= (\tilde{L}^I)_3^3.\end{aligned}\tag{4.9}$$

Before continuing, we must determine if this proposed effective LRSM is physically permitted by the scalar mass hierarchy. That is, we must be able to find parameter space points of $\mathcal{P}_{\text{LRSM}}^{(\text{HS})}$ such that the \tilde{H} and \tilde{l}_R scalars are light, while the other scalars have masses $\mathcal{O}(v)$. For this, we define the parameter constraints which must be satisfied by such a point.

4.2.2 Constraints of the effective LRSM

To further investigate the viability of the proposed effective LRSM, the following parametrization is introduced

$$\begin{aligned} m_{\tilde{H}}^2 &\equiv -(\lambda_2 + \lambda_3 + \lambda_4)v^2 \equiv \xi v^2 \\ m_{\tilde{R}}^2 &\equiv -(\lambda_2 + \lambda_3)v^2 \equiv \delta v^2, \end{aligned} \tag{4.10}$$

such that

$$\begin{aligned} \xi &= -\lambda_2 - \lambda_3 - \lambda_4 \\ \delta &= -\lambda_2 - \lambda_3. \end{aligned} \tag{4.11}$$

The low energy EFT is then further constructed under the requirement that

$$\delta \ll 1, \quad \xi \ll 1, \tag{4.12}$$

while the mass-squared eigenvalues of the \tilde{h} and \tilde{l}_L fields (denoted $m_{\tilde{h}}^2$, $m_{\tilde{L}}^2$ hereafter) should be large. This adds the following constraints

$$-\lambda_3 - \lambda_4 = \mathcal{O}(1), \quad -\lambda_2 - \lambda_4 = \mathcal{O}(1). \tag{4.13}$$

To justify the proposed effective LRSM as a physically viable EFT, parameter space points must exist which satisfy all of the conditions imposed above.

4.2.3 Discussion of the effective LRSM at tree-level

Upon close consideration of the constraints above, it can be concluded that we cannot impose the \tilde{H} and \tilde{l}_R fields to be light compared to others at tree-level. This can be seen directly by using the masses in Table 2, and re-writing

$$m_{\tilde{H}}^2 = \frac{1}{2} (m_{\tilde{h}}^2 + m_{\tilde{L}}^2 + m_{\tilde{R}}^2) \tag{4.14}$$

There is no construction in which $m_{\tilde{H}}^2 \ll m_{\tilde{h}}^2, m_{\tilde{L}}^2$. Thus, taking \tilde{H} to be light automatically enforces that other color-singlet scalars be kept light as well.

This conclusion, however, does not hold for the $\tilde{\Phi}^s$ state. As can be seen in Table 2, this field has a mass dependent on λ_1 . Thus, it can be integrated out by tuning λ_1 to ensure a large mass in comparison to other scalars. Similarly, we can integrate out all scalars in the colored sector, as their masses can be fully tuned by values of $\alpha_{1\dots 4}$.

At this point we can conclude that the proposed effective LRSM does not constitute a viable EFT as desired. Although we can impose the desired hierarchy between scalars in the colored and color-singlet sector, as well as integrate out one heavy scalar, $\tilde{\Phi}^s$, we cannot tune the masses in such a way that $m_{\tilde{H}}^2, m_{\tilde{R}}^2 \ll m_{\tilde{h}}^2, m_{\tilde{L}}^2$.

This conclusion holds when considering tree-level masses only. Thus, at this stage, it becomes significant to hypothesize about the possibility of observing the desired splitting in scalar mass hierarchy upon inclusion of one-loop mass corrections. At one loop, masses of the color-singlet scalars will depend on $\{g, y, \gamma\}$, as well as higher orders of these parameters, in addition to $\{\lambda_{1\dots 4}, v\}$. This suggests that one-loop effects could affect the hierarchy significantly, justifying the choice of light fields in the effective LRSM after all. With this motivation, obtaining the full one-loop scalar mass spectrum for the LRSM becomes an essential component of this work.

However, obtaining this mass spectrum is extensive work. Thus, before embarking on this task, it is well worth investigating whether the effective LRSM successfully breaks to a SM-like theory, as was hypothesized in the previous section, to begin with. If radiative breaking to a theory with desirable SM properties is naturally found in the proposed effective LRSM, then it becomes essential to investigate whether the correct mass hierarchy can be obtained upon inclusion of one-loop corrections.

Thus, this work is continued under the assumption that the proposed effective LRSM can in fact exist as a physical low-energy limit of the trinification model, and its RG evolution is investigated.

4.2.4 Field content and effective Lagrangian

Under this assumption, we continue to construct the effective LRSM. As mentioned, we integrate out all scalars apart from the \tilde{H} , \tilde{l}_R , and $\tilde{\Phi}$ states.

Furthermore, in the fermion sector, the heavy Dirac fermions are also integrated out. From Section 4.1.2, these correspond to the $(Q_L^f)_3^c$ and $(Q_R^f)_c^3$ fields.

Similarly, the heavy massive gauge bosons are integrated out, such that only the gauge fields of the remaining symmetry group are kept in the effective LRSM.

The total particle content of the effective LRSM is given in Table 3. The charges of fields under each symmetry group, found with the method described in Section 3.4, are also listed, such that the allowed interactions can be investigated, and with this, an effective Lagrangian can be written.

The fermion Lagrangian is found by writing all possible combinations of scalars and fermions considering the fact that charges must be conserved for each term. Thus, we write

Table 3: The total particle content of the effective LRSM.

Name	Field	SU(3) _C	SU(2) _L	SU(2) _R	U(1) _{L+R}	{SU(2) _F }	{U(1) _X }	{U(1) _Z }	{U(1) _B }
Scalars									
\tilde{H}	$(\tilde{L}^I)_R^L$	1	2	$\bar{\mathbf{2}}$	0	2	0	+1	0
\tilde{l}_R	$(\tilde{L}^I)_R^3$	1	1	$\bar{\mathbf{2}}$	-1	2	-1	+1	0
$\tilde{\Phi}$	$(\tilde{L}^I)_3^3$	1	1	1	0	2	-2	+1	0
Fermions									
H	$(L^I)_R^L$	1	2	$\bar{\mathbf{2}}$	0	2	0	+1	0
l_L	$(L^I)_3^L$	1	2	1	+1	2	-1	+1	0
l_R	$(L^I)_R^3$	1	1	$\bar{\mathbf{2}}$	-1	2	-1	+1	0
Φ	$(L^I)_3^3$	1	1	1	0	2	-2	+1	0
H^s	$(L^3)_R^L$	1	2	$\bar{\mathbf{2}}$	0	1	+2	0	0
l_L^s	$(L^3)_3^L$	1	2	1	+1	1	+1	0	0
l_R^s	$(L^3)_R^3$	1	1	$\bar{\mathbf{2}}$	-1	1	+1	0	0
Φ^s	$(L^3)_3^3$	1	1	1	0	1	0	0	0
Q_L	$(Q_L^I)_L^c$	3	$\bar{\mathbf{2}}$	1	-1/3	2	-1	0	+1/3
Q_L^s	$(Q_L^3)_L^c$	3	$\bar{\mathbf{2}}$	1	-1/3	1	+1	-1	-1/3
\mathcal{D}_L^s	$(Q_L^3)_3^c$	3	1	1	+2/3	1	+2	-1	+1/3
Q_R	$(Q_R^I)_c^R$	$\bar{\mathbf{3}}$	1	2	+1/3	2	-1	0	-1/3
Q_R^s	$(Q_R^3)_c^R$	$\bar{\mathbf{3}}$	1	2	-1/3	1	+1	-1	-1/3
\mathcal{D}_R^s	$(Q_R^3)_c^3$	$\bar{\mathbf{3}}$	1	1	-2/3	1	+2	-1	+1/3
Gauge Bosons									
G_C	G_C^α	8	1	1	0	1	0	0	0
G_L	G_L^α	1	3	1	0	1	0	0	0
G_R	G_R^α	1	1	3	0	1	0	0	0
G_{L+R}	$\frac{1}{\sqrt{2}}(G_L^8 + G_R^8)$	1	1	1	0	1	0	0	0

$$\begin{aligned}
\mathcal{L}_{\text{F(LRSM)}} = & Y_\alpha (\tilde{H}_I^*)_L^R (H^I)_R^L (\Phi^s) & + Y_\theta (\tilde{H}_I^*)_L^R (Q_L^I)_L^c (Q_R^s)_c^{R'} \epsilon^{LL'} \epsilon_{RR'} \\
& + Y_\beta (\tilde{H}_I^*)_L^R (H^s)_R^L (\Phi^I) & + Y_\kappa (\tilde{l}_{RI}^*)^R (l_R^I)_R (\Phi^s) \\
& + Y_\gamma (\tilde{H}_I^*)_L^R (l_L^I)^L (l_R^I)_R & + Y_\lambda (\tilde{l}_{RI}^*)^R (l_R^s)_R (\Phi^I) \\
& + Y_\delta (\tilde{H}_I^*)_L^R (l_L^I)^L (l_R^s)_R & + Y_\mu (\tilde{l}_R^I)_R (D_L^s)^c (Q_R^J)_c^R \epsilon_{IJ} \\
& + Y_\epsilon (\tilde{H}^I)_R^L (Q_L^s)_L^c (Q_R^J)_c^R \epsilon_{IJ} & + Y_\nu (\tilde{l}_{RI}^*)^R (H^I)_R^L (l_L^s)^L \epsilon_{LL'} \\
& + Y_\zeta (\tilde{H}^I)_R^L (Q_L^J)_L^c (Q_R^s)_c^R \epsilon_{IJ} & + Y_\pi (\tilde{l}_{RI}^*)^R (H^s)_R^L (l_L^I)^L \epsilon_{LL'} \\
& + Y_\eta (\tilde{H}_I^*)_L^R (Q_L^s)_L^c (Q_R^I)_c^{R'} \epsilon^{LL'} \epsilon_{RR'} & + Y_\tau (\tilde{\Phi}_I^*) (\Phi^I) (\Phi^s) \\
& + \frac{m_{\Phi^s}^2}{2} \Phi^s \Phi^s & \\
& + \text{c.c.} &
\end{aligned} \tag{4.15}$$

Here, a Majorana mass term for the Φ^s state arises. For the sake of this work, this term is not very significant. However, as we will see in the following section, $m_{\Phi^s}^2$ will run as a function

of energy, and the RG equations of the other parameters will depend on it.

As predicted, we see that the single unified Yukawa coupling, y , present in the trinification Lagrangian prior to spontaneous symmetry breaking, has split into 14 parameters, $Y_{\alpha\dots\tau}$. The unification of the Yukawa coupling at GUT scale is a unique feature of this model arising as a consequence of the global $\{SU(3)_F\}$ symmetry, and, as discussed in Section 2, significantly reduces the number of parameters in the LRSM.

Next, a scalar potential for the effective LRSM can be carefully constructed using the results in Table 3. Requiring the Lagrangian be real, renormalizable, and Lorentz invariant lets us write a possible most general scalar potential as

$$\begin{aligned}
V_{(\text{LRSM})}^{(0)} = & m_{\tilde{H}}^2 |\tilde{H}|^2 + m_{\tilde{R}}^2 |\tilde{l}_R|^2 + m_{\tilde{\Phi}}^2 |\tilde{\Phi}|^2 \\
& + \lambda_a |\tilde{H}|^4 + \lambda_b |\tilde{l}_R|^4 + \lambda_c |\tilde{\Phi}|^4 \\
& + \lambda_d |\tilde{H}|^2 |\tilde{l}_R|^2 + \lambda_e |\tilde{H}|^2 |\tilde{\Phi}|^2 + \lambda_f |\tilde{l}_R|^2 |\tilde{\Phi}|^2 \\
& + \lambda_g (\tilde{l}_{R1}^{I1})_{R1} (\tilde{l}_{R2}^*)_{R2}^{R2} (\tilde{l}_{R1}^{I1})_{R1'} (\tilde{l}_{R2}^*)_{R2'}^{R2'} \epsilon_{I1I1'} \epsilon^{I2I2'} \epsilon_{R2R2'} \epsilon^{R1R1'} \\
& + \lambda_h (\tilde{H}^{I1})_{R1}^L (\tilde{H}^*)_{R2}^{R2} (\tilde{H}^{I1})_{R1'}^L (\tilde{H}^*)_{R2'}^{R2'} \epsilon_{I1I1'} \epsilon^{I2I2'} \epsilon_{R2R2'} \epsilon^{R1R1'} \\
& + \lambda_i (\tilde{H}^{I1})_{R1}^{L1} (\tilde{H}^*)_{R2}^R (\tilde{H}^{I1})_{R1'}^{L1} (\tilde{H}^*)_{R2'}^R \epsilon_{I1I1'} \epsilon^{I2I2'} \epsilon_{L1L1'} \epsilon^{L2L2'} \\
& + \lambda_j (\tilde{H}^I)_{R1}^{L1} (\tilde{H}^*)_{R2}^{R2} (\tilde{H}^I)_{R1'}^{L1} (\tilde{H}^*)_{R2'}^{R2'} \epsilon_{L1L1'} \epsilon^{L2L2'} \epsilon_{R2R2'} \epsilon^{R1R1'} \\
& + \lambda_k (\tilde{l}_{R1}^{I1})_R (\tilde{l}_{R2}^*)^R (\tilde{\Phi}^{I1}) (\tilde{\Phi}^*)_{I2'} \epsilon_{I1I1'} \epsilon^{I2I2'} \\
& + \lambda_l (\tilde{H}^{I1})_R^L (\tilde{H}^*)_{R2}^R (\tilde{\Phi}^{I1}) (\tilde{\Phi}^*)_{I2'} \epsilon_{I1I1'} \epsilon^{I2I2'} \\
& + \lambda_m (\tilde{H}^{I1})_R^L (\tilde{H}^*)_{R2}^R (\tilde{l}_{R1}^{I1})_R (\tilde{l}_{R2}^*)^R \epsilon_{I1I1'} \epsilon^{I2I2'} \\
& + \lambda_n (\tilde{H}^I)_{R1}^L (\tilde{H}^*)_{R2}^{R2} (\tilde{l}_{R1}^I)_{R1'} (\tilde{l}_{R2}^*)_{R2'}^{R2'} \epsilon_{R2R2'} \epsilon^{R1R1'} \\
& + \lambda_o (\tilde{H}^{I1})_{R1}^L (\tilde{H}^*)_{R2}^{R2} (\tilde{l}_{R1}^{I1})_{R1'} (\tilde{l}_{R2}^*)_{R2'}^{R2'} \epsilon_{I1I1'} \epsilon^{I2I2'} \epsilon_{R2R2'} \epsilon^{R1R1'}.
\end{aligned} \tag{4.16}$$

From these results, we can summarize the free parameters of the effective LRSM in a (low-scale) parameter space. Since the mass-squared of the global Goldstone, $m_{\tilde{\Phi}}^2$, is zero, we exclude it as a free parameter. With this in mind, we can write

$$\mathcal{P}_{\text{LRSM}}^{(\text{LS})} = \{\lambda_{a\dots o}, Y_{\alpha\dots\tau}, m_{\tilde{H}}^2, m_{\tilde{R}}^2, m_{\tilde{\Phi}^s}^2\}. \tag{4.17}$$

With the effective LRSM fully constructed, the next aim of this work is to investigate the RG evolution of its parameters. For this, the Lagrangian of the effective LRSM is matched to the high-scale trinification model at the renormalization scale at which heavy particles are integrated out. The free parameters of the low-scale Lagrangian, $\mathcal{P}_{\text{3HDM}}^{(\text{LS})}$, can then be written in terms of those existing in the high-scale theory, $\mathcal{P}_{\text{LRSM}}^{(\text{HS})}$. These expressions will be used as the initial conditions for the running of model parameters.

4.3 Tree-level matching conditions

Classically, the matching conditions are found by equating tree-level diagrams at the breaking scale. As heavy states are integrated out at this energy, the high-scale theory can contain interactions with particles which are not present in the low-scale theory. Thus, the matching is done by identifying such interactions, and equating n -point functions between the two theories. Any contributions existing in both theories can be excluded, as they cancel out upon matching. The matching is done in the zero-external momentum approximation, because the masses of any propagators will be heavy compared to particles on the diagram legs [18].

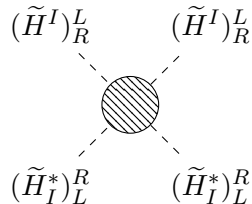
In the Yukawa sector, the tree-level matching conditions are obtained straightforwardly by direct comparison of the Lagrangian of (2.6) and (4.15). Only three low scale Yukawa couplings will have non zero values in terms of the high scale parameters. The results are listed in Section 4.3.2.

Obtaining the full set of matching conditions in the scalar sector involves extensive calculations. The general method used throughout this work is illustrated in this section with a single example.

4.3.1 Example: Tree-level matching conditions for $(\tilde{H}\tilde{H}^*\tilde{H}\tilde{H}^*)$

Consider the 4-point self-interaction term of the Higgs tri-doublet, $\tilde{H}\tilde{H}^*\tilde{H}\tilde{H}^*$, in the low-scale theory. For this field we adopt the notation $(\tilde{H}^I)_R^L$ and $(\tilde{H}_I^*)_L^R$.

The Feynman diagram of this interaction vertex in the low-scale theory is given by



In the high-scale theory, the diagrams of this interaction are formed using Table 2. By enforcing charge conservation in each vertex point, it is clear that the $\tilde{\Phi}^s$ field is the only scalar existing in the high-scale theory that can act as a propagator in tree-level diagrams. Thus, in the high-scale theory we must consider the $\tilde{\Phi}^s\tilde{H}\tilde{H}^*$ vertex, and, consequently, the corresponding t and s -channel tree-level diagrams.

Fermions cannot act as propagators in this interaction, since there are no such tri-linear scalar/fermion terms in the Lagrangian. Gauge boson propagators can form interaction vertices with two incoming scalars. However, by expanding $\mathcal{L}_{\text{gauge}}$ in (2.4), it is clear that these are derivative couplings, and will therefore not contribute in the zero external momentum approximation.

Thus, the matching of this term between the low and high scale theories is illustrated in Figure 1.

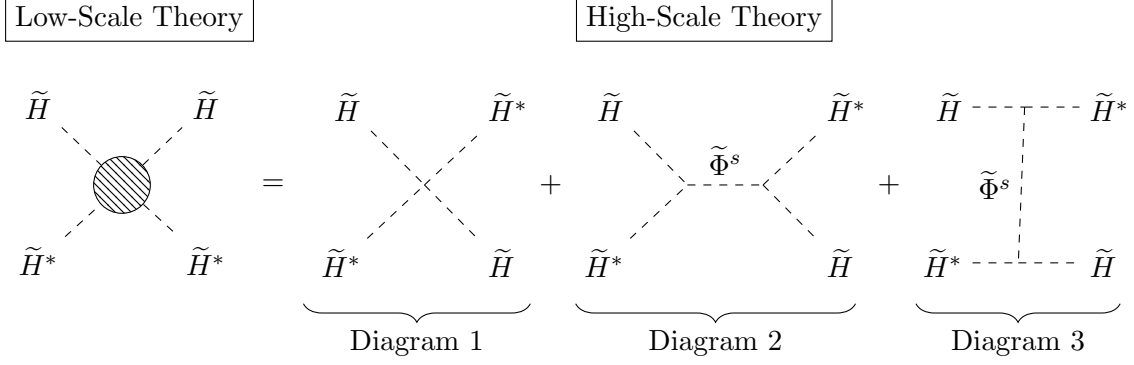


Figure 1: Illustration of matching conditions at the breaking scale. In the high-scale theory, three diagrams contribute.

For the vertex of the diagram in the low-scale theory on the left-hand side of Figure 1, the scalar Lagrangian of (4.16) gives four contributing terms:

$$\begin{aligned}
 V_{(\text{LRSM})}^{(0)} \supset \lambda_a |\tilde{H}|^4 & \quad (4.18) \\
 \lambda_h (\tilde{H}^{I_1})_{R_1}^L (\tilde{H}^{*I_2})_{L_2}^{R_2} (\tilde{H}^{I_1'})_{R_1'}^L (\tilde{H}^{*I_2'})_{L_2'}^{R_2'} \epsilon_{I_1 I_1'} \epsilon^{I_2 I_2'} \epsilon_{R_2 R_2'} \epsilon^{R_1 R_1'} & \\
 \lambda_i (\tilde{H}^{I_1})_R^{L_1} (\tilde{H}^{*I_2})_{L_2}^R (\tilde{H}^{I_1'})_{R_1'}^{L_1'} (\tilde{H}^{*I_2'})_{L_2'}^R \epsilon_{I_1 I_1'} \epsilon^{I_2 I_2'} \epsilon_{L_1 L_1'} \epsilon^{L_2 L_2'} & \\
 \lambda_j (\tilde{H}^I)_{R_1}^{L_1} (\tilde{H}^{*I})_{L_2}^{R_2} (\tilde{H}^I)_{R_1'}^{L_1'} (\tilde{H}^{*I})_{L_2'}^{R_2'} \epsilon_{L_1 L_1'} \epsilon^{L_2 L_2'} \epsilon_{R_2 R_2'} \epsilon^{R_1 R_1'} & .
 \end{aligned}$$

We can choose a specific combination of fields, such that we limit ourselves to consider a single coupling at a time. For instance, taking the field combination, $(\tilde{H}^1)_1^1 (\tilde{H}^{*1})_1^1 (\tilde{H}^1)_1^1 (\tilde{H}^{*1})_1^1$, limits us to examine only the first term of (4.18), as the other three are zero for this combination of indices. Thus, the vertex for the interaction of this specific choice of fields, is given by

$$\begin{array}{ccc}
 (\tilde{H}^1)_1^1 & & (\tilde{H}^1)_1^1 \\
 & \diagdown & / \\
 & \text{---} & \text{---} \\
 & \diagup & \diagdown \\
 (\tilde{H}^{*1})_1^1 & & (\tilde{H}^{*1})_1^1
 \end{array}
 = -4i\lambda_a$$

where the factor of four is added in to account for the combinatorics of the four indistinguishable fields.

We now examine the three contributing high-scale diagrams of Figure 1 separately.

Diagram 1:

The 4-point interaction vertex of this diagram is determined by terms in the V_1 component of $V^{(0)}$, given in (2.7) and (2.8).

To determine the contribution of this diagram, we must first investigate which terms in (2.8) can make up the desired $(\tilde{H}^1)_1^1(\tilde{H}_1^*)_1^1(\tilde{H}^1)_1^1(\tilde{H}_1^*)_1^1$ combination. Each of these terms will affect the total vertex factor.

We begin by determining if λ_1 contributes to this diagram's vertex. The λ_1 term of (2.8) reads

$$\lambda_1 \left[(\tilde{L}^i)_r^l (\tilde{L}_i^*)_{l'}^{r'} \right]^2 \rightarrow \lambda_1 (\tilde{L}^i)_r^l (\tilde{L}_i^*)_{l'}^r (\tilde{L}^j)_{r'}^{l'} (\tilde{L}_j^*)_{l''}^{r'}$$

Making the field replacements

$$(\tilde{L}^i)_r^l \rightarrow (\tilde{L}^I)_R^L \quad \text{and} \quad (\tilde{L}^j)_{r'}^{l'} \rightarrow (\tilde{L}^J)_{R'}^{L'}$$

sets the indices as

$$i = I, \quad l = L, \quad r = R, \quad j = J, \quad l' = L', \quad r' = R',$$

such that

$$\lambda_1 (\tilde{L}^i)_r^l (\tilde{L}_i^*)_{l'}^r (\tilde{L}^j)_{r'}^{l'} (\tilde{L}_j^*)_{l''}^{r'} \rightarrow \lambda_1 (\tilde{L}^I)_R^L (\tilde{L}_I^*)_{L'}^R (\tilde{L}^J)_{R'}^{L'} (\tilde{L}_J^*)_{L''}^{R'}$$

This resulting term is Lorentz invariant, and can make up the desired $(\tilde{H}^1)_1^1(\tilde{H}_1^*)_1^1(\tilde{H}^1)_1^1(\tilde{H}_1^*)_1^1$ combination in the low-scale theory for the case $I, L, R, J, L', R' = 1$. Thus, the coupling λ_1 will contribute to the vertex of this term in the low-scale theory.

Following the same procedure for the λ_2 term, we get

$$\lambda_2 (\tilde{L}^i)_r^l (\tilde{L}^j)_{r'}^{l'} (\tilde{L}_j^*)_{l'}^r (\tilde{L}_i^*)_{l''}^{r'}$$

$$(\tilde{L}^i)_r^l \rightarrow (\tilde{L}^I)_R^L \quad \text{and} \quad (\tilde{L}^j)_{r'}^{l'} \rightarrow (\tilde{L}^J)_{R'}^{L'}$$

such that

$$\lambda_2 (\tilde{L}^i)_r^l (\tilde{L}^j)_{r'}^{l'} (\tilde{L}_j^*)_{l'}^r (\tilde{L}_i^*)_{l''}^{r'} \rightarrow \lambda_2 (\tilde{L}^I)_R^L (\tilde{L}^J)_{R'}^{L'} (\tilde{L}_J^*)_{L'}^R (\tilde{L}_I^*)_{L''}^{R'}$$

Again, this resulting term is Lorentz invariant and can freely take on the desired index combination. Thus, λ_2 also contributes to the vertex at the low energy scale.

When examining the λ_3 term of (2.8), it is clear that it is identical to the λ_2 term upon interchanging the indices r and r' . Due to symmetry about these indices, λ_3 will contribute in the same way as λ_2 .

Similarly, the λ_4 term is identical to the λ_3 term upon interchanging i and j . Thus, it will also contribute to the vertex of Diagram 1.

As no other terms in (2.7) can form $\tilde{L}\tilde{L}^*\tilde{L}\tilde{L}^*$ -like terms, we can conclude that the first diagram is given by Figure 2. This is the first contribution to the low-scale vertex of Figure ??.

$$\begin{array}{ccc}
(\tilde{H}^1)_1^1 & & (\tilde{H}_1^*)_1^1 \\
& \diagdown & / \\
& \times & \\
& / & \diagdown \\
(\tilde{H}_1^*)_1^1 & & (\tilde{H}^1)_1^1
\end{array}
= -4i (\lambda_1 + \lambda_2 + \lambda_3 + \lambda_4)$$

Figure 2: Contribution of Diagram 1 in the high-scale theory. The factor 4 is included to account for the combinatorics of the \tilde{H} fields.

Diagram 2:

Next, the second diagram of Figure 1 is considered. For this, we begin by finding a general expression for the $\tilde{\Phi}^s \tilde{H} \tilde{H}^*$ vertex, and then using this to determine the contribution of the second diagram to the $(\tilde{H}^1)_1^1 (\tilde{H}_1^*)_1^1 (\tilde{H}^1)_1^1 (\tilde{H}_1^*)_1^1$ term.

To find this vertex, we repeat the process described above for this combination of fields. This is done by setting one of the fields components to $\tilde{\Phi}^s \rightarrow \text{Re}[(\tilde{L}^3)_3^3]$, and determining which terms in (2.8) can sustain the additional $\tilde{H} \tilde{H}^*$ combination. As the $\tilde{\Phi}^s$ is the field which obtains a VEV according to (3.1), it can be expanded as such.

Thus, again starting from the λ_1 contribution to the vertex, it is found that

$$\begin{aligned}
\lambda_1 (\tilde{L}^i)_r^l (\tilde{L}_i^*)_l^r (\tilde{L}^j)_{r'}^{l'} (\tilde{L}_j^*)_{l'}^{r'} &\longrightarrow \lambda_1 (\tilde{L}^I)_R^L (\tilde{L}_I^*)_L^R (\tilde{L}^3)_3^3 (\tilde{L}_3^*)_3^3 \\
&\longrightarrow \lambda_1 \tilde{H} \tilde{H}^* \left(\frac{1}{\sqrt{2}} \right)^2 [(\phi + v)(\phi^* + v)] \\
&\longrightarrow \frac{\lambda_1}{2} [\tilde{H} \tilde{H}^* \phi \phi^* + \underbrace{\tilde{H}^* \phi v + \tilde{H} \tilde{H}^* \phi^* v}_{= 2v \tilde{H} \tilde{H}^* \text{Re}[\phi]} + \tilde{H} \tilde{H}^* v^2] \\
&= 2v \tilde{H} \tilde{H}^* \tilde{\Phi}^s
\end{aligned} \tag{4.19}$$

Repeating this process for the $\lambda_{2,3,4}$ terms in (2.8), it quickly becomes clear this field combination cannot be formed in another way. Thus, the λ_1 term is the only contribution, and the vertex $\tilde{\Phi}^s \tilde{H} \tilde{H}^*$ is given by Figure 3.

Using this vertex, the mass-squared eigenvalue of $\tilde{\Phi}^s$ from Table 2, and the $p^2 \rightarrow 0$ approximation, the contribution of the second diagram is given in Figure 4.

$$= -2iv\lambda_1$$

Figure 3: Vertex of the $\tilde{H}\tilde{H}^*\tilde{\Phi}^s$ interaction existing in the high-scale theory. The factor of two is included to account for the combinatorics of the two \tilde{H} fields.

$$= (-2iv\lambda_1) \frac{i}{-2(\lambda_1 + \lambda_2 + \lambda_3 + \lambda_4)v^2} (-2iv\lambda_1)$$

Figure 4: Contribution of Diagram 2 in the high-scale theory.

Diagram 3:

Due to symmetry of incoming and outgoing particles, Diagram 3 gives the same contribution as Diagram 2.

Combining the results of the three diagrams, the matching as illustrated in Figure 1 for the $(\tilde{H}_1)_1^1(\tilde{H}_1^*)_1^1(\tilde{H}_1)_1^1(\tilde{H}_1^*)_1^1$ term becomes

$$-4i\lambda_a = -4i(\lambda_1 + \lambda_2 + \lambda_3 + \lambda_4) + \frac{2i(-2i\lambda_1v)^2}{-2(\lambda_1 + \lambda_2 + \lambda_3 + \lambda_4)v}, \quad (4.20)$$

such that

$$\lambda_a = (\lambda_1 + \lambda_2 + \lambda_3 + \lambda_4) - \frac{\lambda_1^2}{(\lambda_1 + \lambda_2 + \lambda_3 + \lambda_4)}. \quad (4.21)$$

Using the parameterization introduced in (4.11), the expression above can be Taylor expanded, and finally written as

$$\lambda_a = -2\xi + \mathcal{O}(\xi^2) \quad (4.22)$$

4.3.2 Tree-level matching results

The full set of matching conditions can be obtained by repeating the method illustrated by the example above for each $\lambda_{a\dots o}$ in (4.16).

The results of the tree-level matching conditions in terms of the parameterization introduced in (4.11) are given below. All $\mathcal{O}(\xi^2, \delta^2)$ and higher are excluded.

Scalar Matching Conditions:

$$\begin{array}{lll}
\lambda_a = -2\xi & \lambda_f = 0 & \lambda_k = 0 \\
\lambda_b = -2\delta & \lambda_g = 1/2 \delta & \lambda_l = 0 \\
\lambda_c = 0 & \lambda_h = 1/2 \delta & \lambda_m = -2(\lambda_2 - \xi + \delta) \\
\lambda_d = 2\delta & \lambda_i = -1/2 (\lambda_2 - \xi + \delta) & \lambda_n = 2(\lambda_2 + \xi) \\
\lambda_e = 2\xi & \lambda_j = 1/2 (\lambda_2 + \xi) & \lambda_o = 2(\delta - \xi)
\end{array}$$

Yukawa Matching Conditions:

$$Y_\epsilon = Y_\mu = -Y_\xi = y$$

The results of the tree-level matching conditions summarized above, are essential components of the rest of this work. We use these expressions to map the low-scale parameter space $\mathcal{P}_{\text{LRSM}}^{(\text{LS})}$ to the high-scale parameter space $\mathcal{P}_{\text{LRSM}}^{(\text{HS})}$ at the trinification breaking scale, such that

$$\mathcal{P}_{\text{LRSM}}^{(\text{LS})} \Big|_{\mu_{\text{VEV}}} = \{\lambda_2, \delta, \xi, y, g, v\}. \quad (4.23)$$

Here we have used the parameterization in (4.10). In the following section, the β -functions, which describe the RG evolution of the model, are found. The parameters will run starting from the trinification breaking scale, down to lower energies. In this way, the matching conditions provide the initial conditions for the running of the LRSM. As we will see, the β -functions, will depend solely on the parameters of $\mathcal{P}_{\text{LRSM}}^{(\text{LS})}$, as defined in (4.17).

When analyzing the tree-level matching condition results, we can further motivate our previous decision to include one-loop corrections to the model. At tree-level, several scalar couplings, and all but three Yukawa couplings, are zero. Additionally, since ξ and δ are small valued parameters according to the constraints of the effective LRSM outlined in Section 4.2.2, the low scale couplings proportional to these parameters are also only a small off-set from zero. Upon including one-loop corrections to the matching conditions in both the scalar and fermion sectors, this will no longer be the case, and the initial conditions for the RG running can change considerably. This can have significant implications for the RG evolution of the model, and thus for the observation of radiative breaking to the SM. The addition of one-loop corrections to the matching conditions is discussed in Section 8.

Another important result is that each coupling in (4.16) to the global Goldstone, $\tilde{\Phi}$, is matched to zero. Thus, this field decouples at the matching scale⁶.

⁶For a more detailed discussion of this decoupling, refer to [7].

5 RG evolution of the LRSM

In conclusion thus far, spontaneous symmetry breaking of the trinification model was investigated, and an appropriate low-energy effective LRSM was formulated. The high-energy theory was matched to the low-energy theory at the breaking scale, providing the initial conditions for the RG running of the model parameters. The next aim of this work is to calculate the full set of β -functions of the effective LRSM. These will be used to investigate the radiative breaking of the model.

The β -functions of the model form a set of coupled differential equations arising from infinite counterterms used in renormalization [19]. They describe the logarithmic dependence of a parameter, g , on the energy scale, μ , and are defined as [20]

$$\beta(g) = \frac{\partial g}{\partial \log(\mu)}. \quad (5.1)$$

Due to the large number of parameters in $\mathcal{P}_{\text{LRSM}}^{(\text{LS})}$, the β -functions of the effective LRSM are mathematically elaborate and difficult to manually compute. Thus, throughout this work, they are obtained using the software package `PyR@TE` (“PYton Renormalization group equations At Two-loops for Everyone”) [21].

For the sake of this, work RG equations at one-loop are considered only. This is sufficient as a starting point, and more complicated two-loop runnings can be investigated in further research.

5.1 Obtaining β -functions with `PyR@TE`

`PyR@TE` consists of a set of `Python` routines which generate the one or two-loop RG equations for all parameters, given a certain input model. Upon downloading the full software package, `PyR@TE` automatically exports the results to `LATEX` and `Mathematica`.

We begin by implementing the effective LRSM. Firstly, the full symmetry group is encoded by naming and identifying each part of the total product group. The system files are written in such a way that they understand the transformation properties of each group. We continue constructing the model file by adding in the particle content, taking care to split scalars into real and complex components. We specify that the fermions of the model are Weyl fermions, and implement the charges of the fields under each symmetry group.

Next, $V_{(\text{LRSM})}^{(0)}$ and $\mathcal{L}_{\text{F}(\text{LRSM})}$, given in (4.16) and (4.15) respectively, must be written into the `PyR@TE` model file. Because their terms involve contractions of indices corresponding to three different $\text{SU}(2)$ groups, and not all terms involve the same type of contraction (e.g. they are contracted by Kronecker deltas, Levi-Cevita tensors, or both), correctly programming the Lagrangian in `PyR@TE` is relatively complicated.

The difficulty lays in constructing different contractions from pre-defined `PyR@TE` invariants stored in the `PyR@TE` database. In (4.16), we have written a possible most general potential using contractions that best suit the field notation applied throughout this work. That is, we

have written it in a form which we find easiest to read and use in calculating the matching conditions. `PyR@TE`, however, does not share the same notations, and we need to carefully write our specific contractions in terms of `PyR@TE` invariants. Thus, a thorough understanding of the invariants structure of `PyR@TE` is required. This structure, along with the method used to construct `PyR@TE` syntax throughout this work, is outlined with the following example.

5.1.1 Example: constructing contractions from `PyR@TE` invariants

The method of constructing general contractions from pre-defined `PyR@TE` invariants is outlined by first adopting the following notation:

- Define A, B, \dots as labels of a given $SU(2)$ group.
- Define the `PyR@TE` pre-defined invariant with a number $n = \{1, 2, \dots\}$ such that, for example, the first listed invariant for the $SU(2)_A$ gauge group is given as \mathbb{I}_{A1} .
- Define lower-case letters $\{a, b, \dots\}$ as labels of the fields to be contracted, such that in a quartic operator, the first field carries the a -index, the second the b -index, etc.
- The labels $\{1, 2\}$ are added on the field labels $\{a, b, \dots\}$ to denote the first and second field component of an $SU(2)$ -doublet, respectively.

The pre-defined invariants are called up in the `PyR@TE` database by specifying the representation of the given term. If we examine, for example, a quartic coupling transforming under a single $SU(2)_A$ group, this representation corresponds to $\mathbf{2} \times \mathbf{\bar{2}} \times \mathbf{2} \times \mathbf{\bar{2}}$. For such a term, the `PyR@TE` dictionary then yields the following two invariants [21]:

$$\begin{aligned}\mathbb{I}_{A1} &= a_1 b_1 c_1 d_1 + a_1 b_1 c_2 d_2 + a_2 b_2 c_1 d_1 + a_2 b_2 c_2 d_2 \\ \mathbb{I}_{A2} &= a_1 b_1 c_1 d_1 - a_1 b_1 c_2 d_2 + 2a_2 b_1 c_2 d_1 + 2a_1 b_2 c_1 d_2 - a_2 b_2 c_1 d_1 + a_2 b_2 c_2 d_2\end{aligned}$$

Specific contractions can be written as linear combinations of these two invariants. For instance, we can create the following contractions:

$$\begin{aligned}\mathbb{I}_{A1} &= a_1 b_1 c_1 d_1 + a_1 b_1 c_2 d_2 + a_2 b_2 c_1 d_1 + a_2 b_2 c_2 d_2 \\ &= (a_1 b_1 + a_2 b_2)(c_1 d_1 + c_2 d_2) \\ &= \begin{bmatrix} a_1 & a_2 \end{bmatrix} \begin{bmatrix} b_1 \\ b_2 \end{bmatrix} \begin{bmatrix} c_1 & c_2 \end{bmatrix} \begin{bmatrix} d_1 \\ d_2 \end{bmatrix} \equiv \delta^{ab} \delta^{cd}\end{aligned}\tag{5.2}$$

$$\begin{aligned}\mathbb{I}_{A1} + \mathbb{I}_{A2} &= 2(a_1 b_1 c_1 d_1 + a_1 b_2 c_1 d_2 + a_2 b_1 c_2 d_1 + a_2 b_2 c_2 d_2) \\ &= 2(a_1 c_1 + a_2 c_2)(b_1 d_1 + b_2 d_2) \\ &= 2 \begin{bmatrix} a_1 & a_2 \end{bmatrix} \begin{bmatrix} c_1 \\ c_2 \end{bmatrix} \begin{bmatrix} b_1 & b_2 \end{bmatrix} \begin{bmatrix} d_1 \\ d_2 \end{bmatrix} \equiv 2\delta^{ac} \delta^{bd}\end{aligned}\tag{5.3}$$

$$\begin{aligned}
\mathbb{I}_{A1} - \mathbb{I}_{A2} &= 2(a_1 b_1 c_2 d_2 - a_1 b_2 c_1 d_2 - a_2 b_1 c_2 d_1 + a_2 b_2 c_1 d_1) \\
&= 2(a_1 d_2 - a_2 d_1)(b_1 c_2 - b_2 c_1) \\
&= 2 \begin{bmatrix} a_1 & a_2 \end{bmatrix} \begin{bmatrix} 0 & 1 \\ -1 & 0 \end{bmatrix} \begin{bmatrix} d_1 \\ d_2 \end{bmatrix} \begin{bmatrix} b_1 & b_2 \end{bmatrix} \begin{bmatrix} 0 & 1 \\ -1 & 0 \end{bmatrix} \begin{bmatrix} c_1 \\ c_2 \end{bmatrix} \equiv 2\epsilon^{ad}\epsilon^{bc} \quad (5.4)
\end{aligned}$$

If we now wish to construct terms containing contractions between two groups, we add a second $SU(2)_B$ and create combinations of invariants $\mathbb{I}_{A1}, \mathbb{I}_{A2}, \mathbb{I}_{B1}, \mathbb{I}_{B2}$.

More specifically, suppose we have a term in the Lagrangian of the form

$$\lambda F_a F_b^* F_c F_d^* \epsilon_A^{ad} \epsilon_A^{bc} \epsilon_B^{ad} \epsilon_B^{bc}$$

Using (5.4), it is clear that

$$\begin{aligned}
\epsilon_A^{ad} \epsilon_A^{bc} \epsilon_B^{ad} \epsilon_B^{bc} &= \frac{1}{4}(\mathbb{I}_{A1} - \mathbb{I}_{A2})(\mathbb{I}_{B1} - \mathbb{I}_{B2}) \\
&= \frac{1}{2}[\mathbb{I}_{A1}\mathbb{I}_{B1} - \mathbb{I}_{A2}\mathbb{I}_{B2}] - \frac{1}{4}[(\mathbb{I}_{A1} + \mathbb{I}_{A2})(\mathbb{I}_{B1} + \mathbb{I}_{B2})] \\
&= \frac{1}{4}[2\mathbb{I}_{A1}\mathbb{I}_{B1} - 2\mathbb{I}_{A2}\mathbb{I}_{B2} - \mathbb{I}_{A1}\mathbb{I}_{B1} - \mathbb{I}_{A1}\mathbb{I}_{B2} - \mathbb{I}_{A2}\mathbb{I}_{B1} - \mathbb{I}_{A2}\mathbb{I}_{B2}] \\
&= \frac{1}{4}[\mathbb{I}_{A1}\mathbb{I}_{B1} - \mathbb{I}_{A2}\mathbb{I}_{B2} - \mathbb{I}_{A1}\mathbb{I}_{B2} - \mathbb{I}_{A2}\mathbb{I}_{B1}] \quad (5.5)
\end{aligned}$$

Such a term is implemented into the `Python` script in `PyR@TE` by specifying the invariant numbers as the Clebsch Gordon coefficient for each term in (5.5) and adding the normalization factor. Thus, the correct implementation for the example above would be

`{Fields : [[F,F*,F,F*], [F,F*,F,F*], [F,F*,F,F*], [F,F*,F,F*]],`

`CGCs: {A: [1,2,1,2], B: [1,2,2,1]}, Norm : [1/4, -1/4, -1/4, -1/4]},`

Manually finding each term is extensive and inefficient. Thus, a `Mathematica` code is created by defining this `PyR@TE` invariant structure and solving for each desired contraction. In this way, the syntax for each term in (4.16) and (4.15) is found and implemented.

5.2 Results

Once the scalar potential and fermion Lagrangian of the effective LRSM are correctly implemented into `PyR@TE`, the one-loop RG equations for the parameters are found. The resulting full set of RG equations for the couplings $\lambda_{a\dots o}$, the Yukawa's $Y_{\alpha\dots\tau}$, and the fermion singlet Majorana mass term (discussed in Section 4.2.4), are presented in Appendix D.

For radiative breaking, the running of the mass parameters of the two scalars in the effective LRSM are essential. They will be used throughout later sections, and are thus included here. They are found to be

$$\begin{aligned}
(4\pi)^2 \beta_{m_{\mathbb{R}}^2} = & m_{\mathbb{R}}^2 (20\lambda_b - 8\lambda_g - 9/2 g_{\mathbb{R}}^2 - 6g_{\text{LR}}^2) \\
& + 2 m_{\mathbb{R}}^2 (|Y_{\kappa}|^2 + |Y_{\lambda}|^2 + 3|Y_{\mu}|^2 + 3|Y_{\nu}|^2 + 2|Y_{\pi}|^2) \\
& + 16 m_{\mathbb{H}}^2 (\lambda_d + \lambda_m + \lambda_n + \lambda_o) - 4 |m_{\Phi}|^2 |Y_{\kappa}|^2
\end{aligned} \tag{5.6}$$

$$\begin{aligned}
(4\pi)^2 \beta_{m_{\mathbb{H}}^2} = & 48 m_{\mathbb{H}}^2 (3/4 \lambda_a + \lambda_h + \lambda_i + \lambda_j) \\
& - 9/2 m_{\mathbb{H}}^2 (g_{\mathbb{R}}^2 + g_{\text{L}}^2) + 2m_{\mathbb{H}}^2 (4|Y_{\alpha}|^2 + |Y_{\beta}|^2 + |Y_{\gamma}|^2 \\
& + 3|Y_{\epsilon}|^2 + 3|Y_{\eta}|^2 + 3|Y_{\zeta}|^2) \\
& + 2 m_{\mathbb{R}}^2 (8\lambda_d + 8\lambda_n + 8\lambda_m + 8\lambda_o) \\
& - 4|m_{\Phi}|^2 |Y_{\alpha}|^2
\end{aligned} \tag{5.7}$$

From the results above, we can see that the running of the scalar mass-squared parameters is highly dependent on many parameters of the LRSM. Each parameter, in turn, runs independently, making it challenging to find solutions the β -functions analytically.

Furthermore, we can make some statements about the scale at which gauge couplings in the trinification model are unified, by examining the running of each gauge couplings in the LRSM. They are found as

$$(4\pi)^2 \beta_{g_c} = -\frac{19}{3} g_c^3 \qquad (4\pi)^2 \beta_{g_{\text{L}}} = -\frac{2}{3} g_{\text{L}}^3 \tag{5.8}$$

$$\tag{5.9}$$

$$(4\pi)^2 \beta_{g_{\mathbb{R}}} = -\frac{1}{3} g_{\mathbb{R}}^3 \qquad (4\pi)^2 \beta_{g_{\text{LR}}} = \frac{124}{9} g_{\text{L}+\mathbb{R}}^3$$

These are ordinary differential equations, which can be solved analytically using known phenomenological SM values. The running of the gauge couplings is generalized as

$$\beta(g) = \frac{A}{(4\pi)^2} g^3. \tag{5.10}$$

Using the definition of $\beta(g)$ given in (5.1), this becomes a separable differential equation and has the solution

$$\frac{1}{2g^2} = \frac{A}{(4\pi)^2} \ln(\mu) + C, \tag{5.11}$$

where C is an integration constant which can be determined using known values of the coupling constants at the SM energy scale.

To determine the GUT scale at which all the gauge couplings unify, we begin by making the assumption that the running of the gauge couplings is not drastically changed at each symmetry breaking point. That is, we assume the RG running to be smooth over the boundary between the trinification model and the LRSM, as well as over the breaking boundary between the LRSM, and the resulting SM-like theory. Known values from the SM can then be used

as boundary conditions. We take the energy scale of the SM to be roughly the mass of the Z -boson, and used the fact that gauge couplings must equate at the GUT scale, to write a system of equations which, when solved, yields the following expression for the energy of the GUT scale

$$\mu_{\text{GUT}} = \mu_{\text{SM}} \exp \left[\frac{4\pi^2}{(A_C - A_L)} \left(\frac{1}{g_C|_{\mu_{\text{SM}}}} - \frac{1}{g_L|_{\mu_{\text{SM}}}} \right) \right]. \quad (5.12)$$

Then, applying the following known from phenomenology [22]

$$g_C|_{\mu_{\text{SM}}} = 1.18 \quad , \quad g_L|_{\mu_{\text{SM}}} = 0.65 \quad , \quad \mu_{\text{SM}} \approx m_Z \approx 91 \text{ GeV},$$

with the values of A_L and A_C coming from the results given in (5.8) such that

$$A_C = -19/3 \quad , \quad A_L = -2/3,$$

we find that the GUT scale lays at about

$$\mu_{\text{GUT}} \approx 2.1 \times 10^{12} \text{ GeV}.$$

With this, the following value of the unified gauge coupling in the trinification model is found

$$g|_{\mu_{\text{GUT}}} \approx 0.61$$

It should be noted that this is a very rough calculation. Not only is the assumption that parameters run smoothly at each breaking scale not necessarily true, some fields should be integrated out at these intermediate scales. This would change the β -functions of the other parameters. Thus, the result above is only a rough estimate of the GUT scale.

Finally, the expressions in (5.8) along with the results above is plotted in Figure 5, allowing us to examine the behavior of each gauge coupling as the energy scale changes.

In Figure 5, the running of g_{L+R} and g_R has been plotted, even though these gauge couplings are not present in the SM. When the LRSM undergoes radiative breaking to the SM gauge group, these couplings will combine to form the SM hypercharge gauge coupling. In [7], it is shown that the $U(1)_Y$ gauge coupling is related to g_{L+R} and g_R by

$$g_Y = \frac{2g_R g_{L+R}}{\sqrt{4g_{L+R}^2 + g_R^2}} \quad (5.13)$$

6 Radiative breaking to the SM

The next aim of this work is to investigate whether or not the effective LRSM undergoes radiative breaking to a SM-like theory, as hypothesized in Section 4.2.1. We approach this task by first theoretically predicting the simplest scenario in which this occurs. Then, we investigate whether it is possible to tune the model parameters such that breaking occurs

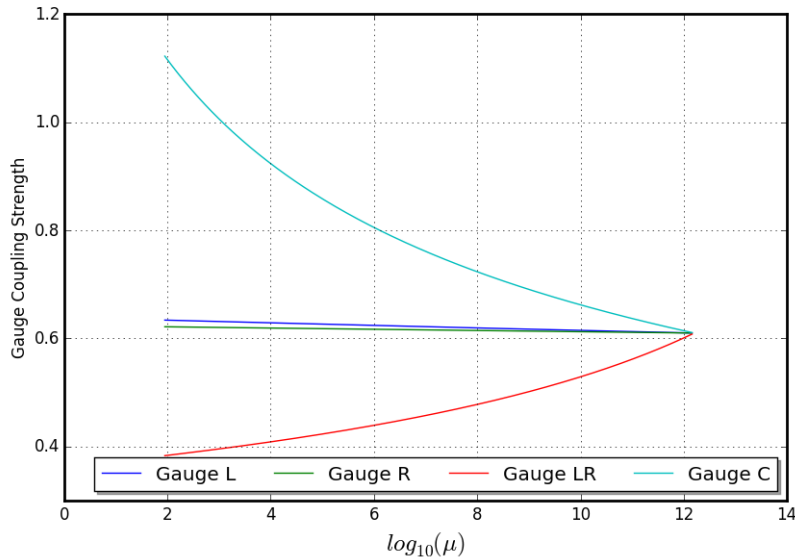


Figure 5: Running of the gauge couplings in the LRSM. Couplings are unified at the GUT scale μ_{GUT} . Couplings of g_L and g_C match SM values at the corresponding energy scale of the mass of the Z-boson.

in this way. In other words, we search for physically valid parameter space points for which spontaneous symmetry breaking is induced and the model breaks naturally to SM-like theory, preserving along the way, the phenomenological SM features discussed in Section 4.2.1.

6.1 Symmetry breaking in the effective LRSM

We begin by considering a possible breaking scheme. In order to break to the SM, part of the LRSM's gauge group must be reduced to $U(1)_Y$ hypercharge. More specifically,

$$[SU(2)_R \times U(1)_{L+R}] \longrightarrow [U(1)_Y] \quad (6.1)$$

The simplest way in which such breaking occurs is if the $(\tilde{L}^2)_2^3$ component of \tilde{l}_R acquires a non-zero VEV, thereby breaking the symmetry of the potential [7]. That is,

$$\langle (\tilde{L}^I)_R^3 \rangle \equiv \delta_2^I \delta_2^R \frac{\rho}{\sqrt{2}} = \frac{1}{\sqrt{2}} \begin{pmatrix} 0 & 0 \\ 0 & \rho \end{pmatrix} \quad (6.2)$$

This field component can acquire a non-zero VEV if its mass-squared parameter runs to a negative value. In other words, radiative breaking can occur when $m_R^2(\mu) < 0$.

We further find the minimization condition for which the scalar potential, $V_{\text{LRSM}}^{(0)}$, has a minimum at this VEV. Repeating the method in Section 3.1, the minimization condition is found by enforcing

$$\left. \frac{\partial V_{\text{LRSM}}^{(0)}}{\partial \phi_i} \right|_{\phi_i = \langle \phi_i \rangle} = 0, \quad (6.3)$$

where now

$$\langle \phi_i \rangle = \begin{cases} \frac{\rho}{\sqrt{2}} & \text{for } \phi_i = (\tilde{L}^2)_2^3 \\ 0 & \text{for } \phi_i = \text{other} \end{cases} \quad (6.4)$$

This leads to the minimization condition

$$-m_{\text{R}}^2 = \lambda_b \rho^2. \quad (6.5)$$

Upon breaking, the \tilde{l}_{R} and \tilde{H} fields undergo a decomposition, similar to that in (4.1). Thus, the physical particle mass spectrum will reflect a splitting in these two fields. Physical masses are obtained by taking the second derivatives of the scalar potential, applying the minimization condition above, and diagonalizing the resulting matrix to find the mass-squared eigenvalues. The resulting particle spectrum is given in Table 4.

Table 4: Splitting of the \tilde{l}_{R} and \tilde{H} fields after spontaneous symmetry breaking in the effective LRSM.

	Name	Field	Mass ²
$\tilde{l}_{\text{R}} \rightarrow$	\tilde{l}_{R1}	$(L^2)_2^3$	$2\lambda_b \rho^2$
	\tilde{l}_{R2}	$(L^1)_1^3$	$2\lambda_g \rho^2$
$\tilde{H} \rightarrow$	\tilde{H}_1	$(L^2)_2^L$	$m_{\text{H}}^2 + \frac{1}{2}\lambda_d \rho^2$
	\tilde{H}_2	$(L^2)_1^L$	$m_{\text{H}}^2 + \frac{1}{2}(\lambda_d + \lambda_n) \rho^2$
	\tilde{H}_3	$(L^1)_2^L$	$m_{\text{H}}^2 + \frac{1}{2}(\lambda_d + \lambda_m) \rho^2$
	\tilde{H}_4	$(L^1)_1^L$	$m_{\text{H}}^2 + \frac{1}{2}(\lambda_d + \lambda_n + \lambda_m + \lambda_o) \rho^2$

In addition, in [7] it is shown that the breaking of $[\text{SU}(2)_{\text{R}} \times \text{U}(1)_{\text{L+R}}]$ into SM hypercharge by the VEV defined in (6.2), leads to three massive gauge bosons which can be identified with the SM W^{\pm} and Z^0 . Their masses are found to be

$$W'^{\pm} = \frac{1}{4}g_{\text{R}}^2\rho^2 \quad , \quad Z'^0 = \left(g_{\text{L+R}} + \frac{1}{4}g_{\text{R}}^2 \right) \rho^2 \quad (6.6)$$

From the particle spectrum, we see that the Higgs tri-doublet field, \tilde{H} , splits into four left-doublets, while the \tilde{l}_{R} field splits into two singlet states. The next step is to create a second effective theory by again integrating out heavy fields at the breaking scale of $\mathcal{O}(\rho)$. The particle content of this EFT should directly lead to the observed spectrum of the SM for a given symmetry breaking scheme.

We propose a three-Higgs-doublet model (3HDM), formulated by integrating out both the \tilde{l}_{R1} and \tilde{l}_{R2} fields, in addition to the \tilde{H}_4 Higgs doublet. In [7], it is argued that the electroweak gauge group of the 3HDM can be broken further into electromagnetism of the SM, when

one component of each left Higgs doublet acquires a VEV. The resulting particle spectrum incorporates a realistic SM mass hierarchy for quarks and the heavy gauge bosons, as well as the correct form of the CKM mixing matrix⁷.

With the promising features of the 3HDM in mind, we investigate whether the discussed breaking scenario is physically viable for the effective LRSM, and if so, whether we can find a region of the parameter space which justifies the choice of the 3HDM as an ETF. We begin by outlining the set of constraints must be satisfied by viable parameter space points. We can then create a parameter scanning algorithm which tests for each of these constraints.

6.2 Parameter constraints for radiative breaking

As was discussed in Section 4.3.2, the low-scale parameters of the effective LRSM can be matched to high-scale parameters at the GUT breaking scale, $\mu|_{\text{VEV}}$. The running is started from this scale, and the values of parameters at a certain energy can be found by solving their respective β -functions, using the mapping in (4.23) as the initial conditions. In this way, values of the high-scale parameters fully determine radiative breaking in the effective LRSM, and we will thus scan for physically viable points of $\mathcal{P}_{\text{LRSM}}^{(\text{HS})}$.

To be considered physically viable, points of $\mathcal{P}_{\text{LRSM}}^{(\text{HS})}$ must pass the following tests and constraints:

1. First, for vacuum stability in both the trinification model and the effective LRSM, mass-squared eigenvalues of all particles must be positive. This places the same constraints on $\mathcal{P}_{\text{LRSM}}^{(\text{HS})}$ as given in (4.7). We further require the masses-squared in Table 4 to be positive at the LRSM breaking scale, $\mu \sim \mathcal{O}(\rho)$.
2. Second, we impose that perturbation theory should be applicable in both the trinification model as well as the effective LRSM. This places perturbativity constraints on the values of the couplings such that

$$\left| \frac{\lambda_i^2}{4\pi} \right| \leq 1 \tag{6.7}$$

3. Third, in order for the $(\tilde{L}^2)_2^3$ scalar component to acquire a non-zero VEV, radiative breaking must be induced by the running of m_{R}^2 to a negative value, while the m_{H}^2 parameter remains positive at the breaking scale.
4. Fourth, the particle spectrum after spontaneous symmetry breaking, summarized in Table 4, must exhibit the correct mass hierarchy to justify integrating out the $\tilde{l}_{\text{R}1}$, $\tilde{l}_{\text{R}2}$, and \tilde{H}_4 fields for the 3HDM. As we will see in the following section, this corresponds to requiring the mass ratio between light and heavy states to be small.

⁷3HDM's have been considered throughout literature as extensions to the more widely studied 2HDM extension of the SM. They have a rich phenomenology, and have for instance been shown to be able to incorporate dark matter candidates, provide an explanation for CP violation, and predict SM particle hierarchies. For an overview of 3HDM physics see [23].

5. Finally, the running must be terminated when any particles obtain a mass of the order of the renormalization scale, such that they can be integrated out accordingly. This occurs when

$$\frac{|m^2(\mu)|}{\mu^2} \approx 1 \quad (6.8)$$

For convenience, logarithmic plots are used, and the following parameterization is introduced

$$t \equiv \log_{10}(\mu) \quad (6.9)$$

such that the requirement for termination of the running in (6.8) becomes

$$|m^2(t)| \simeq 10^{2t} = \mu_t \quad (6.10)$$

The final constraint on the parameter space is that spontaneous symmetry breaking must be induced before the running is terminated. Any points for which this is not the case are discarded.

Taking each of these constraints into account, physically viable parameter space points of $\mathcal{P}_{\text{LRSM}}^{(\text{HS})}$ are found by implementation of a scanning algorithm.

6.3 Scanning the parameter space with simulated annealing

The parameter space $\mathcal{P}_{\text{LRSM}}^{(\text{HS})}$ is scanned for points which satisfy the outlined conditions by implementation of a simulated annealing (SA) algorithm. In this section, we first outline the general principles of SA, and then apply the algorithm to our specific model.

SA is a technique for finding the global minimum of a given function in a multi-dimensional parameter space. It resembles a steepest decent methods, and allows for the “tunneling” between barriers which could otherwise hinder this search [24].

We interpret the function to be minimized as the energy function, $\mathcal{E}(\{x_i\})$ of a given system, where $\{x_i\}$ is a parameter space point describing the physical state of this system. If we imagine the system to be in contact with a thermal source of temperature T , the goal of the SA algorithm is to slowly decrease the temperature until it is approximately zero, at which point the energy function is minimized, and the corresponding parameter space points are found [24].

The general method of SA is outlined in more detail, as follows:

- Being at a given input parameter space point $\{x_0\}$, and implement it into the defined energy function $\mathcal{E}(\{x_0\})$ of the system.
- A small and random change R is made such that $x'_0 = x_0 + R$, and $\mathcal{E}(\{x'_0\})$ is computed.

- The change is either accepted or rejected based on a probability defined by

$$P(x_1 = x'_0) = e^{-\beta[\mathcal{E}(\{x'_0\}) - \mathcal{E}(\{x_0\})]} \quad (6.11)$$

where $\beta = \frac{1}{T}$ is the inverse temperature. A change will be accepted if $P(\{x_1\}) < 1$. The exponential factor will be greater than one if $\mathcal{E}(\{x'_0\}) < \mathcal{E}(\{x_0\})$. Thus, for high values of T , the change will almost always be accepted, while for lower values, the change will be accepted only if it represents a favorable one.

- These steps are repeated many times while systematically lowering T until the energy function is minimized. This occurs when the change in $\mathcal{E}(\{x'_0\})$ becomes smaller than the random change R .

The SA scanning algorithm is implemented in `Python`, and modified for the purpose of this work.

6.3.1 Implementation in Python

We begin by encoding the initial and final values of T , along with the step size between each run over which the SA is carried out. Additionally, a domain for the random values from which each parameter should be chosen is specified, based on a prediction of their physical range of values.

Furthermore, the mass-squared expressions of Table 4 are defined. β -functions of each parameter are called in from the `PyR@TE` results file, and the matching conditions found in Section 4.3.2 are specified as initial values. We set initial and final values of t , as defined in (6.9), and specify the step size over which the running should be calculated. A loop is created which re-calculates the running for each parameter space point used.

Next we require an appropriate energy function. A correctly constructed energy function will return a large constant value for parameter space points which do not satisfy the listed constraints, and return a smaller value, the “better” the suggested point. In this way, as the output of the energy function decreases, the algorithm steers towards more promising parameter space points.

We begin by making the following definitions:

$$m_{\{x\}}^2 = m_{R1}^2 \parallel m_{R2}^2 \parallel m_{H1}^2 \parallel m_{H2}^2 \parallel m_{H3}^2 \parallel m_{H4}^2 \parallel m_{W^\pm}^2 \parallel m_{Z^0}^2, \quad (6.12)$$

$$\begin{aligned} m_{\min} &= \left| \min\{m_{R1}^2, m_{R2}^2, m_{H1}^2, m_{H2}^2, m_{H3}^2, m_{H4}^2, m_{W^\pm}^2, m_{Z^0}^2\} \right| \\ m_{\max} &= \max\{m_{R1}^2, m_{R2}^2, m_{H1}^2, m_{H2}^2, m_{H3}^2, m_{H4}^2, m_{W^\pm}^2, m_{Z^0}^2\}, \end{aligned} \quad (6.13)$$

$$\begin{aligned} r_1 &= \frac{\min\{m_{H1}^2, m_{H2}^2, m_{H3}^2, m_{H4}^2\}}{\min\{m_{W^\pm}^2, m_{Z^0}^2\}} \\ r_2 &= \frac{\min\{m_{H1}^2, m_{H2}^2, m_{H3}^2, m_{H4}^2\}}{\max\{m_{R1}^2, m_{R2}^2, m_{W^\pm}^2, m_{Z^0}^2\}} \end{aligned} \quad (6.14)$$

Defining a parameter space point $\{x_i\} \in \mathcal{P}_{\text{LRSM}}^{(\text{HS})}$, we choose the following energy function

$$\mathcal{E}(\{x_i\}) = \begin{cases} 10, & \text{if } \rho^2, \lambda_b < 0 \\ 5 + \frac{1}{5 m_{\text{max}}} [m_{\text{min}} - 2(m_{\text{R1}}^2 + m_{\text{R2}}^2)], & \text{if } m_{\{x\}}^2 < 0 \\ 2r_1 + r_2, & \text{other} \end{cases} \quad (6.15)$$

This energy function effectively excludes parameter points where $\rho^2 < 0$ and/or $\lambda_b < 0$, which violate the condition that m_{R}^2 is positive just after spontaneous symmetry breaking, by returning the relatively high value 10. It further searches for points where at least one Higgs doublet is light. Points which satisfy $\rho^2 < 0$ and $\lambda_b < 0$ are passed through, and minimum and maximum masses are found. The output is determined by the ratio of these masses. Depending on how well they satisfy the mass positivity of $m_{\text{H1...4}}^2$ and $m_{\text{R1,2}}^2$, and how successful they are in satisfying the mass hierarchy conditions outlined in Section 6.2, the energy function will be larger or smaller. In this way, its output effectively steers towards “better” parameter space points. Thus, when the obtained masses and the ratios between them reflect the desired scalar mass hierarchy, the energy function outputs a lower value. In this way, the algorithm finds not only points which satisfy the constraints, but also the ones which are “most successful” in doing so.

The implemented algorithm carries out the following parameter scanning procedure:

1. Choose a random high scale parameter space point of $\mathcal{P}_{\text{LRSM}}^{(\text{HS})}$, denoted by $\{x_i^{(\text{HS})}\}$ according to the set bounds.
2. Test if $\{x_i^{(\text{HS})}\}$ satisfies the vacuum stability and perturbativity constraints of the trification model. If all constraints are satisfied, accept the point.
3. For an accepted point, apply the matching conditions to get expressions of the low-scale parameters $\{x_i^{(\text{LS})}\}$ in terms of the high-scale $\{x_i^{(\text{HS})}\}$.
4. Implement these as initial conditions for the running of m_{H}^2 and m_{R}^2 . Run the masses down and terminate when one satisfies the condition in (6.10).
5. At the termination point, test if the value of m_{R}^2 is negative while m_{H}^2 is positive. This is necessary for a minimum as defined in (6.2), and the correct breaking scheme will occur. If these conditions are met, pass the point through.
6. Use the accepted point $\{x_i^{(\text{LS})}\}$ to compute masses of $m_{\text{H1...H4}}^2$, $m_{\text{R1,R2}}^2$, and the value of ρ^2 . Accept the parameter point if all are positive, indicating vacuum stability after breaking of the LRSM.
7. For an accepted point $\{x_i^{(\text{LS})}\}$, use these obtained masses as inputs for computing the energy function $\mathcal{E}(\{x_i^{(\text{LS})}\})$.

8. Make a random change in the high scale parameters, $\{x_i^{(HS)}\}$, repeat the matching and running procedures, and compute $\mathcal{E}(\{x_i^{(LS)}\})$
9. Accept or reject the change in parameters based on the value of $P(\{x_i^{(LS)}\})$, as defined in (6.11).
10. Repeat while stepwise decreasing the value of T
11. Stop the process when $\Delta\mathcal{E}(\{x_i^{(LS)}\}) < \epsilon$, where ϵ is a specified small valued parameter

The resulting output file contains a set of physically viable points in $\mathcal{P}_{\text{LRSM}}^{(\text{HS})}$ for which radiative breaking occurs, and for which the 3HDM is justified as a low-energy limit of the effective LRSM.

Using the SA algorithm, points for which radiative breaking occurs are found. For instance, one such point is given by

$$\{\delta = 2.32 \times 10^{-12}, \xi = 2.1 \times 10^{-7}, \lambda_1 = 0.27, \lambda_2 = -7.78 \times 10^{-5}, y = 1.97, g = 0.61, v = 10^{12} \text{ GeV}\}.$$

It can be concluded that there exist viable parameter space points for which spontaneous symmetry breaking is induced, and the 3HDM can be justified as a low-energy limit of the effective LRSM. A more complete picture of the resulting SM-like theory and its parameters, can be found by determining the (un)broken generators and the resulting symmetry group, as was done for the LRSM in Section 3. For the sake of this this part of this work, however, we are interested in verifying the possibility of radiative breaking, by proving that physically viable parameter space points exist. Before continuing to construct the resulting theory, we must first further justify the effective LRSM as a viable low-energy limit of the trinification model.

As discussed in Section 4.2.3, we cannot impose a natural hierarchy between the \tilde{H} and \tilde{l}_R fields and the other color-singlet scalars when taking only tree-level masses into account. Thus, the next aim of this work is to include one-loop corrections to the scalars of the LRSM, in the hope that these will increase the masses of the other fields enough, such that they are heavy compared to \tilde{H} and \tilde{l}_R . This means they can be integrated out, and thus, that the proposed effective LRSM is a low-energy limit of the trinification model at one-loop.

7 The one-loop scalar mass spectrum

With the conclusions presented in the previous section, the final aim of this work is to determine the full one-loop scalar mass spectrum for the LRSM at the GUT scale, and determine whether the correct scalar hierarchy to support the effective LRSM can be naturally obtained upon inclusion of these corrections.

For scalars, the one-loop mass spectrum can be obtained using the effective potential method. Obtaining the full spectrum for such a complex model is both mathematically and computationally extensive. We will build upon the file used to calculate the tree-level masses in

Section 3.2. However, before discussing the computational methods used, a thorough understanding of the theory behind the effective potential method is essential.

7.1 The effective potential method

In Section 3.2, spontaneous symmetry breaking due to the non-zero VEV of a single scalar component in the trinification model was investigated. For the calculation of tree-level particle masses, the classical potential was minimized and leading order effects were considered only.

However, in quantized field theories, fluctuations arising from some arbitrary external source can act on the vacuum and generate the spontaneous breakdown of symmetries or, in theories where there are already broken symmetries, shift the expectation value of the vacuum state. Additionally, such fluctuations will induce a particle's self energy, which forms a contribution to a particle's mass due to interactions with this fluctuating vacuum [25].

To observe the effects of quantum fluctuations, the effective potential is introduced. The effective potential considers higher order radiative corrections as perturbations on the classical potential. To understand the connection between the effective potential and the one-loop mass spectrum, we begin by developing a formalism.

7.1.1 Formalism of the effective potential

In the functional methods description of quantum field theory, n -point correlations functions can be described by a generating functional, Z , which is dependent on an external source of quantum fluctuations, $J(x)$. The details of this formalism are outlined in Appendix C.

Similarly, we can define a generating functional $W[J]$ in the following way

$$Z[J] = e^{iW[J]} = \int \mathcal{D}\phi e^{i[S(\phi)+J\phi]}, \quad (7.1)$$

where $S(\phi)$ is the classical action, and the path integral is defined in (C.2) of Appendix C.1.

Upon examining this definition closely, and using the expression in (C.2), we can interpret $W[J]$ as the vacuum energy as a function of the external source, J .

By taking the functional derivative of W with respect to J , a so-called *classical field* is defined as

$$\phi_c(x) \equiv \frac{\partial W}{\partial J(x)} = \frac{1}{Z[0]} \int \mathcal{D}\phi e^{i[S(\phi)+J\phi]} \phi(x). \quad (7.2)$$

Physically, this represents a weighted average over all the possible fluctuations. We further define the effective action as the Legendre transformation of $W[J]$ such that

$$\Gamma[\phi_c] = -W[J] - \int d^4y J(y)\phi_c(y), \quad (7.3)$$

with the result that the functional derivative of the effective action after some calculus yields the condition

$$\frac{\partial\Gamma(\phi_c)}{\partial\phi_c(x)} = -J(x). \quad (7.4)$$

From this, we can analyze the meaning of the effective action. It's first functional derivative returns the quantum fluctuations on the vacuum state. In other words, this first derivative gives the radiative corrections to the classical VEV.

Furthermore, if we set the external source to zero, indicating that there are no interactions between particles and the vacuum, the relation

$$\frac{\partial\Gamma(\phi_c)}{\partial\phi_c(x)} = 0 \quad (7.5)$$

is obtained. Assuming that the vacuum is invariant under translations in spacetime, then $\phi_c(x)$ (which, as concluded earlier, is a solution to the VEV representing a weighted average over all possible fluctuations) is independent of x . Thus, we can define the *effective potential* as

$$\Gamma[\phi_c] = -V_{\text{eff}}(\phi_c) \int d^4x, \quad (7.6)$$

where the integral over spacetime will be a constant. With this definition, the result of (7.5) will reduce to

$$\frac{\partial V_{\text{eff}}(\phi_c)}{\partial\phi_c(y)} = 0. \quad (7.7)$$

Solutions to this expression are values of the VEV in the absence of any external sources. Thus, when “switching off” quantum fluctuations, the VEV is found by minimization of the potential just as in Section 3.2. In this case, the effective potential simply reduces to the classical potential, $V^{(0)}$ [26].

Combining (7.4) and (7.6), it can be concluded that the effective potential is by definition a function of which the minimization gives the true vacuum state of the quantum field theory.

Furthermore, in Appendix C.3, it is shown that n -point correlation functions can be found by taking the n^{th} functional derivative of the generating functional. Using (C.9) and the definition of the classical field given in (7.2), we derive n -point one-particle irreducible (1PI) Feynman diagrams by taking n^{th} -order derivatives of the effective potential.

More specifically, the effective potential is equal to the classical potential plus the sum of all 1PI connected vacuum graphs, such that it can be written as

$$\begin{aligned} V_{\text{eff}} &= V^{(0)} + \epsilon V^{(1)} + \epsilon^2 V^{(2)} + \epsilon^3 V^{(3)} + \dots \\ &= \sum_n \epsilon^n V^{(n)}. \end{aligned} \quad (7.8)$$

where $\epsilon = \frac{\hbar}{(4\pi)^2}$, and the label on each component V indicates the number of loops considered in the related order correction on the vacuum.

With this, it can be concluded that the i^{th} -derivative of $V^{(n)}$, with respect to ϕ_i , gives the n^{th} -order loop correction to any scalar i -point function of our theory. In other words, this corresponds to the zero-external momentum contribution, arising from interactions with the fluctuating vacuum alone, to a general one-loop diagram with i scalar external legs. This will be the central idea used throughout the rest of this work to obtain the scalar one-loop mass spectrum [12].

7.1.2 The Coleman-Weinberg effective potential

In this work we restrict ourselves to the inclusion of first order corrections to the effective potential only, such that we consistently eliminate any $\mathcal{O}(\epsilon^2)$ or higher arising throughout calculations accordingly.

The formalism developed in the previous section can be used to write an expression for the one-loop effective potential. This was first done for a simple massless scalar theory by Sidney Coleman and Erick Weinberg. In [27] they showed that radiative corrections can generate spontaneous symmetry breaking in theories for which classical tree-level effects do not indicate such breakdowns. Furthermore, they developed the one-loop Coleman-Weinberg effective potential given by [27]

$$\begin{aligned} V_{\text{eff}}^{[1]}(\phi) &= V^{(0)}(\phi) + \epsilon V^{(1)}(\phi) \\ &= V(\phi) - \frac{i}{2} \int \frac{d^4p}{(2\pi)^4} \log \left[p^2 - V''(\phi) \right], \end{aligned} \quad (7.9)$$

where $V''(\phi)$ are the field dependent scalar masses obtained for the massless scalar theory by taking the second derivative of the classical potential in terms of each field.

Before generalizing the one-loop Coleman-Weinberg effective potential into a form which can be applied to the trinification model, it is worth considering the massless scalar theory of [27] in an example, to further understand the connection between derivatives of the effective potential and corrections to n -point functions.

7.1.2.1 Example: massless scalar theory in the effective potential method

Consider the massless scalar theory with the Lagrangian

$$\mathcal{L} = \frac{1}{2}(\partial_\mu\phi)^2 - \left[\frac{1}{2}m_0^2\phi^2 + \frac{\gamma}{3!}\phi^3 + \frac{\lambda}{4!}\phi^4 + \frac{\rho}{5!}\phi^5 + \dots \right]. \quad (7.10)$$

Then the one-loop Coleman-Weinberg effective potential is given by (7.9) where

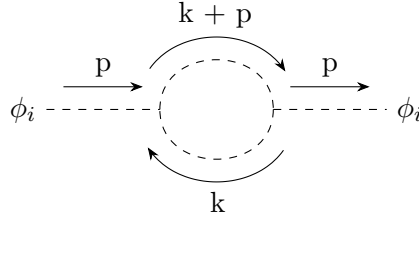
$$V''(\phi) = m_0^2 + \gamma\phi + \frac{1}{2}\lambda\phi^2 + \frac{\rho}{6}\phi^3 + \dots \equiv m(\phi)^2, \quad (7.11)$$

are the field dependent masses. Here, m_0^2 are the tree-level mass-squared terms.

To determine, for example, the one-loop corrections to scalar 3-point functions, we take the third derivative of the one-loop contribution to the effective potential, $V^{(1)}$ such that we have

$$\begin{aligned} \left. \frac{\partial^3 V^{(1)}}{\partial \phi^3} \right|_{\phi=\langle \phi \rangle} &= \frac{i}{2} \rho \int \frac{d^4 p}{(2\pi)^4} \left(\frac{i}{k^2 - m(\phi)^2} \right) \\ &+ \frac{3i}{2} \gamma \lambda \int \frac{d^4 p}{(2\pi)^4} \left(\frac{i}{k^2 - m(\phi)^2} \right)^2 \\ &+ \lambda^3 i \int \frac{d^4 p}{(2\pi)^4} \left(\frac{i}{k^2 - m(\phi)^2} \right)^3 \end{aligned} \quad (7.12)$$

In general, for one-loop Feynman diagrams in the $p \rightarrow 0$ we can write

$$\begin{aligned} \phi_i \text{---} \overset{p}{\rightarrow} \text{---} \phi_i &\propto \int \frac{d^4 k}{(2\pi)^4} \frac{i}{k^2 - m^2} \frac{i}{(k+p)^2 - m^2} \\ &\stackrel{p \rightarrow 0}{=} \int \frac{d^4 k}{(2\pi)^4} \left(\frac{i}{k^2 - m^2} \right)^2 \end{aligned}$$


Recalling that derivatives of the effective potential give corrections to n -point correlation functions in the $p \rightarrow 0$ approximation, we can match each term in the summation of (7.12) to a corresponding 1PI Feynman diagram. Thus, the expression of the third derivative corresponds diagrammatically to:

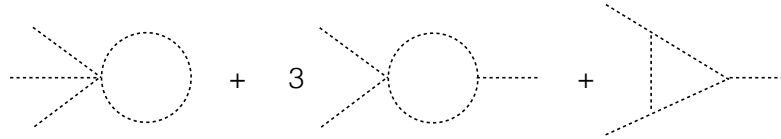


Figure 6: One-loop corrections to scalar 3-point functions in the massless scalar theory. Here, the factor of three before the second diagram is included to account for the combinatorics of external scalars. The 5-point vertex of the first diagram is proportional to ρ , the 4-point vertex of the second diagram is proportional to γ , and all 3-point vertices's are proportional to λ

By comparing (7.12) to Figure 6 above, it is clear that the third derivative of the one-loop correction to the effective potential yields the sum of all zero-external momentum one-loop corrections to the 3-point functions of the theory.

7.2 One-loop scalar masses in the LRSM

With the developed effective potential method as a viable approach for determining one-loop corrections to n -point functions, we can apply this formalism to the scalars of the LRSM to obtain the full one-loop mass spectrum at the GUT scale.

For any scalar in the model, the one-loop mass is the sum of its tree-level (bare) mass with all possible one-loop corrections arising from interactions with the fluctuating vacuum as the particle transitions from an initial state to a final one. Diagrammatically, for scalars in the LRSM this is illustrated as

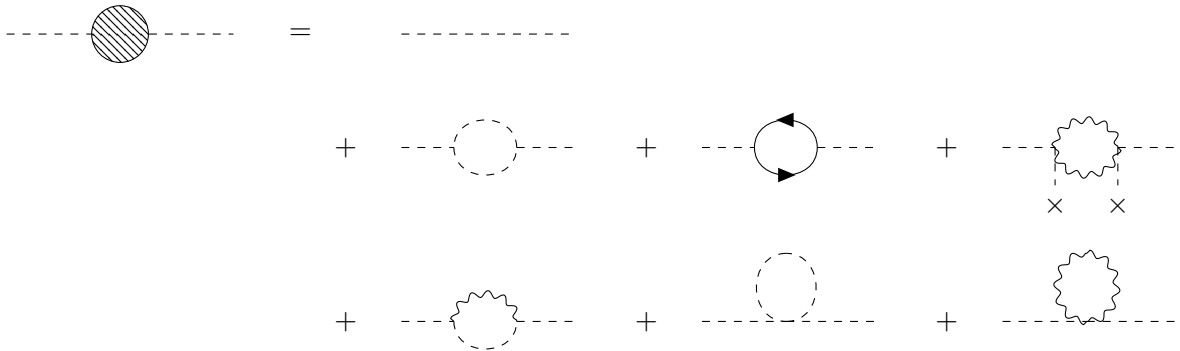


Figure 7: Diagrams contributing to the one-loop mass for scalars in the LRSM

Before the full scalar one-loop mass spectrum for the LRSM can be calculated, the one-loop effective potential of (7.9) must be put into a form which is applicable to this model.

7.2.1 Renormalized one-loop contribution

As mentioned, the effective potential is the classical potential plus the sum of all 1PI connected vacuum graphs. The topology of the one-loop 1PI connected vacuum Feynman diagram does not contain an interaction vertex. Thus, $V^{(1)}$ depends only on the field-dependent squared masses.

In the example of the massless scalar theory, the Lagrangian involved only scalar self-interaction terms, and thus the field dependent masses were functions of ϕ alone. For more complex models, such as the one studied throughout this work, the Lagrangian will also contain interactions between scalars and other particles (fermions and vector bosons) described by cubic and quartic couplings. Because each type of particle can run as a propagator in loop diagrams, the one-loop contribution to the effective potential should sum over all types of particles present in the model.

Furthermore, the integral in the Coleman-Weinberg effective potential in (7.9) contains ultraviolet divergencies. Thus, renormalization theory should be applied by introducing counterterms and setting a cutoff value over which to integrate. After renormalization, the effective potential will be independent of these, since in any dimensional regularization scheme, the divergences are automatically canceled [28].

Considering all interactions in the Lagrangian, the renormalized one-loop contribution to the effective potential can be re-written as

$$V^{(1)} = \frac{1}{4} \sum_{\text{T}} (-1)^{2s_{\text{T}}} (2s_{\text{T}} + 1) \text{Tr}[\Lambda_{(\text{t})}^2 (\overline{\log} \Lambda_{(\text{t})}^2 - k_{\text{T}})], \quad (7.13)$$

where the sum over T is a summation over all types of particles in the theory, such that $\text{T} = \{\text{S}, \text{F}, \text{G}\}$ for scalars, fermions, and gauge bosons respectively. $\Lambda_{(\text{t})}^2$ are the field dependent mass-squared matrices for each particle type, and taking the trace ensures we consider only terms corresponding to 2-point self interactions [8].

Furthermore, s_{T} is the spin of each field of type T, and we introduce the notation

$$\overline{\log}(m^2) \equiv \log\left(\frac{m^2}{Q^2}\right), \quad (7.14)$$

where Q^2 is the renormalization scale. Finally, k_{T} depends on the renormalization scheme. For the sake of this work, we use the $\overline{\text{MS}}$, and the value of k_{T} for each type of particle is⁸

$$k_{\text{T}} = \begin{cases} \frac{3}{2}, & \text{if } \text{T} = \text{S}, \text{F} \\ \frac{5}{6}, & \text{if } \text{T} = \text{G} \end{cases} \quad (7.15)$$

7.2.2 Derivative formulas of the one-loop effective potential

As can be seen in (7.13), at one-loop, field dependent masses enter into the potential as matrix logarithms. Taking n^{th} -order derivatives of such an expression to determine one-loop corrections to n -point functions becomes significantly difficult, unless we evaluate it at a certain minimum.

In [8] general analytic expressions for derivatives of the effective potential with respect to any number of classical scalar fields applicable in any 4-dimensional renormalizable theory, are derived. The use of these expressions instead of taking direct derivatives of (7.13) will allow us to evaluate one-loop contributions while keeping the field dependence throughout the calculation. The formulas hold in the zero-external momentum approximation.

For the sake of this work, we will consider the first and second derivative formulas for the one-loop effective potential. The derivation of these expressions is mathematically extensive, and can be fully found in [8].

The first derivative formula gives the tadpole truncated at one loop. It is given by [8]

$$\partial_i V_{\text{eff}}^{[1]} = \Lambda_{i(s)} + \epsilon O_{(S)i}^j \sum_{\text{T}} \frac{(-1)^{2s_{\text{T}}} (1 + 2s_{\text{T}})}{2} m_{(\text{T})a}^2 \lambda_{(\text{T})a}^a{}_j \left(\overline{\log} m_{(\text{T})a}^2 - k_{\text{T}} + \frac{1}{2} \right), \quad (7.16)$$

⁸In $\overline{\text{MS}}$ each divergent term (arising from loops in Feynman diagrams) plus a constant is absorbed into counterterms. The same constant is used for each divergence, and the different k_{T} values for each particle type arise from the loop integral in each case. The values of k_{T} in (7.15) are derived in [28]. For a detailed discussion of the $\overline{\text{MS}}$ renormalization scheme, see [29].

The second derivative formula essentially sums over all the one-loop scalar 2-point functions allowed by the theory. It is given by [8]

$$\begin{aligned} \partial_{kl} V_{\text{eff}}^{[1]} = & \Lambda_{kl(s)} + \epsilon O_{(S)}^i{}_k O_{(S)}^j{}_l \sum_{\text{T}} \frac{(-1)^{2s_{\text{T}}}(1+2s_{\text{T}})}{2} S_{\{ij\}} \left[\lambda_{(\text{T})i}^{ab} \lambda_{(\text{T})baj} \left(f_{(\text{T})ab}^{(1)} - k_{\text{T}} + \frac{1}{2} \right) \right. \\ & \left. + \lambda_{(\text{T})aij}^a m_{(\text{T})a}^2 \left(\overline{\log} m_{(\text{T})a}^2 - k_{\text{T}} + \frac{1}{2} \right) \right]. \end{aligned} \quad (7.17)$$

Here, $\lambda_{(\text{T})}$ gives cubic or quartic couplings in the mass-eigenbasis, depending on if they are labeled with 3 or 4 indices respectively. Additionally, $O_{(S)}$ is the scalar rotation matrix as defined in (3.9).

$\Lambda_{i(s)}$ is the field dependent first derivative of the classical potential, as defined in (3.3). $\Lambda_{kl(s)}$ the tree-level field dependent scalar mass matrix, as defined in (3.7), and $m_{(\text{T})a}^2$ are the tree-level mass eigenvalues of each particle of type T, as defined throughout Section 3.2.

Furthermore, $S_{\{ij\}}$ is a symmetry operator which symmetrizes with respect to the scalar indices i, j .

Throughout the derivation of (7.16) and (7.17) given in [8], a set of tensors $f_{(\text{T})}^{(k)}$ are defined. Their components are given by

$$f_{(\text{T})a_1 \dots a_N}^{(k)} \equiv \sum_{x=1}^N \frac{m_{(\text{T})a_x}^{2k} \overline{\log} m_{(\text{T})a_x}^2}{\prod_{y \neq x} \left(m_{(\text{T})a_x}^2 - m_{(\text{T})a_y}^2 \right)}. \quad (7.18)$$

To implement the second derivative formula of (7.17), we need to compute f -tensors of rank 2, and of the order $k = 1$. This results in four expressions given by

$$f^{(1)}(x, y) = \begin{cases} 1 + \overline{\log}(0), & \text{if } x = 0, y = 0 \\ \overline{\log}(x), & \text{if } x \neq 0, y = 0 \\ \overline{\log}(y), & \text{if } x = 0, y \neq 0 \\ 1 + \overline{\log}(x), & \text{if } x = y \neq 0 \\ \frac{x \overline{\log}(x)}{(x-y) + y \overline{\log}(y)}, & \text{if } x \neq y \neq 0 \end{cases} \quad (7.19)$$

where x, y are inputted mass-squared eigenstates $m_{(\text{T})a}^2$ for each type (T) summed over in (7.17). The ambiguity in the first case, arising from the $\overline{\log}(0)$, is tackled by substituting a small, non-zero constant, σ , into the logarithm, such that we set $\overline{\log}(0) \rightarrow \overline{\log}(\sigma)$. As can be seen in (7.17), such terms will cancel out of each component of the $\partial_{kl} V_{\text{eff}}^{[1]}$ matrix.

The derivative formulas in (7.16) and (7.17) are valid only in the $p^2 \rightarrow 0$ approximation in which the scalar particles on the external legs in the diagrams are considered light compared to particles propagating in the loop [8].

We can justify that this approximation is valid of the sake of this work. As was discussed in Section 4.2.3 we can integrate the colored scalars of Table 2 out of the effective LRSM at tree-level by tuning the values of $\alpha_{1\dots 4}$. Thus, we are really only interested determining if one-loop contributions will influence the mass hierarchy in the color-singlet sector in such a way that the \tilde{H} and \tilde{l}_R fields are light compared to the others. As each of these fields is light at tree-level, and the largest contributions to their one-loop masses arises from diagrams with at least one heavy loop propagator, the $p^2 \rightarrow 0$ approximation is a good one for the color-singlet scalars of this model.

Finally, (7.16) and (7.17) can be implemented to obtain the full scalar one-loop mass spectrum for the LRSM at GUT scale. The process computationally extensive due to the large number of scalars, fermions, and gauge bosons in the trinification model. As such, it involves several essential components and steps that should be outlined with care.

7.2.3 Tri-linear couplings

Tri-linear couplings involved in scalar mass-corrections correspond to coefficients of cubic scalar field terms in the Lagrangian. As such, they are found by taking third derivatives. As can be seen in Figure 7, tri-linear couplings exist between scalars/scalars, scalars/fermions, and scalars/bosons⁹. Thus, in the $\Lambda(\text{gauge})$ -basis, tri-linear couplings are defined as

$$\frac{\partial \Lambda_{(t)}^{ij}}{\partial \phi_k} = \Lambda_{(t)}^{ijk}, \quad (7.20)$$

and physical couplings are isolated by evaluating in the VEV such that

$$\Lambda_{(t)}^{ijk} \Big|_{\phi_i = \langle \phi_i \rangle} = \Lambda_{(T)}^{ijk}. \quad (7.21)$$

Above, (3.5) defines $\langle \phi_i \rangle$, t and T again denote the type of particle such that $t = \{s, f, g\}$, $T = \{S, F, G\}$, and the term $\Lambda_{(t)}^{ij}$ refers the the expressions given in (3.7), (3.12), and (3.16) respectively.

The resulting $\Lambda_{(T)}^{ijk}$ expressions are a 3-dimensional tensors with dimensions corresponding to the number of derivatives taken such that¹⁰

$$\begin{aligned} [\Lambda_{(S)}^{ijk}] &= 162 \times 162 \times 162 \\ [\Lambda_{(F)}^{Ijk}] &= 81 \times 81 \times 162 \\ [\Lambda_{(G)}^{abk}] &= 24 \times 24 \times 162. \end{aligned} \quad (7.22)$$

Upon implementation of these tri-linear couplings into (7.17), they must first be rotated into the $\lambda(\text{mass})$ -basis. This is done using the rotation matrices $O_{(S)}, O_{(F)}, O_{(G)}$ given in (3.9), (3.14), and (3.18) respectively, according to the following formula

⁹Recall, we use the indices $\{i, j, k, l\}$ for scalars, $\{I, J\}$ for fermions, and $\{a, b\}$ for gauge boson, as defined throughout Section 3.2.

¹⁰Recall, the trinification model has 162 scalar components, 81 Weyl fermions, and 24 gauge bosons.

$$\lambda_{(T)}^{pqr} = \sum_{k=1}^r \sum_{j=1}^q \sum_{i=1}^p O_{(S)_k}^r O_{(T)_j}^q O_{(T)_i}^p \Lambda_{(T)}^{ijk}. \quad (7.23)$$

Due to the relatively large sizes of the $\Lambda_{(T)}^{ijk}$ and $O_{(T)}$ matrices, the computation of these couplings in `Mathematica` is extensive. To optimize the code, we simplify by summing over index values of $O_{(T)}$ for which the product with $\Lambda_{(T)}$ elements will be non-zero. Applying the summation over only such index values, requires us to implement a section of code which first locates non-zero elements of $O_{(T)}$, and then maps each of these, along with their position in the matrix, to a vector. We then substitute the indices i, j, k in (7.23) in for the position indices indicated by this vector, and sum over only those values.

With this optimization, the tri-linear scalar/scalar (S), scalar/fermion (F), and scalar/boson (G) couplings can all be expressed in 3-dimensional tensors in the mass-eigenbasis, denoted by $\lambda_{(T)}^{pqr}$.

7.2.4 Quartic couplings

Similarly, quartic couplings are found by taking fourth derivatives of the Lagrangian. Mathematically, this corresponds to taking the derivatives of $\Lambda_{(t)}^{ijk}$ to a fourth scalar such that

$$\frac{\partial \Lambda_{(t)}^{ijk}}{\partial \phi_l} = \Lambda_{(t)}^{ijkl} \quad (7.24)$$

and again

$$\Lambda_{(t)}^{ijkl} \Big|_{\phi_i = \langle \phi_i \rangle} = \Lambda_{(T)}^{ijkl} \quad (7.25)$$

Due to the fourth index, the dimensions listed in (7.22) increase each by a $\times 162$ to form 4-dimensional tensors.

To obtain couplings the λ -basis, the components are rotated according to

$$\lambda_{(T)}^{pqrs} = \sum_{l=1}^s \sum_{k=1}^r \sum_{j=1}^q \sum_{i=1}^p O_{(S)_l}^s O_{(S)_k}^r O_{(T)_j}^q O_{(T)_i}^p \Lambda_{(T)}^{ijkl} \quad (7.26)$$

Again, due to the extreme size of the $\Lambda_{(T)}^{ijkl}$ tensors, the computational complexity limits the ability for quartic couplings to be calculated in `Mathematica` directly. The code must again be optimized in order to significantly reduce the number of components to be calculated.

For this, we implement the same technique as in the previous section, and sum over only element indices in (7.26) which will yield non-zero values. Secondly, we use the symmetric properties of each $\Lambda_{(T)}^{ijkl}$ to our advantage.

In the scalar sector, it is straightforward to see that $\Lambda_{(S)}^{ijkl}$, is fully symmetric under interchanges of scalar indices, as any order in which we take derivatives of $V^{(0)}$ will give the same

coupling. For the same reason, the $\Lambda_{(G)}^{abkl}$ tensor is symmetric under exchanges of a, b and k, l .

Similarly, the $\Lambda_{(F)}^{IJkl}$ tensor is fully symmetric under exchanges of the scalar indices k, l . Furthermore, we can show that $\Lambda_{(f)}^{IJ}$ is Hermitian using the definition of (3.12), and the fact that M^{IJ} is symmetric, such that

$$\begin{aligned}\Lambda_{(f)}^{IJ} &= M^{*IK} M_K^J \\ &= M^{*KI} M_K^J \\ &= M_K^J M^{*KI} \\ &= \Lambda_{(f)}^{*JI}\end{aligned}$$

As a result, $\Lambda_{(F)}^{IJkl} = \Lambda_{(F)}^{*Jlkl}$.

The symmetric properties of these tensors are used to optimize the code. We create a 4-dimensional tensor with zero's as elements for each $\Lambda_{(T)}$ -quartic coupling tensor, and calculate only the non-zero components in the upper half of these tensors. We then create a function which maps any element with swapped indices to its symmetric counterpart, and places this into the lower half of the corresponding tensor. In this way, we build the full $\Lambda_{(T)}$ -quartic coupling tensors, without having to compute every element individually.

7.2.5 The first derivative formula

Once the tri-linear and quartic couplings of each type have been stored and saved, they can be called up for use in the first derivative formula given in (7.16).

As the $\Lambda_{i(s)}$ component of (7.16) has already be computed in Section 3.1, we are interested solely in determining the one-loop contribution to $\partial_i V_{\text{eff}}^{[1]}$ arising from the fluctuation on the vacuum. Thus, we implement

$$\partial_i V^{(1)} = O_{(S)_i}^j \sum_T \frac{(-1)^{2s_T} (1 + 2s_T)}{2} m_{(T)a}^2 \lambda_{(T)a}^a \lambda_j^a \left(\overline{\log} m_{(T)a}^2 - k_T + \frac{1}{2} \right). \quad (7.27)$$

The result will be a vector of 162 dimensions with one non-zero component corresponding to the correction to the classical VEV as defined in (3.2). This component is solved analytically, and found to be

$$\begin{aligned}
\partial_{\text{VEV}} V^{(1)} = \frac{1}{2} & \left[\frac{1}{9} g^4 v^3 \left\{ 27 \log \left(\frac{g^2}{4} \right) + 24 \log \left(\frac{2g^2}{3} \right) - 17 \right\} \right. \\
& + 6v^3 (\alpha_1 + \alpha_2 + \alpha_3 + \alpha_4) [\alpha_1 + \alpha_2 + \alpha_3 + \alpha_4 - 2(\lambda_1 - \lambda_2 - \lambda_3 - \lambda_4)] \\
& \quad \left. \left\{ \log \left(\frac{1}{2} [\alpha_1 + \alpha_2 + \alpha_3 + \alpha_4 - 2(\lambda_1 - \lambda_2 - \lambda_3 - \lambda_4)] \right) - 1 \right\} \right. \\
& + 24\alpha_1 v^3 [\alpha_1 - 2(\lambda_1 + \lambda_2 + \lambda_3 + \lambda_4)] \\
& \quad \left. \left\{ \log \left(\frac{1}{2} [\alpha_1 - 2(\lambda_1 + \lambda_2 + \lambda_3 + \lambda_4)] \right) - 1 \right\} \right. \\
& + 12v^3 (\alpha_1 + \alpha_2) (\alpha_1 + \alpha_2 - 2(\lambda_1 + \lambda_2 + \lambda_3 + \lambda_4)) \\
& \quad \left. \left\{ \log \left(\frac{1}{2} [\alpha_1 + \alpha_2 - 2(\lambda_1 + \lambda_2 + \lambda_3 + \lambda_4)] \right) - 1 \right\} \right. \\
& + 12v^3 (\lambda_1 + \lambda_2 + \lambda_3 + \lambda_4)^2 \{ \log (2[\lambda_1 + \lambda_2 + \lambda_3 + \lambda_4]) - 1 \} \\
& - 16v^3 (\lambda_2 + \lambda_3) (\lambda_1 + \lambda_4) \{ \log ([\lambda_2 + \lambda_3]) - 1 \} \\
& - 16v^3 (\lambda_1 + \lambda_3) (\lambda_2 + \lambda_4) \{ \log ([\lambda_2 + \lambda_4]) - 1 \} \\
& - 16v^3 (\lambda_1 + \lambda_2) (\lambda_3 + \lambda_4) \{ \log ([\lambda_3 + \lambda_4]) - 1 \} \\
& - 32v^3 \lambda_1 (\lambda_2 + \lambda_3 + \lambda_4) \{ \log ([\lambda_2 + \lambda_3 + \lambda_4]) - 1 \} \\
& - 12v^3 y^4 \left\{ \log \left(\frac{y^2}{2} \right) - 1 \right\} + \left[6 \left(-\frac{\kappa}{\sqrt{2}} + \alpha_1 + \alpha_3 \right) \right. \\
& \quad \left. \left(-\sqrt{2}\kappa + (\alpha_1 + \alpha_3) - 2[\lambda_1 + \lambda_2 + \lambda_3 + \lambda_4] \right) \right] \\
& \quad \left. \left\{ \log \left[\frac{1}{2} \left(-\sqrt{2}\kappa + (\alpha_1 + \alpha_3) - 2[\lambda_1 + \lambda_2 + \lambda_3 + \lambda_4] \right) \right] - 1 \right\} \right. \\
& + 6 \left(\frac{\kappa}{\sqrt{2}} + (\alpha_1 + \alpha_3) - \left(\sqrt{2}\kappa + (\alpha_1 + \alpha_3) - 2[\lambda_1 + \lambda_2 + \lambda_3 + \lambda_4] \right) \right) \\
& \quad \left. \left. \left\{ \log \left(\frac{1}{2} \left(\sqrt{2}\kappa + (\alpha_1 + \alpha_3) - 2[\lambda_1 + \lambda_2 + \lambda_3 + \lambda_4] \right) \right) - 1 \right\} \right] \right].
\end{aligned} \tag{7.28}$$

In this result we have applied several substitutions for convenience. Firstly, the renormalization scale is set at the same order as the classical VEV, v . This amounts to making the substitution $Q^2 \rightarrow v^2$ where Q is the renormalization scale, entering the first derivative in the logarithms under the definition of (7.14). Secondly, μ^2 is eliminated by applying the classical minimization condition of (3.6). Finally, we have made the substitution $\kappa = \frac{\gamma}{v}$. With these manipulations, the above result neatly shows the tree-level mass-squared expression of each scalar, as listed in Table 2, the fermions, and gauge bosons, entering the logarithms and contributing to the one-loop the correction to the VEV.

To ensure that expressions have been correctly implemented into the code, and thus that our results are reliable, several checks can be made. The first essential check involves comparing the result of (7.28) with the result when taking the first derivative of (7.13) to the classical VEV directly. We assign a numerical value to each parameter and apply them to both the resulting derivative and (7.28). We ensure that these numerical values coincide.

7.2.6 One-loop tadpole condition

Once the implementation of the first derivative formula has been checked with this method, the one-loop tadpole condition of the model can be found. As explained in Section 7.1.1, quantum fluctuations shift the classical VEV, such that the vacuum state at first order is given by

$$v + \epsilon\omega, \quad (7.29)$$

where v is the classical VEV, ω is this shift, and ϵ is defined in (7.8).

By definition, the one-loop tadpole condition is found by minimizing the one-loop effective potential. It is found by requiring that

$$\left. \frac{\partial V_{\text{eff}}^{[1]}}{\partial \phi} \right|_{v+\epsilon\omega} = 0. \quad (7.30)$$

Expanding the one-loop effective potential, we obtain

$$\left. \frac{\partial V^{(0)}}{\partial \phi} \right|_{v+\epsilon\omega} + \epsilon \left. \frac{\partial V^{(1)}}{\partial \phi} \right|_{v+\epsilon\omega} = 0. \quad (7.31)$$

The one-loop tadpole condition is then found by expanding this expression to the first order in ϵ and requiring each coefficient in the expansion to be zero.¹¹

Starting from the first term in (7.31), we insert (7.29) into the result of (3.3) and expand. This gives

$$\left. \frac{\partial V^{(0)}}{\partial \phi} \right|_{v+\epsilon\omega} = - \underbrace{\mu^2 v + (\lambda_1 + \lambda_2 + \lambda_3 + \lambda_4) v^3}_{\epsilon_{(0)\text{TP}}^0} + \underbrace{2v^2\omega(\lambda_1 + \lambda_2 + \lambda_3 + \lambda_4)}_{\epsilon_{(0)\text{TP}}^1} \epsilon. \quad (7.32)$$

We then isolate the zeroth order in ϵ by taking $\epsilon \rightarrow 0$. Only the first term in (7.31) will contribute in the zeroth order expansion in ϵ , as the second term, concerning the derivative of the one-loop contribution to the effective potential, enters as a multiple of ϵ . Thus, minimization of the zeroth order in ϵ coefficient gives

$$\epsilon_{(0)\text{TP}}^0 = 0 \quad \longrightarrow \quad \mu^2 = (\lambda_1 + \lambda_2 + \lambda_3 + \lambda_4) v^2, \quad (7.33)$$

which, as expected, corresponds to the tree-level minimization condition given in (3.6) for a stable vacuum at v .

To obtain the minimization condition in the first order of ϵ , the second term in (7.31) must also be considered. Since it enters as a multiple of ϵ , and as terms of $\mathcal{O}(\epsilon^2)$ are to be discarded, it is sufficient to expand this term in v . Thus, we define the coefficient in ϵ arising from the second term in (7.31) as

$$\left. \frac{\partial V^{(1)}}{\partial \phi} \right|_v = \epsilon_{(1)\text{TP}}^1. \quad (7.34)$$

¹¹Throughout calculation in this section we consistently discard $\mathcal{O}(\epsilon^2)$.

Combining (7.32) and (7.34), the coefficient of the first order in ϵ is given by

$$\epsilon_{\text{TP}}^1 = \epsilon_{(0)\text{TP}}^1 + \epsilon_{(1)\text{TP}}^1. \quad (7.35)$$

Finally, requiring $\epsilon_{\text{TP}}^1 = 0$, and solving for ω gives the one-loop tadpole condition for a stable vacuum at (7.29). The result of the one-loop tadpole condition is given in Appendix E.

7.2.7 The second derivative formula

We continue by implementing the second derivative formula in (7.17). As the $\Lambda_{kl(s)}$ matrix has already been computed, it is again sufficient to implement only the rotated $V^{(1)}$ contribution to the effective potential, such that

$$\begin{aligned} \partial_{kl}V^{(1)} = O_{(S)}^i{}_k O_{(S)}^j{}_l \sum_{\text{T}} \frac{(-1)^{2s_{\text{T}}}(1+2s_{\text{T}})}{2} S_{\{ij\}} \left[\lambda_{(\text{T})i}^{ab} \lambda_{(\text{T})baj} \left(f_{(\text{T})ab}^{(1)} - k_{\text{T}} + \frac{1}{2} \right) \right. \\ \left. + \lambda_{(\text{T})aij}^a m_{(\text{T})a}^2 \left(\overline{\log} m_{(\text{T})a}^2 - k_{\text{T}} + \frac{1}{2} \right) \right]. \end{aligned} \quad (7.36)$$

By closely studying the expression above, we see that the computation of the second derivatives involves a summation over both a , and b , applied to the summation over T for each type of particle. As such, the resulting matrix will contain 162×162 components, each of which is calculated by taking two summations over 162 indices each. Finally, the entire matrix is rotated over all the non-zero components of $O_{(S)}$. Thus, the computation of all the components of $\partial_{kl}V^{(1)}$ is strenuous, and obtaining results can require several days of computing time.

Once all the second derivative of the one-loop contribution to the effective potential have been computed and saved in a table, we can once again perform checks on the code to ensure that our results are reliable. Firstly, we can perform the same type of check as in the previous section, by comparing the direct second derivative of (7.13) with respect to v , with the component of $\partial_{kl}V^{(1)}$ which corresponds to the second derivative of the scalar obtaining the classical VEV. From Section 3.1, this is the $(\tilde{L}^3)_3$ field. We apply a numerical rule to each, and ensure they have the same value.

This idea can be used to further check the results. For instance, we can implement additional “toy” VEV’s in other scalar fields. If we place two different VEV’s in two differing scalar components, then we can check the corresponding off-diagonal term of $\partial_{kl}V^{(1)}$ where $k \neq l$. With this, numerous checks can be performed for several cases.

7.2.8 One-loop mass terms

Finally, the one-loop mass spectrum can be obtained by adding the one-loop mass correction terms in the second derivative matrix, $\partial_{kl}V^{(1)}$, to the tree-level mass terms of $\Lambda_{(s)}^{ij}$, found in Section 3.2. This will give the full one-loop mass-squared matrix in the gauge(Λ)-basis, with components defined by (7.17). The diagonalization of this matrix will yield the full scalar one-loop mass-squared eigenvalues at GUT scale, in the $p^2 \rightarrow 0$ approximation.

The one-loop mass spectrum is given by the second derivative of the full one-loop effective potential, evaluated at the shifted vacuum of our theory, defined by (7.29). Thus,

$$\left. \frac{\partial^2 V_{\text{eff}}^{[1]}}{\partial \phi_i \partial \phi_j} \right|_{v+\epsilon\omega} = \left. \frac{\partial^2 V^{(0)}}{\partial \phi_i \partial \phi_j} \right|_{v+\epsilon\omega} + \epsilon \left. \frac{\partial^2 V^{(1)}}{\partial \phi_i \partial \phi_j} \right|_{v+\epsilon\omega}. \quad (7.37)$$

We again expand in power of ϵ . The only term contributing to the zeroth order in ϵ will come from the first term expansion in v such that

$$\left. \frac{\partial^2 V^{(0)}}{\partial \phi_i \partial \phi_j} \right|_v = \epsilon_{(0)\text{M}}^0. \quad (7.38)$$

Clearly, this is equivalent to the tree-level mass-squared matrix obtained in Section 3.2. Thus, we make the replacement

$$\epsilon_{(0)\text{M}}^0 = \Lambda_{(\text{S})}^{ij}.$$

The first term in (7.37) also contributes in the first order expansion of ϵ . This coefficient is found by expanding it in $v + \epsilon\omega$ and extracting the coefficient in front of ϵ . We denote this coefficient by $\epsilon_{(0)\text{M}}^1$.

Similarly, the second term of (7.37) gives a contribution to the first order in ϵ . Just as before, we realize that this term enters as a multiple of ϵ and thus

$$\left. \frac{\partial^2 V^{(1)}}{\partial \phi_i \partial \phi_j} \right|_v = \epsilon_{(1)\text{M}}^1. \quad (7.39)$$

This expression is equivalent to evaluating the result of (7.36) at the classical VEV, v , and applying the classical minimization condition in (3.6).

The one-loop contribution to the masses is then

$$\Lambda_{(\text{S})}^{ij(1)} = \epsilon_{(0)\text{M}}^1 + \epsilon_{(1)\text{M}}^1. \quad (7.40)$$

Finally, we implement the one-loop tadpole condition given in Appendix E into this loop contribution term, and we can write the scalar one-loop mass-squared matrix in the Λ -basis as

$$\Lambda_{(\text{S})}^{ij[1]} = \Lambda_{(\text{S})}^{ij} + \epsilon \Lambda_{(\text{S})}^{ij(1)}. \quad (7.41)$$

The resulting matrix, $\Lambda_{(\text{S})}^{ij[1]}$ has 162×162 elements. Each non-zero element is an extensive mathematical expression, logarithmically dependent on the masses of any particles allowed to run in the loop of the corresponding 2-point function. They are, as such, not included for reference in this section.

In order to obtain physical mass-squared eigenvalues, the $\Lambda_{(\text{S})}^{ij[1]}$ matrix must be diagonalized into to λ -basis. Due to the extensive and lengthy nature of these expressions, analytical digitalization is computationally impossible. Thus, we must apply a numerics to obtain a final mass hierarchy for the scalar sector of the LRSM.

7.3 Numerical results for the one-loop mass spectrum

Once each one-loop mass has been found as an element of $\Lambda_{(S)}^{ij[1]}$, the task of determining the scalar mass hierarchy of the LRSM can be continued. The final aim of this work is to implement a parameter scanning algorithm which searches for physical points of the $\mathcal{P}_{\text{LRSM}}^{(\text{HS})}$ parameter space, which support the existence of the effective LRSM as a low-energy limit of the trinification model. That is, we search for points which impose a naturally occurring hierarchy between the one-loop masses of the Higgs tri-doublet, \tilde{H} , and the bi-doublet, \tilde{l}_R and the other color-singlet scalars in the top portion of Table 2.

7.3.1 Random point parameter scan

A preliminary parameter scan is constructed via an algorithm which passes randomly chosen parameter space points through systematically upon successfully satisfying defined conditions. Firstly, random real values between $\{-1\dots 1\}$ are chosen for each $\lambda_{1\dots 4}$, $\alpha_{1\dots 4}$, and y such that they satisfy the perturbativity requirement of (6.7).

The chosen parameter space point is then first required to pass a positivity test which ensures that the tree-level masses-squared eigenvalues of all particles are positive. In addition to securing vacuum stability, this ensures the real nature of any logarithmic terms in the components of $\Lambda_{(S)}^{ij[1]}$, thus preventing imaginary numbers arising as physical one-loop mass-squared eigenvalues. In conclusion, the first conditions on the chosen parameter space point are given in (4.7). These inequalities are reduced to a set of possible parameter solutions, which are implemented as the first requirement for passing a given point through.

Points which pass this first part of the positivity test are further input into the components of the $\Lambda_{(S)}^{ij[1]}$ matrix. Each mass term is computed numerically, and the resulting matrix is diagonalized. This gives a numerical scalar one-loop mass-squared matrix, which now describes physical mass-squared eigenstates. The final step in the positivity test, is to ensure that these are positive as well for the given parameter space point.

Next, we identify which states correspond to the \tilde{H} and \tilde{l}_R fields after diagonalization, and implement a requirement that these masses be no more than one tenth the size of other scalar masses. This is achieved by defining a function which compares the one-loop mass term to the tree-level scalar mass in the limit $\epsilon \rightarrow 0$. Using the known tree-level mass expression from Table 2 specific fields can be identified, and the same function can then require the corresponding numerical one-loop masses to be small compared to the others.

Parameter points which pass this final requirement are exported to a data file. They are physically viable parameter space points for which the desired scalar mass hierarchy in the effective LRSM is observed.

7.3.1.1 Results and discussion

Although the scanning algorithm outlined in the previous section is run for $\sim 8 \times 10^7$ randomly generated points, not a single parameter space point with satisfies the full set of constraints is found. The difficulty lays in passing the second test which requires the low mass ratio between

color-singlet states. Although they are still relatively rare when considering the large number of attempts, points which pass the positivity test can be found.

Although the lack of physically viable parameter space points obtained by this scanning algorithm makes it tempting to conclude at this stage that the desired hierarchy of the effective LRSM is mathematically prohibited, the ineffectiveness of the scanning design should be taken into careful consideration. The scanning algorithm has no feedback mechanism or bias which steers in towards more promising parameter values. As such, the random number generator could altogether miss small regions of the parameter space in which physically viable points lay.

To test the reliability of the scan, we can run the same algorithm, but this time requiring that the masses of the \tilde{h} and \tilde{l}_R fields be no more than one tenth that of the other scalar masses. As previously discussed, in [7] it is shown that the parameters of the trinification model can be tuned in such a way that these states are light compared to others at tree-level. Thus, we expect that, if our parameter scan is working correctly, and assuming the one-loop effects do not spoil the hierarchy, it should find physically viable parameter space points for this scenario.

Once the scan is run, it can be concluded that this random points algorithm finds roughly 1 in 1000 points which satisfy the conditions of the proposed EFT in [7]. In addition to indicating that the scan seems capable enough to find points for this scenario, the results proves that one-loop mass contributions do not spoil the imposed scalar mass hierarchy in the effective theory proposed in [7]. With this, we can further justify the EFT in [7] at one-loop.

With the scan working, at least for one scenario, we can tune the algorithm to see under which conditions physically viable parameter space points for our proposed EFT can be found. This involves softening the perturbativity constraints by increasing the range of values of the couplings, and/or increasing the required mass ratio between light and heavy scalars.

Upon several manipulations of the code, the scanning algorithm still fails to produce parameter space points. We move to further soften the scanning requirements by removing some of the scalars from the second test completely. For instance, we remove the requirement that \tilde{l}_R be light, and simplify the scan to consider only the Higgs tri-doublet. Furthermore, we increase the ratio between masses such that m_H^2 is required to be at no more than one third of the mass of each other scalar. Still, the scanning algorithm fails to produce a single viable point.

One interesting representation of the data we can look at, is the points passing the positivity test. These parameter space points ensure vacuum stability of the trinification model, and ensure the positiveness of the one-loop mass-squared eigenvalues of our scalars. We recall the relation in (4.14) of Section 4.2.3 which essentially prohibited the possibility that

$$m_H^2 \ll m_h^2, m_L^2,$$

at tree-level. We can plot the same relation, now at one-loop, and look for points for which lay away from the line given by the relation

$$m_{\text{H}}^2{}^{(1)} = \frac{1}{2} \left(m_{\text{h}}^2{}^{(1)} + m_{\text{L}}^2{}^{(1)} + m_{\text{R}}^2{}^{(1)} \right). \quad (7.42)$$

Any points which do not satisfy this relation can be further investigated as they may provide insight into one-loop effects which can possibly, but not necessarily, imply that $m_{\text{H}}^2, m_{\text{R}}^2 \ll m_{\text{h}}^2, m_{\text{L}}^2$.

We find parameter space points which pass the positivity test apply them to calculate the one-loop masses for each scalar field. To best represent the obtained data, we plot the deviation from the tree-level requirement obtained at one-loop, defined as

$$\% \text{ deviation} = \left| \frac{m_{\text{H}}^2{}^{(1)} - \left[\frac{1}{2} \left(m_{\text{h}}^2{}^{(1)} + m_{\text{L}}^2{}^{(1)} + m_{\text{R}}^2{}^{(1)} \right) \right]}{m_{\text{H}}^2{}^{(1)}} \right| \times 100, \quad (7.43)$$

against the one-loop mass-squared of the Higgs tri-doublet. The resulting data is plotted in Figure 8.

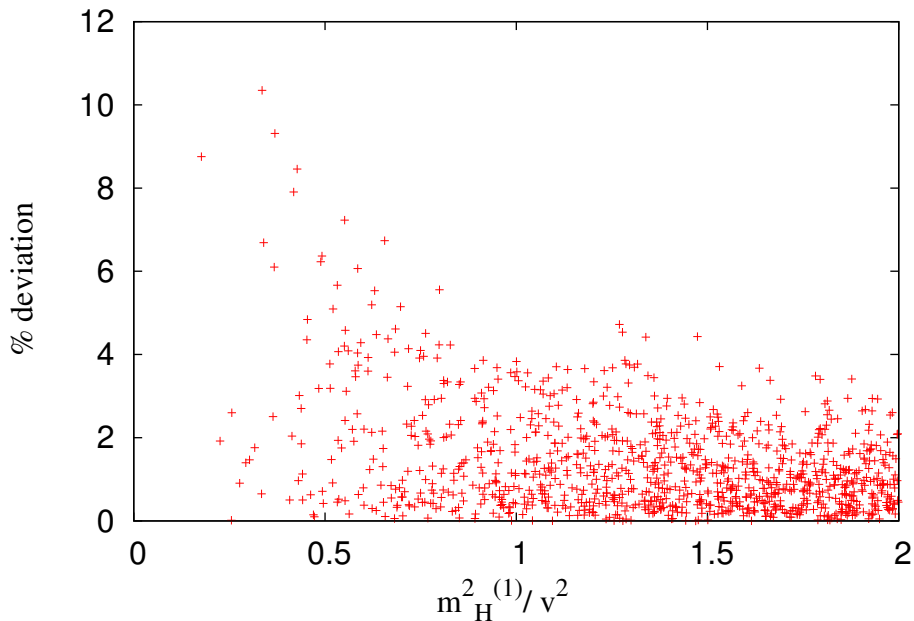


Figure 8: Percentage deviation from the tree-level mass-squared relation in (4.14) at one-loop. Throughout the scan, $v \rightarrow 1$, and squared-masses are expressed in units of $1/v^2$

The data in Figure 8 presents a significant result. Although percentage deviations are small, they take on non-zero values. This implies that at one-loop, the expression of (4.14) no longer holds, indicating that at the very least, one-loop effects can have some effect on the trification scale scalar mass hierarchy. In fact, we see that deviations can reach up to 10% of $m_{\text{H}}^2{}^{(1)}$. However, as the random scanning algorithm still fails to produce points for which the mass ratio between $\tilde{H}, \tilde{l}_{\text{R}}$ and $\tilde{h}, \tilde{l}_{\text{L}}$ is acceptable enough to justify integrating out particles at the GUT scale, a further analysis is needed before any hard conclusions can be made. For

instance, a first step in future research could be to examine points which indicate relatively large deviations in more detail.

As a final attempt to implement this scan for our purpose, we can limit it to consider only the region of the parameter space for which the tree-level masses of the color-singlet scalar states are zero. Limiting ourselves to considering only this case essentially lets us examine the effect of one-loop mass contributions alone. Upon considering tree-level masses only, the correct mass hierarchy could not be observed. Thus, we argued that one-loop contributions could push up the masses of some scalars enough to make them heavy in comparison to the \tilde{H} and \tilde{l}_R . We now tune the scan to consider this one-loop offset without the tree-level masses, and look for points for which the offsets of the \tilde{H} and \tilde{l}_R fields are very small compared to the others.

Theoretically, this is done by removing the positivity constraints and setting $\lambda_{2,3,4} = 0$, while assigning $0 < \lambda_1 \leq 1$. From Section 4.2.3, λ_1 enters only in the mass of the $\tilde{\Phi}^s$ state, and thus, this particle can be tuned independently of the others. However, the code identifies each field after diagonalization of the numerical one-loop mass matrix by comparing the one-loop mass to the tree-level mass as $\epsilon \rightarrow 0$. So, in practice we set each coupling to a small valued parameter, and we remove the mass ratio requirements completely.

After briefly examining the resulting mass-squared off-sets, no apparent trends are found. Because tree-level masses still constitute a significant contribution to the physical masses of the particle, we would require that the ratio between the one-loop mass offsets of light and heavy states be even smaller than when considering the full physical mass. No such trends are found.

With this final attempt, we can conclude that the random point algorithm is unsuccessful in finding points which support the mass ratio required by our effective LRSM.

8 Conclusion

Throughout this work, a trinification based GUT model with an added global $\{SU(3)\}$ family symmetry was investigated. This model is proposed in [7] as a radiative origin of the SM.

We showed that spontaneous symmetry breaking of the trinification model leads to the LRSM. Based on a set of predictions inspired by [7], we constructed a low-energy limit of the LRSM consisting of the tri-triplet, \tilde{H} , and the bi-doublet, \tilde{l}_R , scalars. We further showed that this effective LRSM can undergo radiative breaking due to the running of m_R^2 to a negative value, and that the 3HDM effective theory can be constructed by further integrating out heavy states at the breaking scale. Motivated by the results of [7], we argued that the 3HDM can break into $U(1)_{EM}$, and predicted a realistic SM quark hierarchy and CKM mixing. In summary, we showed that if the effective LRSM can exist as a low-energy limit of the trinification model, then it can be relatively simply broken down to the SM gauge group and account for certain SM phenomenology.

However, we concluded that although we can tune the model parameters such that colored scalars and the $\tilde{\Phi}^s$ state are heavy compared to the other scalar fields, we cannot impose a natural hierarchy between \tilde{H} , \tilde{l}_R and \tilde{h} , \tilde{l}_L when considering tree-level masses at the GUT scale. Thus, we constructed the effective potential method using a set of general expressions for the derivatives of the effective potential, found in [8], and used it to calculate the one-loop scalar mass spectrum in the $p^2 \rightarrow 0$ approximation. Upon including one-loop mass corrections, we searched for physically viable points for which the scalar hierarchy proposed in the effective LRSM can be imposed. We thereby attempted to rescue the effective LRSM, and justify it as a simple and elegant radiative origin of the SM.

Using the results presented throughout this work, we can make several conclusions. First and foremost, we can conclude that with the random scanning algorithm outlined in Section 7.3.1, we are unable to find any points which pass both the positivity test, as well as support the imposed mass-squared ratio between heavy and light scalars in the effective LRSM. Due to the random nature of the scan, we cannot conclude at this point that no such parameter space points exist. Although we test the algorithm for the mass ratio proposed in the EFT in [7], for which the desired mass hierarchy is observed already at tree-level, the results of this test do not let us draw significant conclusions about the capabilities of our scan. They do, however, let us conclude that our desired scalar hierarchy scenario is significantly more rare than that investigated in [7]. Ever so, it remains possible that the scan simply misses regions of the parameter space which satisfy our conditions. The results of the scanning algorithm applied to the EFT of [7], do, however, lead to the conclusion that a scalar hierarchy between the \tilde{h}, \tilde{l}_R and the \tilde{H}, \tilde{l}_L states is preserved at one-loop.

With this conclusion, we can discuss several key points for further research. Firstly, a more intelligent scanning algorithm should be designed. For example, a program similar to the simulated annealing algorithm used in Section 6 can be implemented by defining the ratio between light and heavy scalars, and determining which region of the high-scale parameter space minimizes this ratio. In this way, we can not only determine for which parameter space points we can achieve a small mass ratio, but we can also investigate how close to the desired hierarchy we can get. As a second step, a even more sophisticated algorithm can be implemented. For example, we can design a genetic algorithm, which are commonly implemented to generate high-quality solutions to optimization and search problems.

Before continuing to discuss further extensions of this work, it is worth noting the implications of the results. If a more intelligent parameter scan still fails to find regions of the parameter space for which we can justify the effective LRSM, it still does not imply that it cannot be a low-energy limit of the trinification model. It would, however, indicate that there is no natural splitting in the hierarchy of color-singlet scalars at the GUT scale, and prohibit us from integrating out the \tilde{h} and \tilde{l}_L fields. We would have to further investigate if such a splitting does occur at lower energies by keeping all four color-singlet scalars in the EFT. This would significantly complicate the matching conditions and RG running of the model. However, it is suggestible that this can still lead to an observable splitting at lower energies, allowing us to integrate out fields as done in this work at that scale, and preserve the breaking scheme to the 3HDM.

Furthermore, this study can be extended by considering one-loop corrections to the matching conditions in both the scalar and fermion sectors. As was seen in Section 4.3.2, many tree-level Yukawa and scalar couplings were zero or close to zero. Adding one-loop corrections could significantly affect these matching conditions, and thereby shift the initial conditions for the running of these parameters. In the fermion sector, one-loop corrections to n -point functions must be found diagrammatically. In the scalar sector, however, one-loop corrections to 3, 4-point functions can be computed with the third and fourth derivative formulas given in [8]. Throughout this work, it was attempted to apply these formulas to the trinification model, but calculations were hindered by limited computing time and power. Thus, in further studies, significant optimizations should first be considered.

On a final outlook, if a naturally occurring scalar hierarchy remains unobserved even with extensions of this work, it can motivate the consideration the supersymmetric version of the trinification model, proposed in [10]. In this model, a distinct splitting between scalar mass terms can be observed at the GUT scale at tree-level, and several heavy fields from other sectors can be integrated out at high energies. These effects, as well as several other key features discussed throughout [10], suggest that the supersymmetric trinification model may provide a more favorable topic of research.

Acknowledgements

First and foremost, I would like to thank Roman Paseschnik for his thorough supervision over my project, and specifically, for the all the time he has invested in my understanding of the trinification model and the essential concepts of model building used throughout this work. Thank you for the engaging discussions, and for challenging me throughout these months.

Secondly, I would like to express my sincere gratitude to Jonas Wessén and Eliel Camargo-Molina for their additional guidance throughout this thesis. Their support and approachability was essential to the project, as well as meaningful to me personally. Thank you for all your time, efforts, and for being such exceptional mentors.

Furthermore, I would like to thank António Morais and Marco Sampaio for their notable assistance in the implementation of the derivative formulas used for the scalar one-loop mass spectrum. I greatly appreciate the time you have taken to help me construct a reliable and effective code.

Finally, I would like to thank everyone in the THEP group for the memorable time I have had throughout this year. Particularly the many cups of coffee, awful physics jokes, and the unfailing moral support of my wonderful office mates have proved vital for the success of this project.

Appendices

A Full trinification breaking scheme

Throughout this Appendix the calculations of the breaking scheme of the trinification model are continued from Section 3.3.

In addition to breaking the trinification gauge group $[\text{SU}(3)_C \times \text{SU}(3)_L \times \text{SU}(3)_R]$, the global symmetry group of the model will also undergo spontaneous symmetry breaking upon placement of the VEV. Finding the unbroken generators and the new symmetry group is done in the same way as in Section 3.3 for the gauged trinification group.

Each must still satisfy the condition in (3.23), however, throughout this calculation, the i index should not be suppressed, adding a third transformation term to the condition for unbroken generators, such that

$$0 = i\omega_L^a (T_L^a)_3^l \delta_r^3 \delta_3^i - i\omega_R^a (T_R^a)_r^3 \delta_3^i \delta_3^l + i\omega_F^a (T_F^a)_3^i \delta_3^l \delta_r^3 \quad (\text{A.1})$$

The case $l = 3, r = 3, i \neq 3$ yields the relation

$$0 = \frac{1}{2}\omega^a \quad \text{for } a = 4\dots 7$$

such that just as before, the $\{\text{SU}(3)_F\}$ symmetry is broken into a $\{\text{SU}(2)_F\}$ where

$$T_F^{1\dots 3}$$

remain unbroken generators.

The next, and more algebraically complex, case to consider is when $l = r = i = 3$. For this case, (3.23), with and added i index, is given as

$$0 = i\omega_L^a (T_L^a)_3^3 - i\omega_R^a (T_R^a)_3^3 + i\omega_F^a (T_F^a)_3^3 \quad (\text{A.2})$$

which becomes the condition to satisfy for unbroken generators. Using

$$T^8 = \frac{\lambda^8}{2} = \frac{1}{2\sqrt{3}} \begin{pmatrix} 1 & 0 & 0 \\ 0 & 1 & 0 \\ 0 & 0 & -2 \end{pmatrix} \quad (\text{A.3})$$

we obtain the condition

$$\omega_L^8 - \omega_R^8 + \omega_F^8 = 0 \quad (\text{A.4})$$

which, if its met, indicates that some generator which is a linear combination of T_L^8 , T_R^8 , and T_F^8 will remain unbroken.

Using the results of the previous calculations, which indicate that the T_{L+R}^8 generator remains unbroken, we satisfy the condition above by introducing the following definitions:

$$\omega_L^8 = \omega_{L+R} + \omega_X \quad , \quad \omega_R^8 = \omega_{L+R} - \omega_X$$

The corresponding unbroken generators are found by expanding the infinitesimal transformation in terms of these definitions, such that

$$\begin{aligned} \omega_L^8 T_L^8 + \omega_R^8 T_R^8 + \omega_F^8 T_F^8 &= \omega_L^8 T_L^8 + \omega_R^8 T_R^8 + (\omega_R^8 - \omega_L^8) T_F^8 & (A.5) \\ &= \omega_L^8 (T_L^8 - T_F^8) + \omega_R^8 (T_R^8 + T_F^8) \\ &= (\omega_{L+R} + \omega_X)(T_L^8 - T_F^8) + (\omega_{L+R} + \omega_X)(T_R^8 + T_F^8) \\ &= \omega_{L+R} \underbrace{(T_L^8 - T_F^8)}_{\text{unbroken:}} + \omega_X \underbrace{(T_L^8 - T_R^8 - 2T_F^8)}_{\text{unbroken:}} \\ & \quad T_{L+R} \propto (T_L^8 + T_R^8) \quad \quad T_X \propto (T_L^8 - T_R^8 - 2T_F^8) \end{aligned}$$

Finally, to obtain the full breaking scheme the accidental global $U(1)_A$ and $U(1)_B$ symmetries must be included. As mentioned in Section (2.3), the $U(1)_B$ symmetry, referring to the conservation of baryon number, should remain intact when breaking to a SM-like theory. Adding the $U(1)_A$ symmetry into (A.2), we obtain the condition

$$0 = i\omega_L^a (T_L^a)_3^3 - i\omega_R^a (T_R^a)_3^3 + i\omega_L^a (T_L^a)_3^3 + i\omega_A T_A \delta_3^l \delta_r^3 \delta_3^i \quad (A.6)$$

Examining again the case $l = r = i = 3$, this condition leads to

$$\frac{1}{\sqrt{3}} \underbrace{(\omega_L^8 - \omega_R^8 + \omega_F^8)}_{\omega_Z} + \omega_A^8 = 0 \quad (A.7)$$

such that we need to satisfy

$$\omega_A^8 - \frac{\omega_Z}{\sqrt{3}} = 0 \quad (A.8)$$

to obtain an expression for an unbroken generator.

Repeating the same process of re-parameterization and algebraical expansion as in (A.5) yields the result:

$$T_Z \equiv \frac{2}{3}(T_A + \sqrt{3}T_F^8)$$

B Gell-Mann matrices

The Gell-Mann matrices are a set of linearly independent traceless Hermitian matrices. Throughout this work, they are used as the 8 generators of the SU(3)-space, such that $T^a = \frac{\lambda^a}{2}$. As such, they are essential in the calculations performed in Section 3.3 and Appendix A, and are given by

$$\begin{aligned} \lambda^1 &= \begin{pmatrix} 0 & 1 & 0 \\ 1 & 0 & 0 \\ 0 & 0 & 0 \end{pmatrix}, \quad \lambda^2 = \begin{pmatrix} 0 & -i & 0 \\ i & 0 & 0 \\ 0 & 0 & 0 \end{pmatrix}, \quad \lambda^3 = \begin{pmatrix} 1 & 0 & 0 \\ 0 & -1 & 0 \\ 0 & 0 & 0 \end{pmatrix}, \quad \lambda^4 = \begin{pmatrix} 0 & 0 & 1 \\ 0 & 0 & 0 \\ 1 & 0 & 0 \end{pmatrix} \\ \lambda^5 &= \begin{pmatrix} 0 & 0 & -i \\ 0 & 0 & 0 \\ i & 0 & 0 \end{pmatrix}, \quad \lambda^6 = \begin{pmatrix} 0 & 0 & 0 \\ 0 & 0 & 1 \\ 0 & 1 & 0 \end{pmatrix}, \quad \lambda^7 = \begin{pmatrix} 0 & 0 & 0 \\ 0 & 0 & -i \\ 0 & i & 0 \end{pmatrix}, \quad \lambda^8 = \frac{1}{\sqrt{3}} \begin{pmatrix} 1 & 0 & 0 \\ 0 & 1 & 0 \\ 0 & 0 & -2 \end{pmatrix} \end{aligned} \tag{B.1}$$

C Functional methods in quantum field theory

In this section we examine the quantization of scalar fields using the method of generating functionals. This formulation is essential in quantizing particles after symmetry breaking in quantum field theories. Additionally, it will prove essential to this work because we require a solid formalism in which to construct the effective potential. The effective potential is used to obtain the full scalar one-loop mass spectrum throughout Chapter 7.

C.1 Path integral formulation

In the path integral formulation of quantum mechanics we compute the transition amplitudes of particles as a sum over the infinite trajectories which are quantum mechanically allowed. We define the path integral by dividing the total time of transition, T , into small intervals of duration ϵ , and then integrating over the spatial coordinate, q_k , of each interval. Thus,

$$\int Dq(t) \equiv \frac{1}{C(\epsilon)} \prod_k \int_{-\infty}^{\infty} \frac{dq_k}{C(\epsilon)} \quad (\text{C.1})$$

where $C(\epsilon)$ is a constant [12].

Using this expression, we can write the probability amplitude for a particle to propagate from an initial state q_I to a final state q_F using the unitary time evolution operator as

$$\langle q_F | e^{-iHT} | q_I \rangle = \int Dq(t) e^{i \int_0^T dt L(\dot{q}, q)} \quad (\text{C.2})$$

Essentially, the expression above indicates that the scattering amplitude of the system is given by the integral over all possible paths such that the initial state is q_I and the final state is q_F [26].

C.2 Correlation functions

In quantum field theory, we study interacting theories in which the Hamiltonian

$$H = H_0 + H_{\text{int}} \quad (\text{C.3})$$

can be studied as a perturbation, H_{int} , on a free theory, H_0 . We define the vacuum state of the free theory as $|0\rangle$ with $E_0 = 0$ and the vacuum state of the interacting theory as $|\Omega\rangle$ with $E_\Omega \neq 0$. Instead of systems of particles we now study quantum fields, which correspond to particles once the theory has been quantized.

Correlation functions then describe the probability of transition from the vacuum state in the far past to the vacuum state in the far future, in the presence of some external source which disturbs the vacuum. They are the Green's functions of the system, and are defined as the vacuum expectation value of time ordered product of fields. Thus, the n -point correlation function is defined as

$$\begin{aligned}\langle\phi(x_1)\dots\phi(x_n)\rangle &\equiv\langle\Omega|T\phi(x_1)\dots\phi(x_n)|\Omega\rangle \\ &\equiv G_n(x_1\dots x_n)\end{aligned}\tag{C.4}$$

We consider a theory with a single scalar field, ϕ , and add the effect of a coupling to the external source, $J(x)$, such that

$$\mathcal{L}(\phi, \partial_\mu\phi) \longrightarrow \mathcal{L}(\phi, \partial_\mu\phi) + J(x)\phi(x)\tag{C.5}$$

For a free theory, the two-point correlation function is given by the Feynman Propagator, defined as

$$\begin{aligned}\langle 0|T\phi(x)\phi(y)|0\rangle &= \int \frac{d^4p}{(2\pi)^4} \frac{ie^{-ip\cdot(x-y)}}{(p^2 - m^2 + i\epsilon)} \\ &= D_F(x - y)\end{aligned}\tag{C.6}$$

To calculate higher order correlation functions for the interacting theory, however, we need to relate the correlation functions defined in (C.4) to the expectation value of the fields on the free vacuum $|0\rangle$, which are significantly easier to compute. This results in a general expression for computing correlation functions using path integrals, as

$$\langle\phi(x_1)\dots\phi(x_n)\rangle = \frac{\int \mathcal{D}\phi e^{i\int_{-T}^T \mathcal{L}[\phi]} \phi(x_1) \dots \phi(x_n)}{\int \mathcal{D}\phi e^{i\int_{-T}^T \mathcal{L}[\phi]}}\tag{C.7}$$

C.3 Generating functionals

Alternatively, we can introduce a function, Z , dependent on the source, J , which acts as a *generating functional* of the correlation functions.

We define the generating functional integral of a correlation function in the presence of the external source as

$$Z[J] = \int \mathcal{D}\phi e^{i\int d^4x(\mathcal{L}[\phi]+J\phi)}\tag{C.8}$$

The functional derivative relates the change in the functional at hand, to the change in a function on which the functional depends. Correlation functions can thus be found by taking the functional derivative of $Z[J]$, such that

$$\frac{1}{i^n} \frac{1}{Z[0]} \left(\frac{\partial^n}{\partial J(x_1) \dots \partial J(x_n)} \right) Z[J] \Big|_{J=0} = \langle\phi(x_1)\dots\phi(x_n)\rangle\tag{C.9}$$

Mathematically, a generating functional is the sum over the series expansion which expresses any infinite sequence of numbers as coefficients. Thus, another way to write the above relation between the generating functional and the n -point correlation functions in a field theory is

$$Z[J] = Z[0] \sum_{n=0}^{\infty} \frac{i^n}{n!} \int d^4x_1 \dots d^4x_n G_n(x_1, \dots, x_n) \cdot J(x_1) \dots J(x_n) \quad (\text{C.10})$$

In Section 7.1.1, we use the functional above to construct the *effective action*, which allows us to connect the functional methods formalism described throughout this Appendix to renormalization theory. For this, it is important to realize that the coefficients in the expansion of the generating functional are the connected Green's functions. G_n is the sum of all connected Feynman diagrams with n external lines [12].

In conclusion, we can define n -point correlations functions of any quantum field theory using the generating functional integral, $Z[J]$. This functional expresses the correlation functions as coefficients in an expansion in powers of J .

D Full RG equations of the effective LRSM

D.1 Running of Yukawa couplings

$$\begin{aligned}
(4\pi)^2 \beta_{Y_\pi} &= \left(-\frac{9}{2}g_L^2 - 3g_{LR}^2 - \frac{9}{4}g_R^2 + 4|Y_\pi|^2 + 3|Y_\mu|^2 + 2|Y_\nu|^2 + |Y_\beta|^2 + |Y_\delta|^2 + |Y_\kappa|^2 + |Y_\lambda|^2 \right) Y_\pi \\
(4\pi)^2 \beta_{Y_\nu} &= \left(-\frac{9}{4}g_R^2 - 3g_{LR}^2 - \frac{9}{2}g_L^2 + 3|Y_\mu|^2 + 2|Y_\pi|^2 + 5|Y_\nu|^2 + \frac{1}{2}|Y_\alpha|^2 + |Y_\kappa|^2 + 2|Y_\gamma|^2 + |Y_\lambda|^2 \right) Y_\nu \\
(4\pi)^2 \beta_{Y_\beta} &= \left(-\frac{9}{4}g_R^2 - \frac{9}{4}g_L^2 + |Y_\delta|^2 + 4|Y_\beta|^2 + |Y_\gamma|^2 + \frac{1}{2}|Y_\tau|^2 + |Y_\lambda|^2 + |Y_\pi|^2 + |Y_\alpha|^2 + 3[|Y_\zeta|^2 \right. \\
&\quad \left. + |Y_\eta|^2 + |Y_\epsilon|^2 + |Y_\theta|^2] \right) Y_\beta \\
(4\pi)^2 \beta_{Y_\tau} &= \left(2|Y_\kappa|^2 + |Y_\tau|^2 Y_\tau + |Y_\lambda|^2 + 4|Y_\alpha|^2 + \frac{3}{2}|Y_\tau|^2 + 2|Y_\beta|^2 \right) Y_\tau \\
(4\pi)^2 \beta_{Y_\gamma} &= \left(-\frac{9}{4}g_L^2 - 6g_{LR}^2 - \frac{9}{4}g_R^2 + |Y_\alpha|^2 + 3|Y_\eta|^2 + 3|Y_\zeta|^2 + \frac{1}{2}|Y_\kappa|^2 + |Y_\delta|^2 + 3|Y_\theta|^2 \right. \\
&\quad \left. + 2|Y_\nu|^2 + |Y_\beta|^2 + 3|Y_\epsilon|^2 + |Y_\gamma|^2 \right) Y_\gamma \\
(4\pi)^2 \beta_{Y_\kappa} &= \left(-\frac{9}{4}g_R^2 - 3g_{LR}^2 |Y_\tau|^2 + 3|Y_\mu|^2 + |Y_\gamma|^2 + |Y_\lambda|^2 + 2|Y_\pi|^2 + 4|Y_\alpha|^2 + 5|Y_\kappa|^2 + 2|Y_\nu|^2 \right) Y_\kappa \\
(4\pi)^2 \beta_{Y_\lambda} &= \left(-3g_{LR}^2 - \frac{9}{4}g_R^2 + |Y_\kappa|^2 + \frac{1}{2}|Y_\tau|^2 + 3|Y_\lambda|^2 + 3|Y_\mu|^2 + 2[|Y_\delta|^2 + |Y_\beta|^2 + |Y_\nu|^2 + |Y_\pi|^2] \right) Y_\lambda \\
(4\pi)^2 \beta_{Y_\delta} &= \left(-\frac{9}{4}g_R^2 + |Y_\gamma|^2 - \frac{9}{4}g_L^2 + 3|Y_\eta|^2 - 6g_{LR}^2 + |Y_\pi|^2 + |Y_\beta|^2 + |Y_\alpha|^2 + 3|Y_\zeta|^2 + |Y_\lambda|^2 \right. \\
&\quad \left. + 4|Y_\delta|^2 + 3|Y_\theta|^2 + 3|Y_\epsilon|^2 \right) Y_\delta \\
(4\pi)^2 \beta_{Y_\zeta} &= \left(-\frac{9}{4}g_L^2 - \frac{9}{4}g_R^2 - \frac{2}{3}g_{LR}^2 - 8g_c^2 + |Y_\beta|^2 + 3|Y_\theta|^2 + |Y_\alpha|^2 + |Y_\gamma|^2 + 3|Y_\theta|^2 + 3|Y_\eta|^2 + |Y_\delta|^2 \right. \\
&\quad \left. + 3|Y_\epsilon|^2 + 4|Y_\zeta|^2 \right) Y_\zeta \\
(4\pi)^2 \beta_{Y_\eta} &= \left(-\frac{2}{3}g_{LR}^2 - \frac{9}{4}g_R^2 - \frac{9}{4}g_L^2 - 8g_c^2 + 3[|Y_\zeta|^2 + |Y_\theta|^2 + |Y_\epsilon|^2] + |Y_\alpha|^2 + |Y_\delta|^2 + |Y_\gamma|^2 \right. \\
&\quad \left. + |Y_\beta|^2 + 6|Y_\eta|^2 \right) Y_\eta \\
(4\pi)^2 \beta_{Y_\epsilon} &= \left(-\frac{9}{4}g_L^2 - \frac{9}{4}g_R^2 - \frac{2}{3}g_{LR}^2 - 8g_c^2 + \frac{1}{2}|Y_\mu|^2 + 6|Y_\epsilon|^2 + 3|Y_\eta|^2 + |Y_\gamma|^2 + 3|Y_\theta|^2 + |Y_\beta|^2 \right. \\
&\quad \left. + |Y_\alpha|^2 + 3|Y_\zeta|^2 + 3|Y_\eta|^2 + |Y_\delta|^2 \right) Y_\epsilon \\
(4\pi)^2 \beta_{Y_\alpha} &= \left(-\frac{9}{4}g_R^2 - \frac{9}{4}g_L^2 + |Y_\delta|^2 + \frac{11}{2}|Y_\alpha|^2 + 3|Y_\theta|^2 + 2|Y_\kappa|^2 + |Y_\tau|^2 + |Y_\beta|^2 + 3|Y_\epsilon|^2 + 3|Y_\zeta|^2 \right. \\
&\quad \left. + \frac{1}{2}|Y_\nu|^2 + 3|Y_\eta|^2 + |Y_\gamma|^2 \right) Y_\alpha \\
(4\pi)^2 \beta_{Y_\theta} &= \left(-\frac{2}{3}g_{LR}^2 - \frac{9}{4}g_R^2 - 8g_c^2 - \frac{9}{4}g_L^2 + |Y_\alpha|^2 + |Y_\delta|^2 + 3[|Y_\eta|^2 + |Y_\epsilon|^2] + |Y_\gamma|^2 \right. \\
&\quad \left. + |Y_\beta|^2 + 6[|Y_\theta|^2 + |Y_\zeta|^2] \right) Y_\theta \\
(4\pi)^2 \beta_{Y_\mu} &= \left(-8g_c^2 - \frac{5}{3}g_{LR}^2 - \frac{9}{4}g_R^2 + 6|Y_\mu|^2 + \frac{|Y_\eta|^2}{72} + |Y_\kappa|^2 + 2|Y_\nu|^2 + 2|Y_\pi|^2 + |Y_\lambda|^2 + |Y_\epsilon|^2 \right) Y_\mu
\end{aligned}$$

D.2 Running of quartic couplings

$$\begin{aligned}
(4\pi)^2 \beta_{\lambda_a} = & 96\lambda_a \lambda_j + 2\lambda_e^2 + 4\lambda_e \lambda_l + 128\lambda_h \lambda_i - 9\lambda_a g_L^2 + 4\lambda_l^2 + 8\lambda_n^2 + 16\lambda_o^2 + 12\lambda_a |Y_\zeta|^2 \\
& - 2|Y_\gamma|^4 + 4\lambda_a |Y_\beta|^2 + 320\lambda_j^2 - 2|Y_\alpha|^4 + 4\lambda_a |Y_\delta|^2 + 12\lambda_a |Y_\theta|^2 + 8\lambda_d \lambda_n + 96\lambda_a \lambda_i + 8\lambda_d \lambda_o \\
& + 320\lambda_i^2 + 128\lambda_i \lambda_j + \frac{3}{4}g_L^2 g_R^2 - 9\lambda_a g_R^2 + 4\lambda_d^2 + \frac{9}{8}g_L^4 + 12\lambda_a |Y_\epsilon|^2 + 320\lambda_h^2 + \frac{9}{8}g_R^4 + 8\lambda_d \lambda_m \\
& - 6|Y_\eta|^4 - 6|Y_\epsilon|^4 - 2|Y_\delta|^4 - 6|Y_\zeta|^4 + 128\lambda_h \lambda_j + 16\lambda_n \lambda_o - 2|Y_\beta|^4 + 4\lambda_a |Y_\alpha|^2 - 6|Y_\zeta|^4 \\
& + 48\lambda_a^2 + 4\lambda_a |Y_\gamma|^2 + 8\lambda_m^2 + 8\lambda_m \lambda_n + 96\lambda_a \lambda_h + 12\lambda_a |Y_\eta|^2 + 16\lambda_m \lambda_o
\end{aligned}$$

$$\begin{aligned}
(4\pi)^2 \beta_{\lambda_b} = & 32\lambda_b^2 - 16\lambda_b \lambda_g + 32\lambda_n \lambda_o - 12\lambda_b g_{LR}^2 + 3g_{LR}^2 g_R^2 - 2|Y_\kappa|^4 + 4\lambda_b |Y_\lambda|^2 + 8\lambda_b |Y_\nu|^2 - 6|Y_\mu|^4 \\
& - 4|Y_\pi|^4 + 16\lambda_d \lambda_m + 32\lambda_m \lambda_o + 6g_{LR}^4 + 4\lambda_b |Y_\kappa|^2 + 12\lambda_b |Y_\mu|^2 + 8\lambda_d^2 + 16\lambda_m^2 + 16\lambda_d \lambda_o \\
& + 16\lambda_n^2 - 2|Y_\lambda|^4 + 16\lambda_d \lambda_n + 16\lambda_g^2 - 9\lambda_b g_R^2 + \frac{9}{8}g_R^4 + 4\lambda_k^2 + 32\lambda_o^2 + 8\lambda_b |Y_\pi|^2 \\
& + 16\lambda_m \lambda_n - 4|Y_\nu|^4
\end{aligned}$$

$$(4\pi)^2 \beta_{\lambda_c} = 8\lambda_e^2 + 8\lambda_k^2 - 2|Y_\tau|^4 + 16\lambda_l^2 + 24\lambda_c^2 + 16\lambda_e \lambda_l + 4\lambda_c |Y_\tau|^2 + 16\lambda_m \lambda_n - 4|Y_\nu|^4$$

$$\begin{aligned}
(4\pi)^2 \beta_{\lambda_d} = & -6\lambda_d g_{LR}^2 + 2\lambda_d |Y_\beta|^2 + 4\lambda_e \lambda_k + 6\lambda_d |Y_\mu|^2 - |Y_\beta|^2 |Y_\lambda|^2 + 32\lambda_a \lambda_m + 192\lambda_h \lambda_o - 3|Y_\epsilon|^2 |Y_\mu|^2 \\
& + 6\lambda_d |Y_\theta|^2 - |Y_\delta|^2 |Y_\pi|^2 - 32\lambda_g \lambda_o - 3|Y_\mu|^2 |Y_\epsilon|^2 + 20\lambda_b \lambda_d + 8\lambda_k \lambda_l - |Y_\alpha|^2 |Y_\nu|^2 + 48\lambda_d \lambda_h \\
& + 2\lambda_d |Y_\lambda|^2 + 4\lambda_d |Y_\pi|^2 + 8\lambda_n^2 - |Y_\gamma|^2 |Y_\nu|^2 + 96\lambda_h \lambda_n - |Y_\kappa|^2 |Y_\gamma|^2 - |Y_\gamma|^2 |Y_\nu|^2 - |Y_\delta|^2 |Y_\pi|^2 \\
& + 2\lambda_d |Y_\alpha|^2 + 6\lambda_d |Y_\eta|^2 + 48\lambda_d \lambda_j - |Y_\gamma|^2 |Y_\kappa|^2 + 16\lambda_b \lambda_m - |Y_\pi|^2 |Y_\beta|^2 - 16\lambda_g \lambda_m \\
& - |Y_\alpha|^2 |Y_\nu|^2 + \frac{9}{4}g_R^4 - |Y_\lambda|^2 |Y_\delta|^2 - |Y_\delta|^2 |Y_\lambda|^2 - |Y_\pi|^2 |Y_\delta|^2 - 9\lambda_d g_R^2 - |Y_\lambda|^2 |Y_\beta|^2 + 6\lambda_d |Y_\epsilon|^2 \\
& + 2\lambda_d |Y_\gamma|^2 - |Y_\lambda|^2 |Y_\beta|^2 + 4\lambda_d^2 + 96\lambda_h \lambda_m + 96\lambda_j \lambda_n - |Y_\gamma|^2 |Y_\nu|^2 + 32\lambda_j \lambda_m - |Y_\lambda|^2 |Y_\delta|^2 \\
& - |Y_\kappa|^2 |Y_\alpha|^2 - |Y_\nu|^2 |Y_\alpha|^2 + 16\lambda_b \lambda_n + 48\lambda_d \lambda_i - \frac{9}{2}\lambda_d g_L^2 + 64\lambda_j \lambda_o + 96\lambda_i \lambda_m - |Y_\pi|^2 |Y_\beta|^2 \\
& - 16\lambda_g \lambda_n - |Y_\delta|^2 |Y_\pi|^2 - |Y_\nu|^2 |Y_\gamma|^2 - 3|Y_\mu|^2 |Y_\epsilon|^2 + 16\lambda_b \lambda_o - 3|Y_\mu|^2 |Y_\epsilon|^2 - |Y_\beta|^2 |Y_\pi|^2 \\
& - |Y_\alpha|^2 |Y_\kappa|^2 - 8\lambda_d \lambda_g + 32\lambda_i \lambda_n + 64\lambda_i \lambda_o - |Y_\lambda|^2 |Y_\beta|^2 - |Y_\delta|^2 |Y_\lambda|^2 + 32\lambda_a \lambda_n \\
& - |Y_\alpha|^2 |Y_\kappa|^2 + 36\lambda_a \lambda_d - |Y_\gamma|^2 |Y_\kappa|^2 + 32\lambda_a \lambda_o - |Y_\nu|^2 |Y_\gamma|^2 + 2\lambda_d |Y_\kappa|^2 - |Y_\alpha|^2 |Y_\kappa|^2 \\
& + 4\lambda_d |Y_\nu|^2 + 32\lambda_o^2 - |Y_\nu|^2 |Y_\alpha|^2 + 2\lambda_d |Y_\delta|^2 + 8\lambda_m^2 - |Y_\gamma|^2 |Y_\kappa|^2 + 6\lambda_d |Y_\zeta|^2
\end{aligned}$$

$$\begin{aligned}
(4\pi)^2 \beta_{\lambda_e} = & 32\lambda_a \lambda_l + 32\lambda_j \lambda_l - |Y_\alpha|^2 |Y_\tau|^2 + 36\lambda_a \lambda_e + 8\lambda_c \lambda_l + 8\lambda_d \lambda_k + 96\lambda_i \lambda_l + 16\lambda_k \lambda_m \\
& + 2\lambda_e |Y_\beta|^2 + 6\lambda_e |Y_\eta|^2 + 12\lambda_c \lambda_e + 6\lambda_e |Y_\epsilon|^2 - |Y_\beta|^2 |Y_\tau|^2 + 4\lambda_e^2 + 6\lambda_e |Y_\zeta|^2 \\
& + 96\lambda_h \lambda_l + 8\lambda_k \lambda_n - \frac{9}{2}\lambda_e g_L^2 - |Y_\beta|^2 |Y_\tau|^2 + 2\lambda_e |Y_\delta|^2 - |Y_\alpha|^2 |Y_\tau|^2 + 48\lambda_e \lambda_h + 48\lambda_e \lambda_i \\
& + 2\lambda_e |Y_\tau|^2 + 8\lambda_l^2 + 2\lambda_e |Y_\alpha|^2 + 16\lambda_k \lambda_o - |Y_\tau|^2 |Y_\alpha|^2 - |Y_\tau|^2 |Y_\beta|^2 + 48\lambda_e \lambda_j + 6\lambda_e |Y_\theta|^2 \\
& - |Y_\alpha|^2 |Y_\tau|^2 - |Y_\beta|^2 |Y_\tau|^2 - \frac{9}{2}\lambda_e g_R^2 + 2\lambda_e |Y_\gamma|^2
\end{aligned}$$

$$\begin{aligned}
(4\pi)^2 \beta_{\lambda_f} = & +4\lambda_f |Y_\pi|^2 - |Y_\kappa|^2 |Y_\tau|^2 + 6\lambda_f |Y_\mu|^2 - |Y_\tau|^2 |Y_\lambda|^2 - \frac{9}{2}\lambda_f g_R^2 - |Y_\lambda|^2 |Y_\tau|^2 - 16\lambda_f \lambda_g \\
& - Y_\tau |Y_\kappa|^2 Y_\tau + 2\lambda_f |Y_\kappa|^2 + 4\lambda_f |Y_\nu|^2 - 6\lambda_f g_{LR}^2 + 2\lambda_f |Y_\lambda|^2 + 2\lambda_f |Y_\tau|^2 \\
& + 4\lambda_b \lambda_f + 12\lambda_c \lambda_f + 8\lambda_f \lambda_k
\end{aligned}$$

$$\begin{aligned}
(4\pi)^2\beta_{\lambda_g} = & 12\lambda_g|Y_\mu|^2 + 3g_{LR}^2g_R^2 - \frac{1}{2}\lambda_f^2 + 8\lambda_n^2 - \frac{15}{8}|Y_\mu|^4 - \frac{5}{4}|Y_\pi|^4 - \frac{5}{4}|Y_\nu|^4 + 4\lambda_g|Y_\kappa|^2 \\
& + 4\lambda_g|Y_\lambda|^2 - \frac{5}{8}|Y_\lambda|^4 - 16\lambda_g^2 - 12\lambda_gg_{LR}^2 + 2\lambda_k^2 + 16\lambda_n\lambda_o - 9\lambda_gg_R^2 \\
& - \frac{5}{8}|Y_\kappa|^4 + 24\lambda_b\lambda_g + 8\lambda_g|Y_\nu|^2 + 8\lambda_g|Y_\pi|^2 + 8\lambda_m^2 + 16\lambda_m\lambda_o
\end{aligned}$$

$$\begin{aligned}
(4\pi)^2\beta_{\lambda_h} = & 4\lambda_h|Y_\gamma|^2 - \frac{3}{32}|Y_\eta|^2|Y_\epsilon|^2 + 24\lambda_a\lambda_h - 32\lambda_h\lambda_j - \frac{1}{2}\lambda_l^2 - 9\lambda_hg_L^2 + 4\lambda_h|Y_\beta|^2 \\
& - \frac{3}{16}g_L^2g_R^2 + 64\lambda_h^2 - 32\lambda_h\lambda_i + \frac{5}{32}|Y_\beta|^4 - \frac{3}{32}|Y_\epsilon|^2|Y_\eta|^2 + 12\lambda_h|Y_\eta|^2 \\
& - \frac{9}{32}|Y_\zeta|^2|Y_\theta|^2 - \frac{9}{32}|Y_\theta|^2|Y_\zeta|^2 + \frac{5}{32}|Y_\gamma|^4 + \frac{5}{32}|Y_\delta|^4 + \frac{15}{32}|Y_\zeta|^4 \\
& + \frac{5}{32}|Y_\alpha|^4 + 4\lambda_h|Y_\delta|^2 + \frac{15}{32}|Y_\epsilon|^4 + 12\lambda_h|Y_\epsilon|^2 - \lambda_m^2 - 2\lambda_m\lambda_o - \lambda_n^2 \\
& - 2\lambda_n\lambda_o - 9\lambda_hg_R^2 - 32\lambda_i^2 - 32\lambda_j^2 + \frac{15}{32}|Y_\zeta|^4 + 4\lambda_h|Y_\alpha|^2 + \frac{15}{32}|Y_\eta|^4 \\
& + 12\lambda_h|Y_\zeta|^2 + 64\lambda_i\lambda_j + 12\lambda_h|Y_\theta|^2
\end{aligned}$$

$$\begin{aligned}
(4\pi)^2\beta_{\lambda_i} = & 4\lambda_i|Y_\alpha|^2 - \frac{1}{2}\lambda_l^2 - \frac{3}{16}g_L^2g_R^2 - 32\lambda_h\lambda_i + 12\lambda_i|Y_\epsilon|^2 - 2\lambda_o^2 + 64\lambda_i^2 \\
& - 9\lambda_ig_R^2 + \frac{5}{32}|Y_\beta|^4 - 9\lambda_i g_L^2 + 4\lambda_i|Y_\gamma|^2 + \frac{5}{32}|Y_\gamma|^4 + \frac{5}{32}|Y_\delta|^4 + \frac{15}{32}|Y_\zeta|^4 \\
& - 32\lambda_i\lambda_j - \frac{9}{32}|Y_\epsilon|^2|Y_\eta|^2 + \frac{5}{32}|Y_\alpha|^4 - 32\lambda_h^2 + 64\lambda_h\lambda_j + \frac{15}{32}|Y_\epsilon|^4 \\
& - \frac{9}{32}|Y_\eta|^2|Y_\epsilon|^2 + 4\lambda_i|Y_\beta|^2 - \lambda_m^2 - 2\lambda_m\lambda_o - \frac{3}{32}|Y_\zeta|^2|Y_\theta|^2 + 4\lambda_i|Y_\delta|^2 \\
& + 12\lambda_i|Y_\theta|^2 - 32\lambda_j^2 + 12\lambda_i|Y_\eta|^2 + \frac{15}{32}|Y_\zeta|^4 + 12\lambda_i|Y_\zeta|^2 + \frac{15}{32}|Y_\eta|^4 + 24\lambda_a\lambda_i \\
& - \frac{3}{32}|Y_\theta|^2|Y_\zeta|^2
\end{aligned}$$

$$\begin{aligned}
(4\pi)^2\beta_{\lambda_j} = & -32\lambda_h\lambda_j - 9\lambda_jg_L^2 + 4\lambda_j|Y_\gamma|^2 + 64\lambda_j^2 - 2\lambda_o^2 + \frac{5}{32}|Y_\beta|^4 + 12\lambda_j|Y_\epsilon|^2 + 12\lambda_j|Y_\zeta|^2 + 24\lambda_a\lambda_j \\
& - \frac{9}{32}|Y_\zeta|^2|Y_\theta|^2 + 4\lambda_j|Y_\delta|^2 + \frac{3}{8}g_L^2g_R^2 - \frac{9}{32}|Y_\theta|^2|Y_\zeta|^2 + \frac{5}{32}|Y_\gamma|^4 \\
& + \frac{5}{32}|Y_\delta|^4 + 4\lambda_j|Y_\alpha|^2 + \frac{15}{32}|Y_\zeta|^4 - 32\lambda_i\lambda_j + \frac{5}{32}|Y_\alpha|^4 - 32\lambda_h^2 - 9\lambda_jg_R^2 \\
& + \frac{15}{32}|Y_\epsilon|^4 + 64\lambda_h\lambda_i + 12\lambda_j|Y_\eta|^2 - 32\lambda_i^2 - \lambda_n^2 - 2\lambda_n\lambda_o \\
& + \frac{3}{32}|Y_\epsilon|^2|Y_\eta|^2 + \frac{15}{32}|Y_\zeta|^4 + 4\lambda_j|Y_\beta|^2 + \frac{15}{32}|Y_\eta|^4 + 12\lambda_j|Y_\theta|^2 \\
& + \frac{3}{32}|Y_\eta|^2|Y_\epsilon|^2
\end{aligned}$$

$$\begin{aligned}
(4\pi)^2\beta_{\lambda_k} = & 8\lambda_e\lambda_n + 8\lambda_e\lambda_o + 4\lambda_k|Y_\nu|^2 + 2\lambda_k|Y_\tau|^2 + 12\lambda_b\lambda_k + 8\lambda_c\lambda_k + 2\lambda_k|Y_\lambda|^2 + 8\lambda_l\lambda_n \\
& - \frac{1}{2}|Y_\tau|^2|Y_\kappa|^2 + 8\lambda_d\lambda_l - \frac{1}{2}|Y_\kappa|^2|Y_\tau|^2 + 8\lambda_e\lambda_m + 6\lambda_k|Y_\mu|^2 + 4\lambda_k|Y_\pi|^2 \\
& + 2\lambda_k|Y_\kappa|^2 - \frac{1}{2}|Y_\kappa|^2|Y_\tau|^2 + 8\lambda_d\lambda_e + 12\lambda_k^2 - \frac{1}{2}Y_\tau|Y_\kappa|^2Y_\tau \\
& - 6\lambda_k g_{LR}^2 - \frac{9}{2}\lambda_k g_R^2
\end{aligned}$$

$$\begin{aligned}
(4\pi)^2\beta_{\lambda_l} = & + 2\lambda_l|Y_\alpha|^2 + \frac{1}{4}|Y_\tau|^2|Y_\beta|^2 + 16\lambda_j\lambda_l + \frac{1}{4}|Y_\beta|^2|Y_\tau|^2 + 8\lambda_e\lambda_l - \frac{9}{2}\lambda_l g_L^2 + \frac{1}{4}|Y_\alpha|^2|Y_\tau|^2 \\
& + 2\lambda_l|Y_\gamma|^2 + 6\lambda_l|Y_\zeta|^2 + \frac{1}{4}|Y_\alpha|^2|Y_\tau|^2 + 4\lambda_a\lambda_l + 2\lambda_l|Y_\tau|^2 - 8\lambda_k\lambda_m \\
& + 2\lambda_l|Y_\beta|^2 + 4\lambda_c\lambda_l - 48\lambda_h\lambda_l + \frac{1}{2}|Y_\beta|^2|Y_\tau|^2 + 2\lambda_l|Y_\delta|^2 \\
& + \frac{1}{2}|Y_\beta|^2|Y_\tau|^2 - 48\lambda_i\lambda_l + 8\lambda_l^2 + 6\lambda_l|Y_\epsilon|^2 - \frac{9}{2}\lambda_l g_R^2 + 6\lambda_l|Y_\eta|^2 \\
& + 6\lambda_l|Y_\theta|^2 - 8\lambda_k\lambda_o
\end{aligned}$$

$$\begin{aligned}
(4\pi)^2\beta_{\lambda_m} = & + \frac{1}{2}|Y_\pi|^2|Y_\delta|^2 + \frac{1}{4}|Y_\alpha|^2|Y_\kappa|^2 + \frac{1}{4}|Y_\nu|^2|Y_\gamma|^2 + \frac{3}{2}|Y_\mu|^2|Y_\epsilon|^2 + 2\lambda_m|Y_\lambda|^2 + \frac{1}{4}|Y_\gamma|^2|Y_\kappa|^2 \\
& + \frac{1}{2}|Y_\nu|^2|Y_\alpha|^2 + \frac{3}{2}|Y_\mu|^2|Y_\epsilon|^2 + \frac{1}{2}|Y_\gamma|^2|Y_\kappa|^2 + 32\lambda_j\lambda_o - 9\lambda_m g_R^2 \\
& + \frac{1}{4}|Y_\delta|^2|Y_\lambda|^2 - 48\lambda_i\lambda_m + 2\lambda_m|Y_\kappa|^2 + \frac{1}{2}|Y_\alpha|^2|Y_\nu|^2 + \frac{1}{2}|Y_\nu|^2|Y_\alpha|^2 \\
& + \frac{1}{4}|Y_\beta|^2|Y_\pi|^2 + 16\lambda_j\lambda_m + \frac{1}{2}|Y_\delta|^2|Y_\pi|^2 + \frac{1}{2}|Y_\lambda|^2|Y_\beta|^2 + \frac{1}{2}|Y_\kappa|^2|Y_\gamma|^2 \\
& - 96\lambda_h\lambda_o - 4\lambda_k\lambda_l + \frac{3}{4}|Y_\epsilon|^2|Y_\mu|^2 - 32\lambda_i\lambda_o + 2\lambda_m|Y_\beta|^2 \\
& + \frac{1}{4}|Y_\beta|^2|Y_\lambda|^2 + 2\lambda_m|Y_\alpha|^2 + \frac{1}{4}|Y_\gamma|^2|Y_\nu|^2 + \frac{3}{2}|Y_\mu|^2|Y_\epsilon|^2 + 6\lambda_m|Y_\eta|^2 \\
& + \frac{1}{2}|Y_\gamma|^2|Y_\kappa|^2 - \frac{9}{2}\lambda_m g_L^2 + 6\lambda_m|Y_\epsilon|^2 + 6\lambda_m|Y_\mu|^2 + \frac{1}{2}|Y_\lambda|^2|Y_\beta|^2 \\
& + \frac{1}{4}|Y_\delta|^2|Y_\pi|^2 + 8\lambda_d\lambda_m + \frac{1}{4}|Y_\delta|^2|Y_\lambda|^2 + 6\lambda_m|Y_\zeta|^2 + \frac{1}{4}|Y_\alpha|^2|Y_\kappa|^2 \\
& + 4\lambda_b\lambda_m - 48\lambda_h\lambda_m + \frac{1}{2}|Y_\delta|^2|Y_\pi|^2 + 2\lambda_m|Y_\gamma|^2 + 16\lambda_n\lambda_o + 2\lambda_m|Y_\delta|^2 \\
& + \frac{1}{4}|Y_\pi|^2|Y_\beta|^2 + 6\lambda_m|Y_\theta|^2 + \frac{1}{4}|Y_\alpha|^2|Y_\nu|^2 + 4\lambda_m|Y_\nu|^2 + \frac{1}{2}|Y_\lambda|^2|Y_\beta|^2 \\
& + 4\lambda_a\lambda_m + 8\lambda_g\lambda_m + 16\lambda_g\lambda_o + 8\lambda_m^2 - 6\lambda_m g_{LR}^2 + 4\lambda_m|Y_\pi|^2
\end{aligned}$$

$$\begin{aligned}
(4\pi)^2\beta_{\lambda_n} = & 6\lambda_n|Y_\epsilon|^2 + 4\lambda_n|Y_\pi|^2 + \frac{1}{2}|Y_\pi|^2|Y_\beta|^2 - 32\lambda_j\lambda_o + \frac{1}{4}|Y_\alpha|^2|Y_\kappa|^2 + \frac{1}{4}|Y_\nu|^2|Y_\gamma|^2 + \frac{1}{4}|Y_\gamma|^2|Y_\kappa|^2 \\
& - 6\lambda_n g_{LR}^2 + \frac{1}{4}|Y_\gamma|^2|Y_\nu|^2 + 6\lambda_n|Y_\eta|^2 + \frac{1}{2}|Y_\nu|^2|Y_\alpha|^2 + \frac{1}{2}|Y_\lambda|^2|Y_\delta|^2 \\
& + 6\lambda_n|Y_\mu|^2 + \frac{3}{2}|Y_\mu|^2|Y_\epsilon|^2 + 8\lambda_n^2 + 2\lambda_n|Y_\alpha|^2 + 2\lambda_n|Y_\kappa|^2 + 6\lambda_n|Y_\theta|^2 \\
& + \frac{1}{2}|Y_\pi|^2|Y_\beta|^2 + 6\lambda_n|Y_\zeta|^2 + \frac{1}{4}|Y_\lambda|^2|Y_\beta|^2 + \frac{1}{2}|Y_\nu|^2|Y_\alpha|^2 + \frac{1}{4}|Y_\beta|^2|Y_\pi|^2 \\
& + 8\lambda_d\lambda_n + \frac{1}{2}|Y_\kappa|^2|Y_\gamma|^2 - 96\lambda_h\lambda_o + \frac{3}{4}|Y_\epsilon|^2|Y_\mu|^2 + \frac{1}{4}|Y_\beta|^2|Y_\lambda|^2 \\
& + \frac{1}{2}|Y_\delta|^2|Y_\lambda|^2 - 48\lambda_h\lambda_n + \frac{1}{4}|Y_\gamma|^2|Y_\nu|^2 + 4\lambda_b\lambda_n + \frac{3}{2}|Y_\mu|^2|Y_\epsilon|^2 \\
& + 2\lambda_n|Y_\gamma|^2 + \frac{1}{4}|Y_\lambda|^2|Y_\delta|^2 - 48\lambda_j\lambda_n + \frac{1}{2}|Y_\gamma|^2|Y_\kappa|^2 + 4\lambda_n|Y_\nu|^2 \\
& + \frac{1}{4}|Y_\delta|^2|Y_\pi|^2 + 4\lambda_a\lambda_n + \frac{1}{4}|Y_\delta|^2|Y_\lambda|^2 + \frac{1}{4}|Y_\delta|^2|Y_\pi|^2 \\
& + \frac{3}{4}|Y_\mu|^2|Y_\epsilon|^2 + 8\lambda_g\lambda_n - 9\lambda_n g_R^2 + \frac{1}{4}Y_\pi Y_\delta Y_\lambda Y_\beta + 32\lambda_i\lambda_o \\
& + \frac{1}{4}|Y_\gamma|^2|Y_\kappa|^2 + \frac{1}{4}|Y_\alpha|^2|Y_\nu|^2 - \frac{9}{2}\lambda_n g_L^2 + \frac{1}{4}|Y_\alpha|^2|Y_\kappa|^2 + 16\lambda_i\lambda_n \\
& + \frac{1}{4}|Y_\alpha|^2|Y_\nu|^2 + 2\lambda_n|Y_\lambda|^2 - \frac{1}{4}Y_\lambda Y_\beta Y_\pi Y_\delta + 16\lambda_g\lambda_o + 2\lambda_n|Y_\beta|^2 \\
& + 16\lambda_m\lambda_o + 2\lambda_n|Y_\delta|^2
\end{aligned}$$

$$\begin{aligned}
(4\pi)^2\beta_{\lambda_o} = & -\frac{1}{8}|Y_\beta|^2|Y_\pi|^2 - \frac{1}{4}|Y_\nu|^2|Y_\alpha|^2 + 6\lambda_o|Y_\zeta|^2 - \frac{3}{8}|Y_\mu|^2|Y_\epsilon|^2 + 2\lambda_o|Y_\alpha|^2 - \frac{1}{8}|Y_\alpha|^2|Y_\kappa|^2 \\
& + \frac{1}{8}Y_\nu Y_\alpha Y_\kappa Y_\gamma - \frac{3}{4}|Y_\mu|^2|Y_\epsilon|^2 + 2\lambda_o|Y_\delta|^2 - \frac{1}{8}|Y_\beta|^2|Y_\lambda|^2 \\
& + 48\lambda_h\lambda_o - \frac{1}{8}|Y_\pi|^2|Y_\beta|^2 - \frac{1}{8}|Y_\gamma|^2|Y_\kappa|^2 - 16\lambda_i\lambda_o - \frac{1}{8}|Y_\alpha|^2|Y_\kappa|^2 \\
& - 8\lambda_g\lambda_o + 6\lambda_o|Y_\epsilon|^2 + 2\lambda_o|Y_\gamma|^2 - \frac{3}{4}|Y_\mu|^2|Y_\eta|^2 - \frac{9}{2}\lambda_o g_L^2 \\
& - \frac{3}{4}|Y_\mu|^2|Y_\epsilon|^2 - \frac{3}{8}|Y_\eta|^2|Y_\mu|^2 + 2\lambda_o|Y_\kappa|^2 - \frac{1}{4}|Y_\nu|^2|Y_\alpha|^2 + 8\lambda_d\lambda_o \\
& - 16\lambda_j\lambda_o - \frac{1}{8}Y_\kappa Y_\gamma Y_\nu Y_\alpha - 9\lambda_o g_R^2 - \frac{1}{8}|Y_\gamma|^2|Y_\kappa|^2 + 4\lambda_o|Y_\nu|^2 \\
& - \frac{1}{8}|Y_\alpha|^2|Y_\nu|^2 + 2\lambda_o|Y_\beta|^2 + 6\lambda_o|Y_\eta|^2 + 4\lambda_b\lambda_o - \frac{1}{8}|Y_\nu|^2|Y_\gamma|^2 \\
& + 4\lambda_a\lambda_o - 6\lambda_o g_{LR}^2 + 2\lambda_o|Y_\lambda|^2 - \frac{1}{8}|Y_\gamma|^2|Y_\nu|^2 - \frac{1}{4}|Y_\delta|^2|Y_\pi|^2 \\
& - \frac{1}{8}|Y_\alpha|^2|Y_\nu|^2 - \frac{1}{8}|Y_\delta|^2|Y_\lambda|^2 + 16\lambda_n\lambda_o + 6\lambda_o|Y_\mu|^2 - \frac{1}{8}|Y_\lambda|^2|Y_\beta|^2 \\
& + 32\lambda_o^2 + 6\lambda_o|Y_\theta|^2 - \frac{3}{8}|Y_\eta|^2|Y_\mu|^2 + 8\lambda_m\lambda_n - \frac{1}{8}|Y_\delta|^2|Y_\lambda|^2 \\
& - \frac{1}{4}|Y_\kappa|^2|Y_\gamma|^2 + 4\lambda_o|Y_\pi|^2 - \frac{1}{4}|Y_\gamma|^2|Y_\kappa|^2 + 16\lambda_m\lambda_o - \frac{3}{8}|Y_\epsilon|^2|Y_\mu|^2
\end{aligned}$$

D.3 Running of the Majorana mass term

$$(4\pi)^2\beta_{m_\Phi} = (3|Y_\kappa|^2 + 2|Y_\tau|^2 + 5|Y_\alpha|^2) m_\Phi$$

References

- [1] A De Rújula, H Georgi, SL Glashow, et al. Fifth workshop on grand unification. *World Scientific, Singapore*, 1984.
- [2] Jamil Hetzel. Phenomenology of a left-right-symmetric model inspired by the trinification model. *arXiv:1504.06739*, 2015.
- [3] Ernest Ma. Neutrino masses in an extended gauge model with E_6 particle content. *Physics Letters B*, 380(3):286–290, 1996.
- [4] Christophe Cauet, Heinrich Päs, and Sören Wiesenfeldt. Trinification, the hierarchy problem, and inverse seesaw neutrino masses. *Physical Review D*, 83(9):093008, 2011.
- [5] J. Sayre, S. Wiesenfeldt, and S. Willenbrock. Minimal trinification. *Phys. Rev. D*, 73:035013, Feb 2006.
- [6] Berthold Stech. Neutrino properties from $E_6 \times SO(3) \times Z(2)$. *Fortschritte der Physik*, 58(7-9):692–698, 2010.
- [7] José Eliel Camargo-Molina, António P Morais, Roman Pasechnik, and Jonas Wessén. On a radiative origin of the standard model from trinification. *Journal of High Energy Physics*, 2016(9):129, 2016.
- [8] José Eliel Camargo-Molina, António P Morais, Roman Pasechnik, Marco OP Sampaio, and Jonas Wessén. All one-loop scalar vertices in the effective potential approach. *arXiv preprint arXiv:1606.07069*, 2016.
- [9] Luis Alvarez-Gaumé. An introduction to anomalies. In *Fundamental problems of gauge field theory*, pages 93–206. Springer, 1986.
- [10] José E Camargo-Molina, António P Morais, Astrid Ordell, Roman Pasechnik, Marco OP Sampaio, and Jonas Wessén. Reviving trinification models through an E_6 -extended supersymmetric GUT. *Physical Review D*, 95(7):075031, 2017.
- [11] David J Gross, Jeffrey A Harvey, Emil Martinec, and Ryan Rohm. Heterotic string. *Physical Review Letters*, 54(6):502, 1985.
- [12] Michael E Peskin and Daniel V Schroeder. An introduction to quantum field theory, 1996.
- [13] Kovalenko Serguei. Phenomenology of physics beyond the Standard Model. 2016.
- [14] Mark Thomson. *Modern particle physics*. Cambridge University Press, 2013.
- [15] Francesco Decarolis, Ricardo Mayer, and Martin Santamaria. Homotopy continuation methods, 2002.
- [16] Howard Georgi and Richard Slansky. Lie algebras in particle physics. *Physics Today*, 36:62, 1983.
- [17] Howard Georgi. Effective field theory. *Annual review of nuclear and particle science*, 43(1):209–252, 1993.

- [18] Alexander Gall. Matching in nonrelativistic effective quantum field theories. *arXiv preprint hep-ph/9910364*, 1999.
- [19] Gerard't Hooft. The glorious days of physics-renormalization of gauge theories. *arXiv preprint hep-th/9812203*, 1998.
- [20] Luminita N Mihaila, Jens Salomon, and Matthias Steinhauser. Renormalization constants and beta functions for the gauge couplings of the standard model to three-loop order. *Physical Review D*, 86(9):096008, 2012.
- [21] Florian Lyonnet, Ingo Schienbein, Florian Staub, and Akin Wingerter. Pyr@ te: renormalization group equations for general gauge theories. *Computer Physics Communications*, 185(3):1130–1152, 2014.
- [22] K. A. Olive et al. Review of Particle Physics. *Chin. Phys.*, C38:090001, 2014.
- [23] IP Ivanov and CC Nishi. Symmetry breaking patterns in 3hdm. *arXiv preprint arXiv:1410.6139*, 2014.
- [24] Scott Kirkpatrick, C Daniel Gelatt, Mario P Vecchi, et al. Optimization by simulated annealing. *science*, 220(4598):671–680, 1983.
- [25] Martin B Einhorn and DR Timothy Jones. The effective potential, the renormalisation group and vacuum stability. *Journal of High Energy Physics*, 2007(04):051, 2007.
- [26] Anthony Zee. *Quantum field theory in a nutshell*. Princeton university press, 2010.
- [27] Sidney Coleman and Erick Weinberg. Radiative corrections as the origin of spontaneous symmetry breaking. *Physical Review D*, 7(6):1888, 1973.
- [28] Stephen P Martin. Two-loop effective potential for a general renormalizable theory and softly broken supersymmetry. *Physical Review D*, 65(11):116003, 2002.
- [29] Gerard't Hooft. Dimensional regularization and the renormalization group. *Nucl. Phys. B*, 61:455–68, 1973.